THE LEVEL STRUCTURE OF SOME LIGHT NUCLEI

by

L.G. Earwaker

A Thesis Submitted to
The Australian National University
for the Degree of
Doctor of Philosophy

December, 1963

PREFACE

This thesis describes a series of experiments which were carried out on the Canberra Tandem Van de Graaff accelerator in the Department of Nuclear Physics of the Australian National University.

The work described in chapters 1 to 5 inclusive was carried out in collaboration with Mr. J.G. Jenkin under the supervision of Professor E.W. Titterton. Approximately 50 percent of the supervised effort was my own. The remaining experiment, described in chapter 6, was carried out in collaboration with Dr. D.F. Hebbard. Again 50 percent of the effort was my own.

The experiments described in this thesis have been published under the following titles:

Half Lives of C^{10} and Ne^{19}
L.G. Earwaker, J.G. Jenkin and E.W. Titterton,
Nature (Lond.) 195 (1962) 217.

The $B^{10}(p,n)C^{10}$ Excitation Function from Threshold to 10.6 MeV
L.G. Earwaker, J.G. Jenkin and E.W. Titterton,
Nuclear Physics 42 (1963) 521.

The $F^{19}(p,n)Ne^{19}$ Reaction Between 5 and 11 MeV.
J.G. Jenkin, L.G. Earwaker and E.W. Titterton,
Nuclear Physics 44 (1963) 453.

The $B^{10}(p,He^3)Be^8$ Reaction
J.G. Jenkin, L.G. Earwaker and E.W. Titterton,
Physics Letters 4 (1963) 142.

The $B^{10}(p,\alpha)Be^{7}$ Reaction Between 2 and 11 MeV.
J.G. Jenkin, L.G. Earwaker and E.W. Titterton,
Nuclear Physics (in press).

Energy Levels of B^{9}.
L.G. Earwaker, J.G. Jenkin and E.W. Titterton,
Nuclear Physics (in press).

States in N^{14} Near the Proton Threshold.
L.G. Earwaker and D.F. Hebbard,
Nuclear Physics (in press).

It is a pleasure to thank the many people who have helped in the work described in this thesis. I would especially like to thank Professor E.W. Titterton for his constant encouragement during the past three years. Thanks are also due to Dr. D.F. Hebbard for his patient supervision during the latter part of this work and for his many helpful comments during the preparation of this thesis.

It has been a pleasure to work with Mr. J.G. Jenkin, whose friendship over the course of this work has been invaluable.

I appreciate the work done by Mr. F.A. Howe and associates at A.W.R.E., U.K., who made the self-supporting B^{10} targets used in three of the experiments described in this thesis.

I am grateful to Dr. F.C. Barker who gave much helpful advice during the preparation of some of the above papers, and also Dr. T.R. Ophel for his many helpful discussions on experimental techniques.

Finally I would like to thank the Australian Institute of Nuclear Science and Engineering whose scholarship I held throughout the course of this work.

No part of this thesis has been submitted for a degree at any other university.

L. G. Earwaker.

TABLE OF CONTENTS

INTRODUCTION

One of the major fields of research in nuclear physics is the accumulation of experimental data on the properties of energy levels in the various light nuclei. In general, the most useful information that can be obtained is whether or not an energy level exists, its excitation energy, its width, its total angular momentum or spin, its relative probability of different modes of decay and its isobaric spin admixtures. Such information should be useful in acquiring further understanding of nuclear forces and nuclear structure.

The research reported in this thesis is a part of this systematic search for and classification of nuclear energy levels. Five separate experiments have been carried out and data has been collected on part of the level structure of the nuclei B^9, C^{10}, C^{11}, N^{14}, O^{15} and Ne^{20}.

Chapter 1 describes the design features and associated electronics for an activation apparatus which was constructed for use in investigating reactions in which the residual nucleus is positron active.

A formula was derived for the absolute cross section of reactions measured by the activation apparatus. Chapters 2 and 3

describe cross sections measured in this manner, for the $F^{19}(p,n)Ne^{19}$ and $B^{10}(p,n)C^{10}$ reactions respectively. In addition to the usual quantities that must be measured to obtain cross sections, the radioactive decay constant is also required. Because an accurate evaluation of this had not previously been made for either Ne^{19} or C^{10}, the half life for each element was measured.

Considerable structure was found in the $F^{19}(p,n)Ne^{19}$ excitation function. From a comparison with the structure observed in other reactions leading to the compound nucleus Ne^{20}, an interpretation of the structure has been made in terms of compound nucleus states, influenced at higher energies by a strong direct interaction contribution. Several new levels in C^{11} were found from the study of the $B^{10}(p,n)C^{10}$ reaction, and a more accurate value was obtained for the energy of the first excited state of C^{10}.

The α particles from the $B^{10}(p,\alpha)Be^{7}$ reaction were studied in an effort to confirm, and to measure some of the properties of the levels in C^{11} observed in the $B^{10}(p,n)C^{10}$ reaction (described in chapter 3). Excitation functions were measured at close energy intervals at two angles, and thirty angular distributions were measured for both the ground and first excited state α-particle groups. These were analysed in terms of a series expansion of Legendre polynomials. The spin of the α particle is zero, and this

reduced the number of unknown parameters entering into the theoretical distributions sufficiently to allow an assignment to be made of a spin and parity to one of the levels. The experiment, and the analysis of the results, are described in chapter 4, together with the results of an investigation of the $B^{10}(p,He^3)Be^8$ reaction which was measured concurrently with the (p,α) work.

Chapter 5 describes the results of an investigation of the level structure of B^9 from a study of the α particles from the $B^{10}(He^3,\alpha)B^9$ reaction. No new levels were seen. However, several possible levels, reported by other workers, were not seen. The excited compound nucleus N^{13} in this reaction is extremely unstable to breakup into $3\alpha + p$. The shape of this continuum of α particles and two possible modes of decay which could result in the observed continuum are discussed.

In order to compute the C^{12}/C^{13} abundance ratio produced at equilibrium in stars burning in the Carbon-Nitrogen-Oxygen cycle, the $C^{13}(p,\gamma)$ cross section at stellar energies must be known. The usual extrapolation of the measured $C^{13}(p,\gamma)$ cross sections down to stellar energies assumes that there are no levels in N^{14} just above the $C^{13} + p$ threshold. Unfortunately, a level just above the threshold has been reported from a study of the $N^{14}(p,p')$ reaction. The purpose of the experiment described in chapter 6 is to repeat this

inelastic proton scattering experiment under as nearly as possible identical conditions to check on the reported level. The experiment was repeated over a range of proton energies and observation angles completely covering that of the previous measurements. The interpretation of the previous results was found to be in error. However, an adequate explanation has been found which does not require a level in N^{14} near the C^{13} + p threshold.

Appendix A describes the results of some calculations on the effect of observed beam current variations on the cross sections measured using the activation apparatus. The cross section formula given in chapter 2 was derived using the assumption that the beam current was constant throughout the bombardment.

Finally, appendix B describes calculations which were carried out to determine the energy resolution of charged particle groups from N^{14} + p reactions, obtainable with the gas target described in chapter 6. Broadening of the groups due to both geometrical effects and to energy straggling are treated.

CHAPTER 1

THE ACTIVATION TECHNIQUE AND APPARATUS

1.1 Introduction

The work described in this thesis is directed towards a better understanding of the level structure and properties of some light nuclei. Much useful information can be obtained from experiments in which the nucleus concerned is studied as the intermediate or compound nucleus. A study of the reaction cross section as a function of bombarding energy will often provide information on the number, positions and widths of the levels in a given excitation region. If the level spacing in the region of interest is much greater than the level width, the levels can be analysed in terms of compound nucleus formation. Properties of the levels, such as spin, parity and reduced width can then often be determined from a study of the angular distribution of the reaction products.

In the simplest experiments, the reaction cross section is measured, as a function of energy, at a single angle with respect to the incident beam. Because of interference between various levels, and between the levels and background contributions, this information may need to be supplemented. Interference effects in the excitation functions, measured at a single angle only, manifest themselves as displacements of the resonance energy, as modifications of the total

level width and even as additional minor anomalies.

If the differential cross section is integrated over 4π steradians however, interference effects, except those due to levels of the same spin and parity, are eliminated. The experimental procedure which provides the most information is one in which the excitation functions are measured at a large number of angles relative to the incident beam direction. The cross section can then be integrated over 4π steradians to give the resonance energy and total width, and the angular distributions can often be used to derive the spin, parity and reduced width of the level.

When the residual nucleus of a nuclear reaction is radioactive, a relatively simple method of measuring the integrated cross section is available. This is the activation technique, which consists in measuring the reaction cross section by recording the radioactivity produced. The technique is most powerful when the incident beam is monoenergetic and can be controlled in energy. High energy resolution can then be obtained by using very thin targets and measuring the cross section as a function of the incident beam energy. If, on the other hand, the incident beam is monoenergetic but cannot be so controlled, a method known as the stacked foil technique can be used. In this method, the target is a stack of thin foils through which the beam is passed. As the beam passes through the stack, it loses energy. Hence, the reaction

cross section corresponding to the average beam energy in each foil can be found from a separate measurement of those foils. In this way a complete excitation function can be measured after one irradiation. However, because of the severe energy straggling of the beam in the foils, the energy resolution obtained using this technique is very poor.

The detection system used with an activation apparatus depends upon the mode of decay of the residual nuclei. The most common modes of decay are by positron and electron emission. These electrons can be measured using CsI or organic scintillators, or with a magnetic or electrostatic focusing spectrometer. A γ-ray spectrometer however, is probably the most generally useful detector for many activities. When the β rays themselves are not detected, the characteristic γ rays from the excited states of the daughter nuclei can be measured. Also, in the case of positron emission, the 0.511 MeV annihilation quanta can be measured, either singly or in coincidence. Other radiations which can be measured by γ-ray spectrometers are the X rays from electron capture, and the γ-decay of isomeric states.

The activation technique is a useful method of investigating many reactions. It is especially useful when the emitted reaction particles are neutrons. Neutron detection is difficult, and no really satisfactory directional neutron counter is available. It is therefore very difficult to discriminate between reaction and background neutrons.

This problem is particularly severe when (p,n) reactions are measured at proton energies near 10 MeV, because of the large neutron background produced in the beam collimators, target backings and the Faraday cup. The activation technique is also very useful for distinguishing between simple and complex reactions such as (a,b) and (a,2b) respectively. Here again this is particularly true when one or both of the reaction particles are neutrons. A third type of measurement where the activation technique may be very useful is in cases where it is very difficult to separate the charged reaction particles of interest from other charged particle groups. This is particularly true for low yield reactions emitting low energy particles, provided the delayed radiation is sufficiently different from that of competing reactions. An example of this class of reaction might be the observation of (He^3,t) reactions in the face of strong competition from the (He^3,α) and (He^3,p) reactions. The tritons can often be separated from α particles and protons by magnetic analysis. However this involves a loss of detection efficiency which can generally be avoided by use of an activation technique.

Competing reactions can generally be separated by their decay half-lives, or by their different characteristic γ rays. Difficulty may be experienced however, when both the half-lives and the characteristic radiations are comparable for the competing reactions.

1.2 The Activation Apparatus

The activation apparatus described in this chapter was designed for use in investigating nuclear reactions in which the residual nucleus is positron-active. It was used, in conjunction with the Canberra tandem Van de Graaff accelerator, to investigate two (p,n) reactions at proton energies up to 11.0 MeV. The positrons were detected by measuring coincidences between the positron annihilation quanta using two NaI(Tℓ) γ-ray spectrometers placed on either side of the target. This method enabled backgrounds, other than those from positron activities, to be eliminated.

The design of such an apparatus may take many forms. However there are certain basic requirements which must be incorporated. The factors considered in the design of the present apparatus are outlined below:

(i) Over periods of time, contaminants such as carbon from backing pump or roughing pump vapours and mercury from the diffusion pump, build up a layer on the target surface. Such layers may produce unwanted background positron activities, and can also produce a shift in the energy at which a sharp resonance is observed. This build up can be reduced by placing a liquid air trap near the target.

(ii) If the measurements are to be consistent, the geometry of the counting system must be well known and reproducible. Hence the provision of a beam viewing device, usually in the form of a quartz disk, is essential to enable the position of the proton beam to be adjusted and monitored.

(iii) When the activity to be measured has a relatively long half life, (greater than a few minutes) the targets are often removed from the target chamber after irradiation, and taken to a shielded counting system for measurement. This procedure greatly reduces all unwanted background activities except those actually present on the target. However, the present apparatus was designed for experiments in which the activity can have a decay half life as short as a few seconds. For this reason it was decided to keep the targets fixed, and to place the counting system beside the target chamber.

(iv) When the above counting procedure is adopted, the interior of the target chamber must be constructed from a material which does not become positron active when irradiated by scattered beam.

(v) In order to make the equipment sensitive to very small cross sections, it is desirable to arrange the counting

equipment in such a manner that the detection efficiency is as high as possible. The activity is measured by detecting coincidences between the two annihilation quanta from a positron at rest. Because of the 180^{o} correlation between the two annihilation quanta, the positrons must be made to annihilate in some relatively small central region between the two counters in order that they be detected.

(vi) Of the readily available target backing materials which do not become positron active when irradiated with protons, a suitable one was tantalum. Tantalum was used on some target backings and was also used to line the inside of the faraday cup. For proton energies above about 5 MeV, the (p,n) reaction cross section for tantalum (Ha 62) increases rapidly. These neutrons activate the Na and I nuclei in the NaI(Tℓ) crystal detectors, and the resulting activity can build up to prohibitively high backgrounds after two or three hours of measurements. The most damaging neutron reactions are $I^{127}(n,\gamma)I^{128}$ and $Na^{23}(n,\gamma)Na^{24}$ giving β^{-} activities with 25 minute and 15 hour half lives respectively. It is therefore essential to protect the crystal detectors with neutron moderating material. Adequate shielding from γ-ray backgrounds from the target chamber and from the quartz viewer must also be provided.

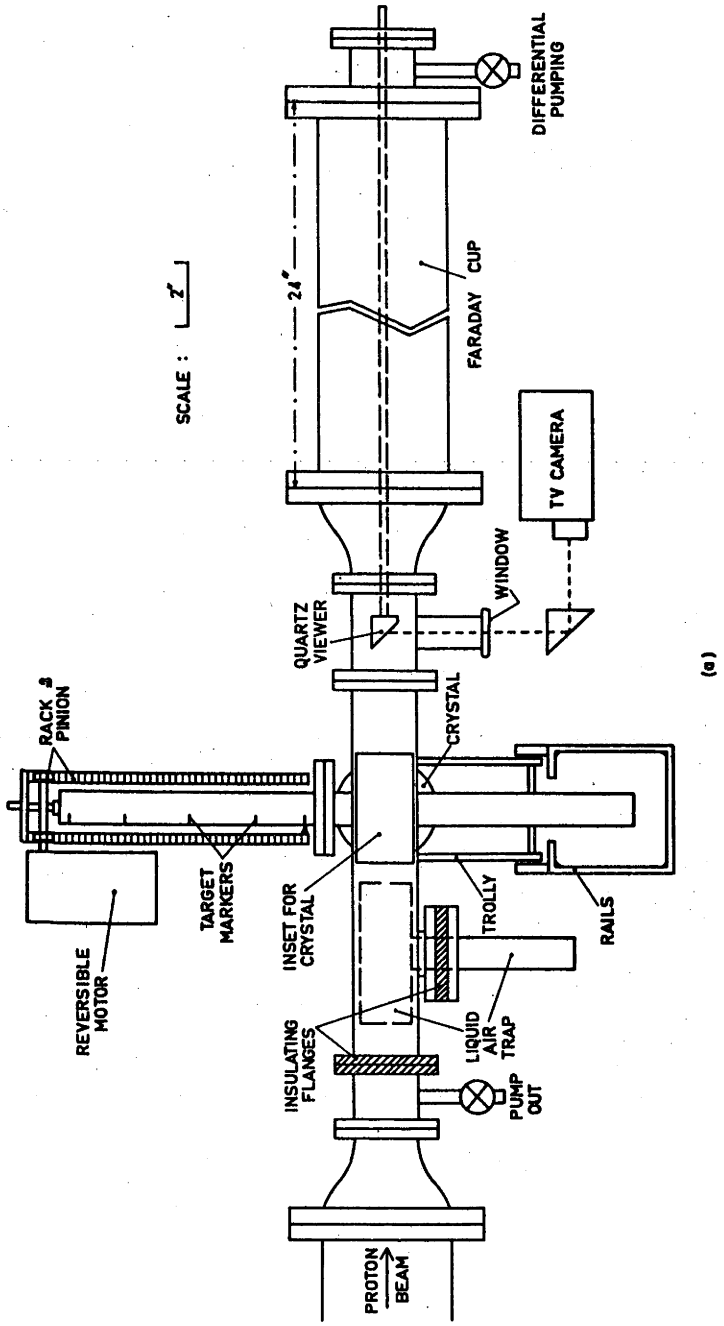

FIG. 1.1 Schematic representation of the activation apparatus.

1.3 Description of Apparatus

The target chamber and counter system is shown in fig. 1.1. The vacuum chamber was made from brass, and the portions visible to the beam were lined with 0.02 cm. tantalum sheet. The tantalum, which does not become positron active when irradiated with protons, prevented scattered protons from activating the Cu and Zn nuclei in the brass. Principal reactions which would lead to positron activity in the brass are $Cu^{63}(p,n)Zn^{63}$, 38 min β^+; $Zn^{64}(p,n)Ga^{64}$, 2.5 min β^+; $Zn^{67}(p,\gamma)Ga^{68}$ and $Zn^{68}(p,n)Ga^{68}$, 68 min β^+.

The targets were held in a vertical tantalum tube 0.05 cm. thick, 2 cm. in diameter and 23 cm. long. Five holes, each 1.6 cm. in diameter, were cut horizontally through the tube. Targets were mounted in four of these spaces, the fifth being left empty to allow the beam to pass through on to a quartz disk, allowing the position and focus of the beam to be observed. The position of the targets could be changed by means of a small reversible direction motor which operated a rack and pinion attached to the target holding assembly. The position of the targets could be accurately reproduced by lining up a small pointer mounted on the rack with a marker on the side of the target chamber. A small O-ring clamped around a 0.63 cm. diameter silver steel rod attached to the tantalum tube made an adequate sliding vacuum seal.

A slightly modified High Voltage Engineering Corporation quartz viewer and viewing port were placed in the beam line about 15 cm behind the target position. A fine tantalum mask defined an area 0.2 cm in diameter in the centre of the quartz, and this allowed the beam always to be focussed in the same position throughout the experiment. When the quartz was bombarded with protons of energy greater than about 5 MeV, several reactions led to positron active nuclei. The most serious reaction was $O^{16}(p,\alpha)N^{13}$ which has a 10 minute half-life β^+ activity. When the beam was positioned and focussed on the viewer, the quartz became highly activated and it was necessary to shield the counters from this source of background. The viewer was therefore mounted on the end of a 72 cm long 2 cm diameter silver steel rod which could be withdrawn along the beam axis to the end of the beam tube when not being used. Because of the large diameter of the steel rod, a double O-ring vacuum seal, and differential pumping was used. When the quartz was in the viewing position, it was accurately located by guide rails attached to the inside of the target chamber. A small tantalum cover was hinged on to the viewer in such a manner that it did not obstruct the beam or viewing window while the viewer was in use, but folded across the face of the quartz when the viewer was rotated through an angle of 90^o. This prevented the beam, which passed through thin self supporting targets

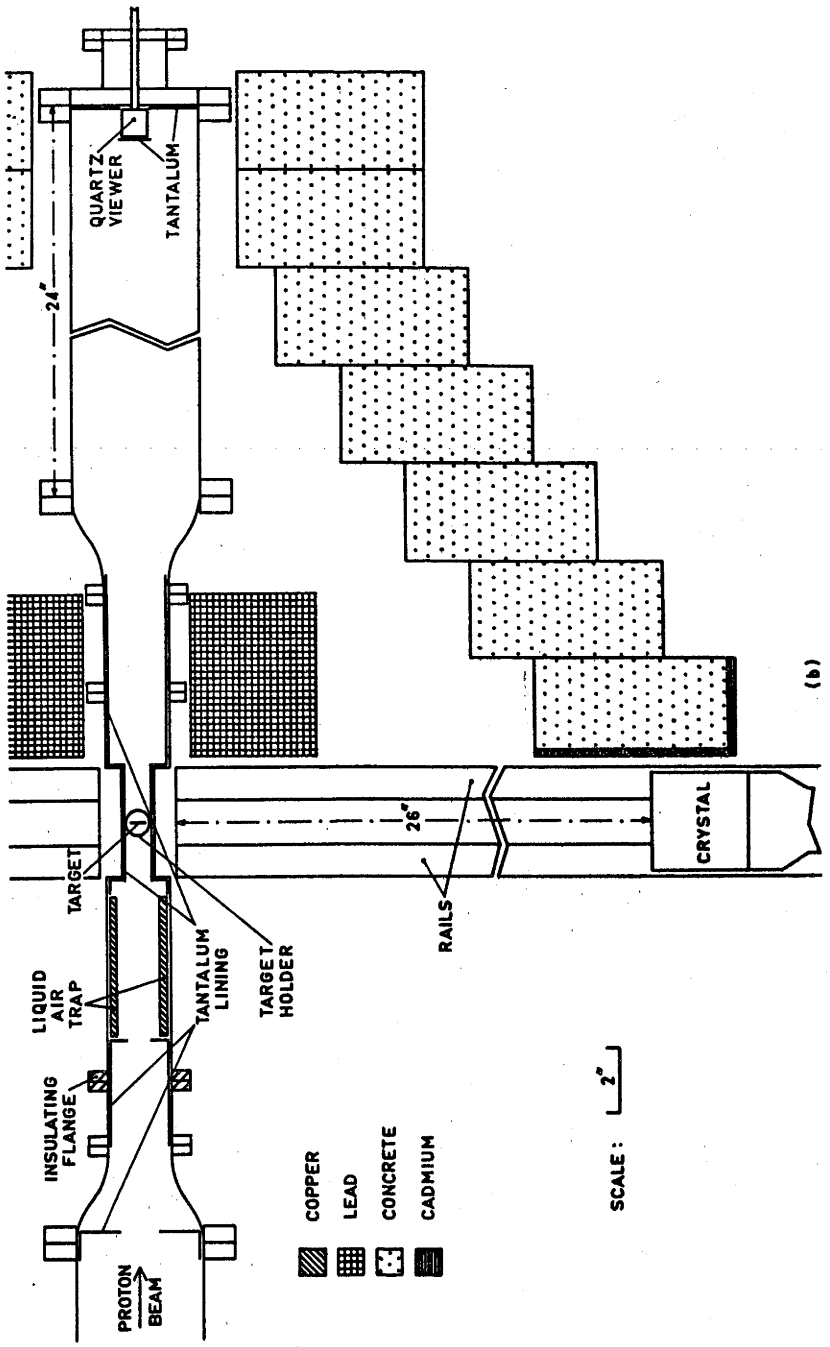

FIG. 1.2 A horizontal section of the activation apparatus showing the tantalum lining and distribution of shielding materials for the NaI(Tl) crystals.

onto the viewer, from activating the quartz.

In order to minimize build-up of contaminants on the targets, a simple liquid air trap was placed in front of the targets. The design was essentially the same as that used previously (Ba 62) in this laboratory, except that here, the beam passed axially down the cylindrical trap.

Two 7.6 cm x 7.6 cm NaI(Tℓ) crystals were used to detect the γ rays associated with the positron decay. Detection efficiency was increased by inserting two flat sections into the side of the target chamber which allowed the two crystals to be placed within 1.25 cm of the target. In order to reduce neutron activation of the Na and I nuclei in the crystals, the crystals were mounted on small pneumatically controlled trolleys which were moved away from the target during the irradiation period.

The crystals were shielded from neutrons originating in the Faraday cup by 100 cm of concrete lined with cadmium sheet. (See fig 1.2). Lead sheet 0.3 cm thick was wrapped around the crystals to reduce the intensity of low energy γ rays from the target and also from slow-neutron capture in the cadmium. When the crystals were in the counting position on either side of the target, they were protected from residual activity in the quartz viewer by 15 cm of lead.

The most energetic positrons encountered in the activation

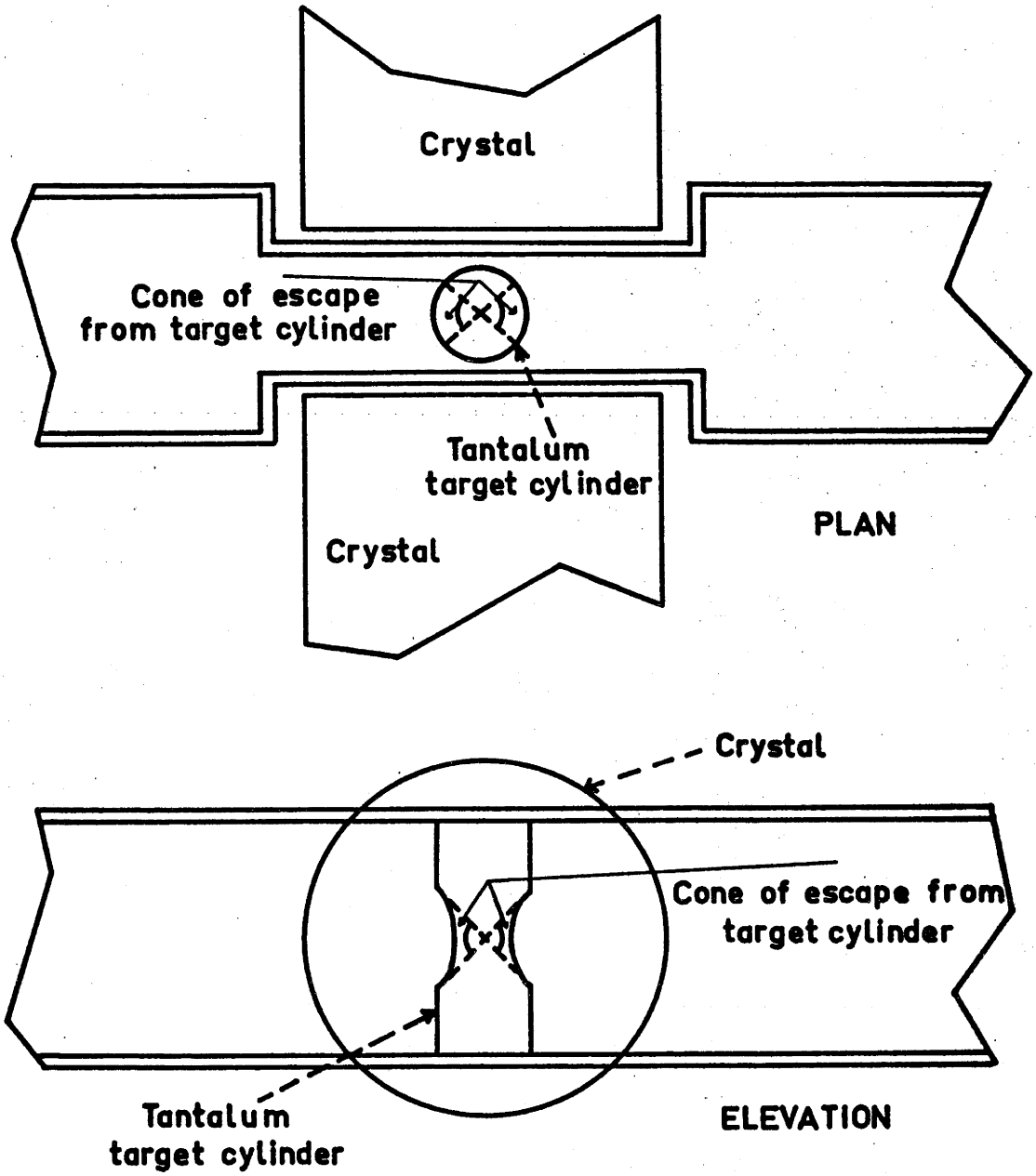

FIG 1.3 Sections of the activation apparatus showing the relative position of the two detectors and the tantalum target holding cylinder in which a large fraction of the positrons are made to annihilate.

experiments were from Ne^{19}, and these had an energy of 2.2 MeV. The tantalum cylinder which contained the targets was capable of stopping only 1.9 MeV positrons. Because of the energy distribution of the positrons, only about 8 percent have energies between 1.9 and 2.2 MeV. However, of all the positrons striking the tantalum cylinder, only about 3.5 percent, which strike the cylinder almost perpendicularly, will pass through it. These will still stop between the crystals (see fig 1.3), and the detection efficiency for them does not differ significantly from that for those stopped in the cylinder. Positrons from C^{10}, which were also measured, have a maximum energy of 2.1 MeV, and less than 1 percent of these which strike the cylinder pass through it. The beam entry and exit holes in the cylinder subtend a solid angle of $0.23 \times 4\pi$ steradians at the target. Most of the positrons emitted into this solid angle travel up or down the beam tube and are lost to the counting region. However, some strike the side of the chamber between the counters (see fig 1.3). Positron escape vertically, up or down the target cylinder, was prevented by tantalum sheets 0.06 cm thick. The detection efficiency was measured using a calibrated Na^{22} source which gives positrons with $E_{max} = 0.5$ MeV. The source was mounted on a thin mylar foil and placed on a target holder of the type used in the experiment. This was then mounted in the target chamber under the same physical conditions as the targets. The same fraction

of positrons would therefore be lost from the counting region during the calibration as would be lost during an actual experiment.

1.4 Associated Electronics

Pulses from the two photomultipliers were amplified by charge sensitive preamplifiers feeding double delay line linear amplifiers. (Franklin Electronics Inc. model 358). Double delay line amplifiers are particularly suitable because of their ability to handle heavy overload pulses without introducing excessive dead time, and their ability to handle high count rates without excessive base line shifts. Also, time jitter can be greatly reduced by using discriminators and single channel analysers which trigger off the "cross-over" point of these pulses. Such reduced time jitter allows smaller resolving times to be used in the coincidence circuits and therefore reduces the accidental coincidence rate.

Pulses from the photopeaks of the coincident γ-rays to be measured were selected by means of single channel analysers and fed into a coincidence unit. The position of the analyser windows was adjusted before each day's run and the gain of the system was checked periodically during the run. Initially it was found that the gains of the photomultipliers were affected by the very high count rates experienced during the target irradiation; changes of up to 25 percent occurred, taking up to 30 minutes to recover. This effect was eliminated by

applying a reverse bias of -90 volts between the photocathodes and focus grids of the photomultipliers (Fa 58) to disable them during irradiation. Any subsequent slow gain drifts during a run were corrected by adjusting the high voltage supply of each photomultiplier. Fine control was obtained by means of a ten turn helipot controlling 15 percent of the high voltage.

Throughout the $B^{10}(p,n)C^{10}$ experiment, described in chapter 3, a Dynatron Radio Ltd., type 1036C coincidence unit, having a resolving time $2\tau = 0.2\ \mu$sec was used. Accidental coincidences were recorded with a second coincidence unit having a 1 μsec delay in one channel. For the $F^{19}(p,n)Ne^{19}$ experiment, described in chapter 2, a Cosmic Radiation Lab. Inc., model 801 multiple fast/slow coincidence unit became available. This unit contained low level discriminators for use with the fast channels and single channel analysers for amplitude selection for the slow channels. The resolving time of the slow unit was $2\tau = 2\ \mu$sec and that of the fast unit was set at $2\tau = 0.050\ \mu$sec. The resolving time of the fast unit was capable of variation from O to 0.180 μsec. The lowest value which could be used without losing true coincidences however, was limited to 0.050 μsec by the time jitter of the "cross-over" points of the pulses from the amplifiers. The increased time resolution obtained with this unit eliminated the need for a second coincidence unit to record accidental

coincidences. The beam current was measured by an Elcor model A 309 A current integrator which was accurate to $\pm$ 1 percent.

CHAPTER 2

THE $F^{19}(p,n)Ne^{19}$ REACTION BETWEEN 5 AND 11 MeV

2.1 Introduction

The $F^{19}(p,n)Ne^{19}$ reaction is particularly suitable for study using the activation apparatus described in chapter 1. The product nucleus, Ne^{19}, decays by positron emission with a half-life of approximately 17 seconds, and there are no competing reactions which result in positron activity. The reaction is extremely difficult to study (above about 5 MeV proton energy) by any other technique because of the difficulty of obtaining a fluorine compound for the target, which does not also produce large numbers of neutrons by (p,n) reactions. The activation technique can distinguish these reactions by the differing residual activities.

The excitation region in Ne^{20} above about 13 MeV has been investigated mainly through F^{19} + p reactions. At this excitation energy, the levels of Ne^{20} are very closely spaced, and only experiments carried out with good energy resolution have been able to see the fine structure. Several groups of workers (Bl 51), (Wi 52), (Ma 55) have studied the (p,n) reaction up to about 6 MeV proton energy while the (p,γ) reaction has been studied (Ge 59), (Br 60) over the proton energy range 0 to 11 MeV. States in Ne^{20} have also been studied through the (p,α) reaction in the proton energy range up to 12 MeV.

TABLE 2.1

RESONANCES IN THE COMPOUND SYSTEM Ne^{20}

PROTON ENERGIES (MEV)

$F^{19}(p,n)$ *	$F^{19}(p,n)$ (Wi 52)	$F^{19}(p,n)$ (Bl 51)	$F^{19}(p,n)$ (Ma 55)	$F^{19}(p,\gamma)$ (Br 60)	$F^{19}(p,\alpha\gamma)$ (Wi 52)	$F^{19}(p,\gamma)$ (Ge 59)	$F^{19}(p,\alpha_0)$ (Wa 63)	$F^{19}(p,\alpha_0)$ (Ra 58)	$F^{19}(p,\alpha_\pi)$ (Ra 58)	$F^{19}(p,\alpha_0)$ (Br 60)	$O^{16}(\alpha,\alpha)$ *** (Hu 62)	$Ex(Ne^{20})$ MeV
10.2							10.22					
9.8							9.82					22.1
							9.60					
9.5							9.50					
				9.30			9.32					
9.2												
9.08												
8.82							8.88			8.80		
8.70							8.70					21.1
8.37												
8.28				8.30			8.30			8.32		
8.15												
8.02												
							7.80			7.82		
7.74										7.70		
							(7.60)					
7.52				7.55			7.50			7.50		20.0
7.41						(7.65)**					7.37	
7.27										7.27		
7.14												
							7.03					
											6.91	
										6.87		
6.81												
											6.66	
6.53		6.5		6.50		(6.65)**	6.45			6.50		19.0
6.35							6.35					
							(6.25)			6.25		
6.15		6.1									6.16	
6.03							6.00				5.96	
							(5.88)					
5.73		5.8	5.75				5.80			5.66	5.72	
											5.53	
5.37		5.4	5.4				5.38			5.37	5.38	18.0
5.26			5.3									
	5.20			5.20	5.20	(5.5)**			5.17	5.20	5.19	
5.11	5.07		5.1		5.07							
5.03							5.05					
4.96	4.99		5.0		4.99			4.97	5.00	4.95	4.95	
	(4.85)						4.85	4.90	4.90			
	4.78	4.8	4.8		4.78							
	4.71				4.71			4.68	4.71	4.70	4.71	
	4.62		4.64				4.65					
	4.57				4.57							
	4.49		4.49		4.49		4.50					
	4.46							4.46		4.47		
								4.36	4.37	4.35		17.0
	4.29				4.29		4.32				4.26	
4.02	4.01	4.1	4.05	4.05	4.01	4.1	4.02	4.01	4.01	4.02	4.05	

* The present experiment

** It has been suggested (Br 60) that these figures are approximately 300 keV too large.

*** Resonances seen in $O^{16}(\alpha,\alpha)$ expressed in terms of the proton energy giving the same excitation to Ne^{20}.

(Br 60), (Ra 58), (Wi 52), (Wa 63). At the higher excitation energies, it is difficult to relate the energy levels reported by different reactions. However, a complete summary of the reported levels, and their possible relationship is given in table 2.1.

Blaser et al. (Bl 51) have studied the (p,n) reaction using an activation technique. A fixed energy cyclotron provided 6.84 MeV protons, and aluminium absorbers were used to vary the incident beam energy. The resulting energy resolution was poor, and only the gross structure was seen. Willard et al. (Wi 52) studied the (p,n) and (p,$\alpha\gamma$) reactions, using protons from a 6 MV Van de Graaff accelerator. Neutrons were detected by a long counter, and the γ rays by a NaI(Tℓ) crystal. The energy resolution obtained was good, and many sharp resonances were observed in both reactions. The (p,n) reaction was also studied, using a long counter, by Marion et al. (Ma 55). Protons from a 6 MV Van de Graaff accelerator were used. However a relatively thick target was used and only moderate energy resolution was obtained.

Gemmell et al. (Ge 59) carried out a study of the γ rays from the F^{19}(p,γ) reaction using 7.7 MeV protons from a cyclotron. The beam energy was modified by absorber foils. Their excitation function is notable for its lack of structure, but this is probably due in part to the poor energy resolution. The same reaction was studied by

Broude and Gove (Br 60), up to proton energies of 11 MeV using a tandem Van de Graaff accelerator. Although their energy resolution (100 keV) was much better than that obtained by Gemmell et al., their excitation function showed the same striking lack of structure. These authors also studied the $F^{19}(p,\alpha_0)$ reaction over the same energy range, with somewhat better resolution. This excitation function showed considerably more structure than did that from the γ-ray work.

Using protons from a 5 MV Van de Graaff accelerator, Ranken et al. (Ra 58) obtained excitation functions with good energy resolution for the (p,α_π), (p,α_0), $(p,\alpha\gamma)$ and $(p,p'\gamma)$ reactions. Considerable structure was evident in all the excitation functions, and good agreement was obtained with the results of other workers. The (p,α_0) reaction data has been extended up to a proton energy of 12 MeV with good energy resolution by Warsh et al. (Wa 63). The proton beam was obtained from a tandem Van de Graaff accelerator. Here again considerable structure was reported. The energy levels of Ne^{20} have been investigated between the excitation energies of 16 and 20 MeV by Hunt et al. (Hu 62) by means of the $O^{16}(\alpha,\alpha)$ reaction. Quite good agreement was obtained with levels reported by other workers in the lower excitation energy region.

Close agreement is found for the levels in Ne^{20} up to about

18 MeV excitation as seen by various different reactions. However, above this energy considerable differences exist in the amount of structure seen by different reactions. It was therefore apparent that an extension of the earlier (p,n) work into the proton energy region up to 11 MeV, with good energy resolution, would provide useful information on the level structure, and possibly the reaction mechanism.

2.2 Experimental Apparatus

The activation apparatus and the triple (fast-slow) coincidence unit used in this experiment have been described in chapter 1.

The fluorine target was obtained by vacuum evaporation of MnF_2 onto a thin gold foil. The compound MnF_2 was chosen for the target for two reasons. Because of its low melting point of 856°C, it is very easily evaporated under vacuum from a tantalum boat. Also, manganese is a single isotope which does not become positron active when irradiated with protons. Only the $Mn^{55}(p,n)Fe^{55}$ reaction leads to a radioactive nucleus. However the X rays resulting from this 2.9 year K capture activity do not affect the present experiment.

The target backing was chosen to be as thin as possible in order to reduce the number of neutrons produced by it. Shielding cannot easily be provided to prevent these neutrons from activating the NaI crystal detectors. The thickness of the foil however, was

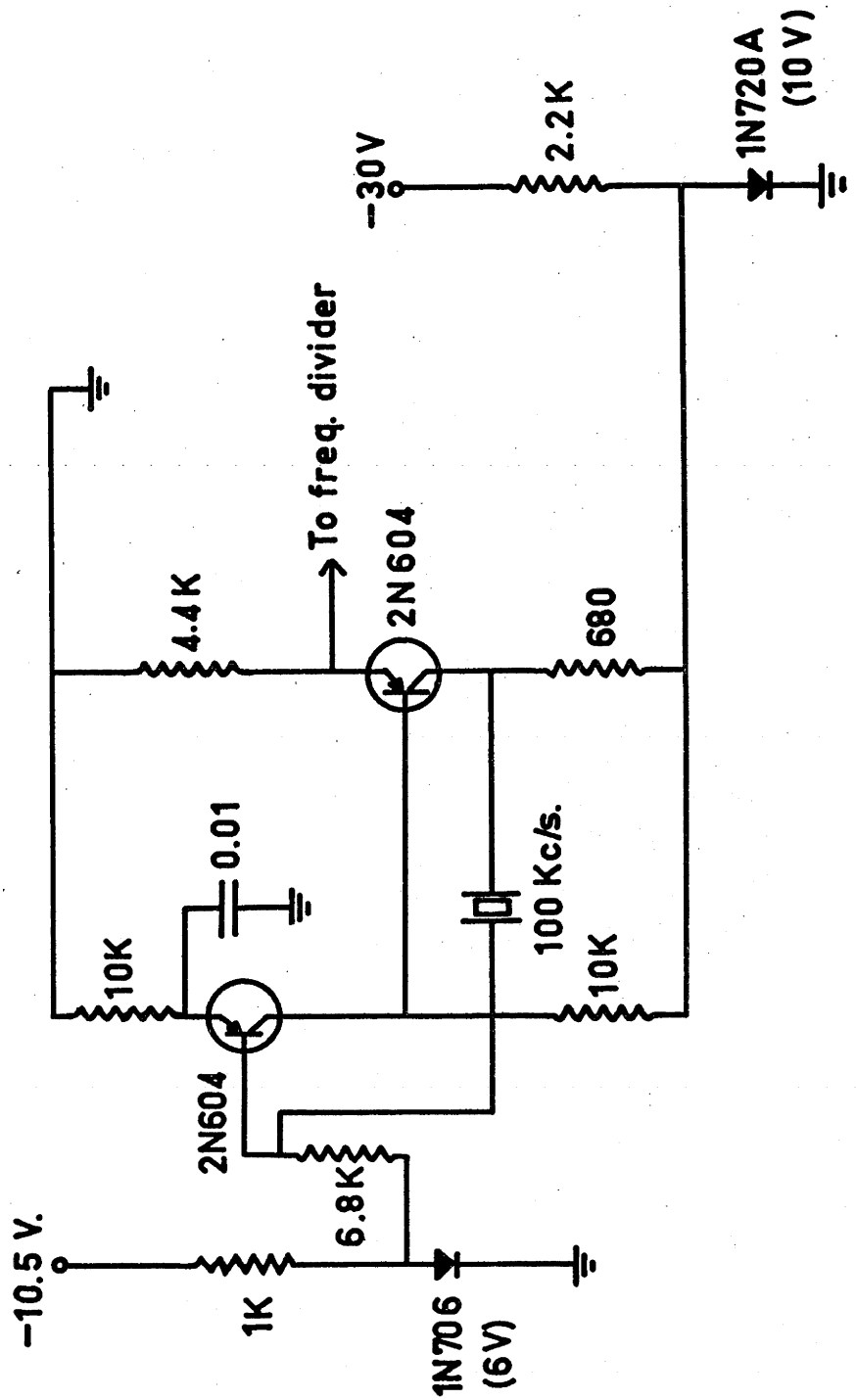

FIG 2.1 Circuit diagram for a 100 Kc/s crystal controlled oscillator. All resistances are in ohms and all capacitances in micro-farads.

thick enough to prevent the Ne^{19} nuclei recoiling out of the target and being lost from the counting region. Gold foils 3 mgm/cm^2 thick were found to be suitable for this purpose.

2.3 The Half-Life of Ne^{19}

The half-life of Ne^{19} was not well known, and many conflicting values, ranging from 17.4 ± 0.2 sec. up to 20.3 ± 0.5 sec., had been reported (Aj 59). For this reason, and because an accurate value of the decay constant was required for an absolute cross section measurement (see section 2.5), it was decided to measure the Ne^{19} decay half-life.

A 400 channel pulse height analyser, operated in its time analyser (multi-channel scaler) mode, was used to follow the decay of the activity. Part of the analyser behaves as a simple scaler which records the incoming pulses. On an external signal from a pulse generator, the contents of the scaler are recorded in an appropriate channel of the pulse height analyser, the scaler is cleared, and the counting is begun again. This cycle is repeated, stepping from channel to channel for as long as is desired. The decay half-life is of the order of 17 seconds. Hence a counting interval of 2 seconds was chosen. This allowed reasonable statistical accuracy to be built up for each point. It also gave a reasonable number of points on the first two or three half-lives of the curve, from which an accurate

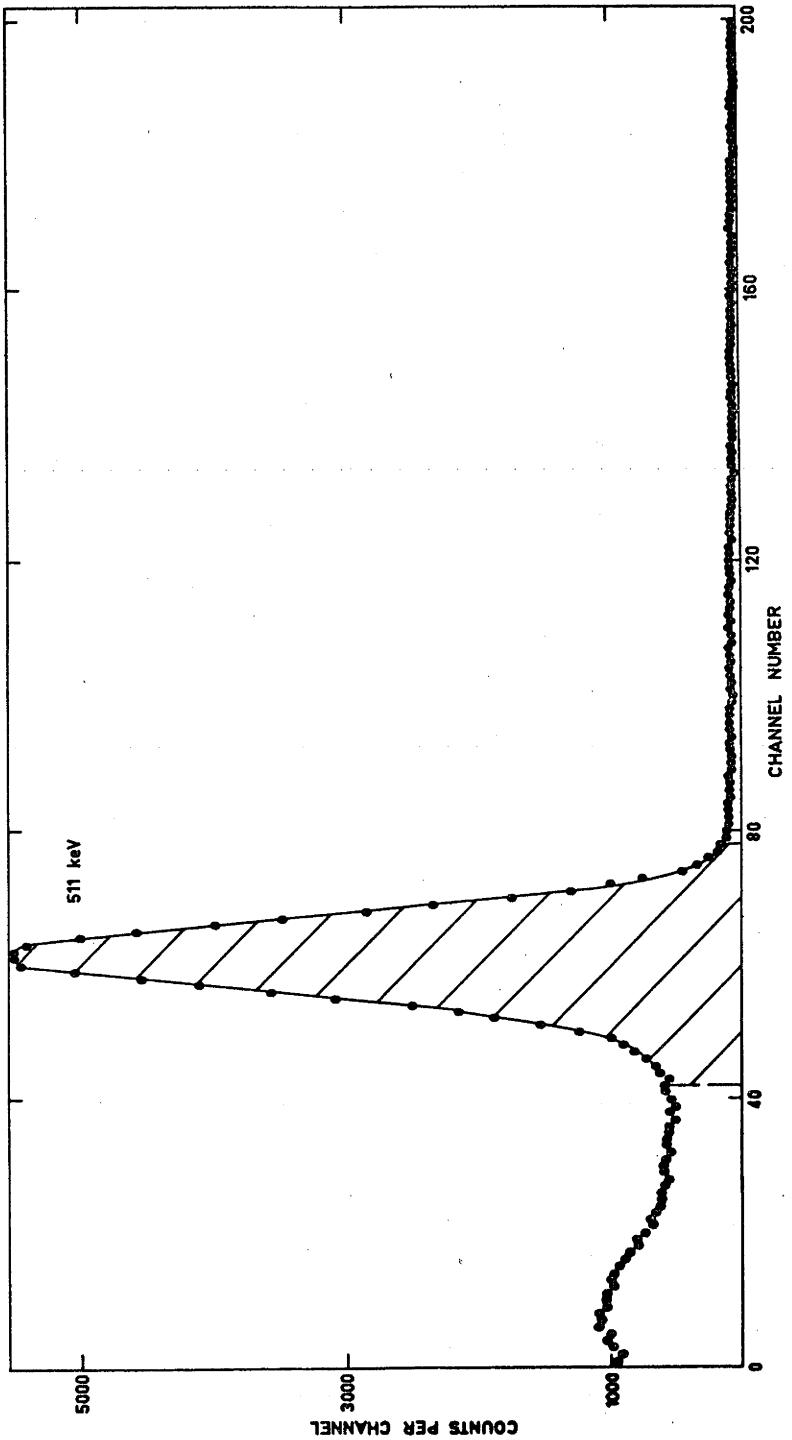

FIG. 2.2 A gamma ray spectrum taken with one of the 7.6 cm x 7.6 cm spectrometers after bombardment with 4.8 MeV protons. The hatched area indicates the energy interval selected for the coincidence measurements.

estimate of the half life could be made. The channel advance pulses were controlled by a scaled down 100 Kc/sec. crystal oscillator. The simple oscillator circuit used (see fig 2.1), was measured to have a stability better than one part in 10^5. The introduction, in the last four or five years, of multi-channel analysers which can be operated in the time analyser mode has greatly increased the ease with which half-life measurements can be made. Using these instruments, as many as four or five hundred points can be measured on one decay curve. This allows the decay to be followed over very many half-lives and leads to a more accurate estimate of background contributions. Fortunately, the introduction of computing facilities to most laboratories has greatly lightened the burden of analysing this increased volume of data.

The F^{19} target was bombarded for 60 sec. with 0.1μA of 4.8 MeV protons, and the decay of the induced activity followed for 290 secs., that is about 15 half-lives. The Ne^{19} decay goes 100 percent to the ground state of F^{19} (Aj 59), and therefore the 0.511 MeV annihilation quanta are the only characteristic γ rays. Pulses from each γ-ray detector were fed into single channel analysers with the windows set over the γ-ray photopeaks (see fig 2.2). By following the decay of counts in the window, single component decay curves on constant, low backgrounds were obtained. The statistical accuracy

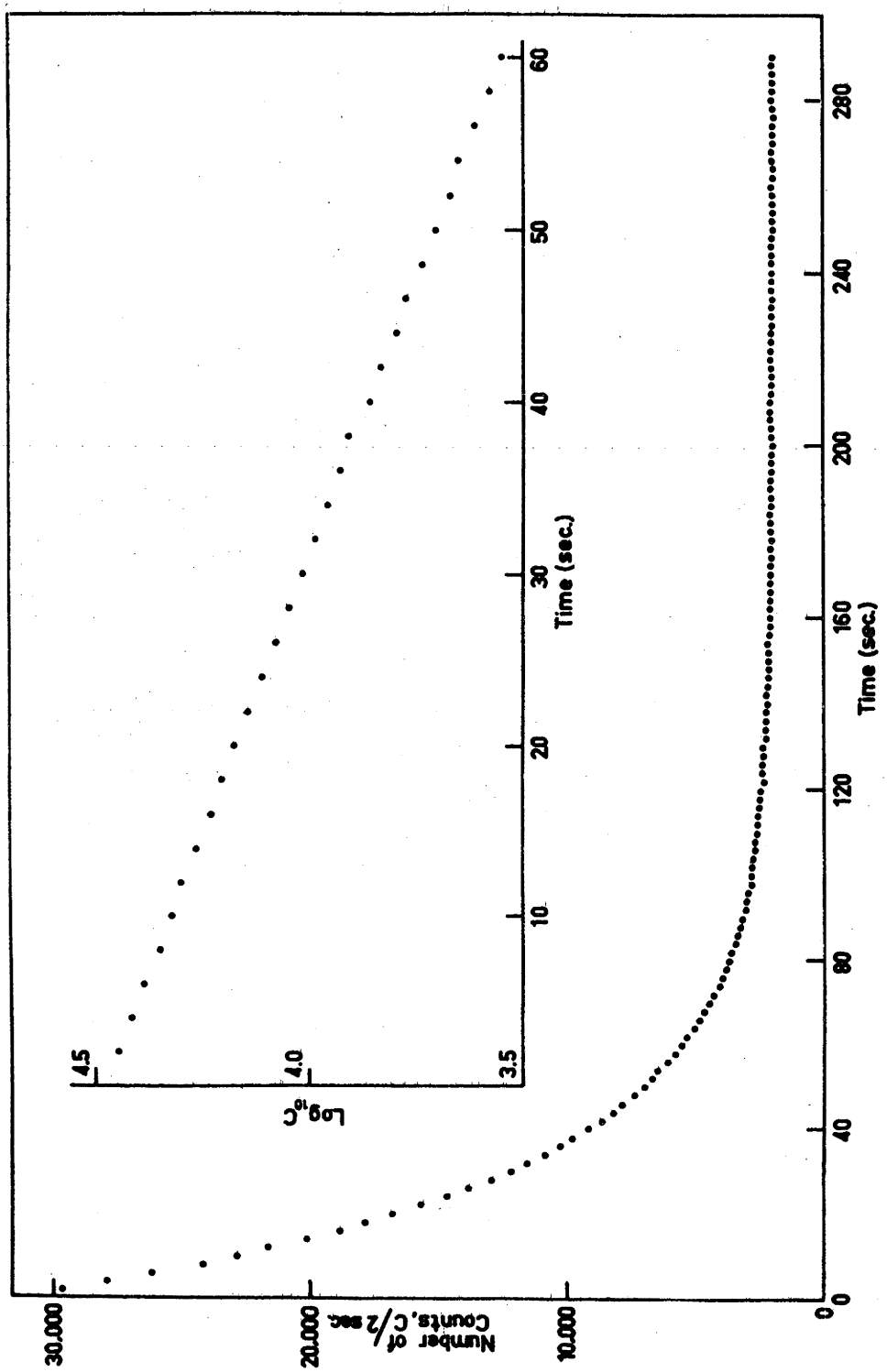

FIG. 2.3 A typical Ne^{19} decay curve, together with a logarithmic plot of the data after background subtraction. This curve consists of the sum of a number of runs, in each of which counting losses and gain-change effects were negligible.

of the decay curves was increased by adding a large number of runs, in each of which counting losses and gain-change effects were negligible. As a check that other activities were not affecting the results, several determinations were made by following the decay of the count rate of coincidences between the annihilation quanta. This does not exclude from the measurement, other positron activities possibly present on the target. No attempt was made to check for other activities. However, it was apparent from the linearity of the logarithmic plots (see fig 2.3) that the effect of any such impurities, except those giving positron activities with a half-life very close to that of Ne^{19}, was negligible.

The Ne^{19} half-life was determined for each measurement, by a weighted least-squares fit of a straight line to the logarithm of the nett counting rate (i.e., total counts minus the constant background) plotted against time. The reciprocal of the standard deviation was used as a weighting factor for each point. If the actual measured number is N, then the standard deviation is $\sigma(N) = N^{\frac{1}{2}}$. The numbers plotted however, are of the form $y = \log N$. Differentiation gives

$$dy = \frac{dN}{N}$$

Therefore if the assumption is made that the standard deviation of the two numbers follows the same form,

$$\sigma(y) = \frac{\sigma(N)}{N}$$

Substitution for $\sigma(N)$ gives

$$\sigma(y) = N^{-\frac{1}{2}}$$

and therefore the appropriate weighting factor for log N is

$$\frac{1}{\sigma(y)} = N^{\frac{1}{2}}$$

A total of five independent measurements were made and analysed at different times. The results from these measurements showed that the equipment was functioning consistently. The results for the Ne^{19} half-life are 17.40, 17.48, 17.29, 17.32 and 17.64 sec. (all $\pm$ 0.13 sec.) From this data, the half-life and its standard deviation was determined as

$$\tau(Ne^{19}) = 17.43 \pm 0.06 \text{ sec.}$$

2.4 Absolute Cross Section

2.4.2 Cross Section Formula

In this section, the factors involved in the determination of an absolute cross section using an activation technique are outlined.

Assuming a constant current arriving at the target, the number of reactions per second induced in the target is

$$R\sigma\frac{x}{M} \text{ / sec} \qquad (2.1)$$

where R is the number of protons/sec. striking the target.

σ is the reaction cross section in cm^2.

x is the target thickness in gm/cm^2,

and M is the mass of a F^{19} nucleus in gms.

It follows therefore, that the number of radioactive Ne^{19} nuclei present in the target after t_1 seconds bombardment is

$$N = \frac{R\sigma x}{M\lambda} (1 - e^{-\lambda t_1}) \qquad (2.2)$$

where λ is the Ne^{19} decay constant.

In order to determine the cross section σ, a relation must be found between the number of events recorded, and the number of radioactive nuclei produced by the bombardment. The total efficiency ε of the detector for 0.511 MeV γ rays will be defined as the probability that an 0.511 MeV annihilation quantum emitted into 4π steradians, will be detected by the crystal. It is convenient to define an intrinsic efficiency ε' by the relation $\varepsilon = (\Omega/4\pi)\ \varepsilon'$, where ε' is now the probability that an 0.511 MeV annihilation quantum will be detected, provided it enters the crystal which subtends a solid angle of Ω at the target. For every positron decay, two 0.511 MeV quanta are produced. Hence the probability that one will be counted in one of the detectors is 2ε. For positrons decaying at rest, there is a 180^o correlation between the annihilation quanta. Also the two γ-ray counters

are placed symmetrically about the target. Hence if one γ ray is detected in one of the crystals, the other γ ray must enter the second crystal. The probability of this second γ ray being detected is ε'. Therefore the probability of detecting a coincident event is $2\,\varepsilon\,\varepsilon'$. In the present experiment, coincidences were measured between pulses in the γ ray photopeaks. Hence the coincidence efficiency must be modified by the ratio P, of the photopeak counts to the total counts. The probability of observing a positron decay as a coincidence between the annihilation quanta is therefore

$$(2\,\varepsilon P_1\,\varepsilon' P_2) \tag{2.3}$$

where the suffices refer to the different crystals.

We require to know the fraction of the active nuclei produced during the bombardment from $t = 0$ to $t = t_1$ which decay during the counting interval from time $t = t_2$ to $t = t_3$ seconds. The fraction of the active nuclei left at time $t = t_2$ seconds is $e^{-(t_2 - t_1)\lambda}$ and the fraction left at time $t = t_3$ seconds is $e^{-(t_3 - t_1)\lambda}$. Hence the fraction which have decayed during the time interval from t_2 to t_3 seconds is

$$\left[e^{-(t_2 - t_1)\lambda} - e^{-(t_3 - t_1)\lambda} \right] \tag{2.4}$$

Combining equations 2.4 and 2.3 gives the fraction of the radioactive nuclei present immediately after bombardment, which are detected by the counter system. This is

$$\left[2\,\varepsilon P_1 \varepsilon' P_2\right]\left[e^{-(t_2 - t_1)\lambda} - e^{-(t_3 - t_1)\lambda}\right] \qquad (2.5)$$

Hence the actual number of decays measured is found from equations 2.5 and 2.2 to be

$$Y = \frac{R\sigma x}{M\lambda}\left[1 - e^{-t_1\lambda}\right]\left[2\,\varepsilon P_1 \varepsilon' P_2\right]\left[e^{-(t_2 - t_1)\lambda} - e^{-(t_3 - t_1)\lambda}\right] \qquad (2.6)$$

The number of protons striking the target per second is found from the integrated current I, (assuming a constant current) to be

$$R = \frac{I}{t_1 \cdot 1.60 \cdot 10^{-19}} \quad \text{protons / sec} \qquad (2.7)$$

where t_1 is the time of the bombardment,

I is measured in coulombs,

and 1.60×10^{-19} coulombs is the charge on a proton.

Substituting equation 2.7 into 2.6 and re-arranging gives,

$$\sigma = \frac{Y \lambda M\, t_1 \cdot 1.60 \cdot 10^{-19}}{I x\left[2\,\varepsilon P_1 \varepsilon' P_2\right]\left[1 - e^{-t_1\lambda}\right]\left[e^{-(t_2 - t_1)\lambda} - e^{-(t_3 - t_1)\lambda}\right]} \text{ cm} \qquad (2.8)$$

2.5.1 Cross Section Determination

The target thickness was measured using protons from the Canberra 1.2 MV Cockcroft-Walton accelerator. The evaporation of the MnF_2 target was carried out with a piece of thick aluminium foil placed alongside the gold backing. It was found experimentally that the thickness of the target layer was uniform. The displacement of

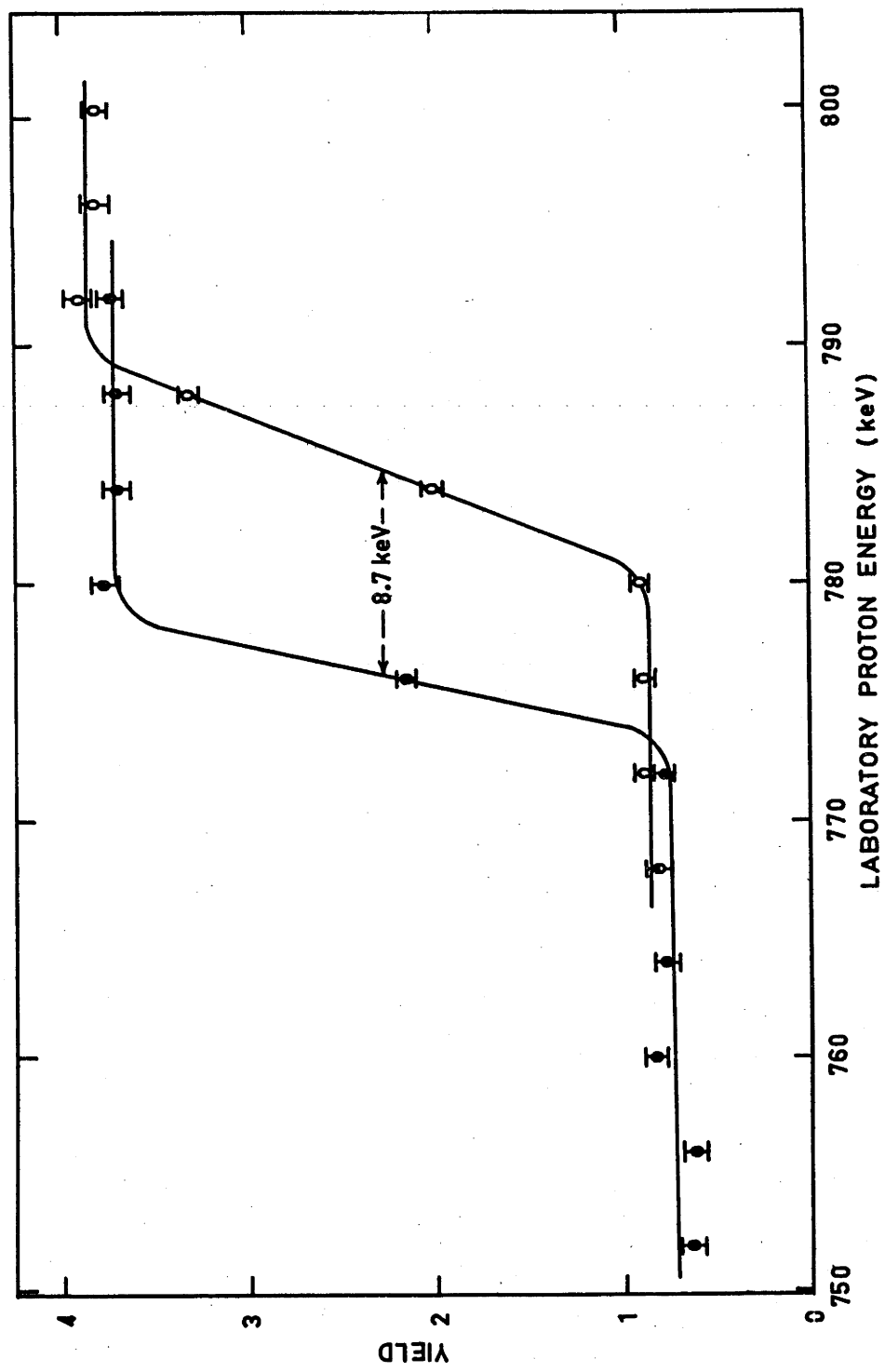

FIG. 2.4 The measurement of the MnF_2 target thickness. The closed circles represent the yield of 12.3 MeV γ rays from the thick Al target around the 773 keV $Al^{27}(p,\gamma)Si^{28}$ resonance. The open circles show the apparent energy shift of this resonance when the MnF_2 coated side of the Al target was presented to the proton beam.

the narrow 773 keV $Al^{27}(p,\gamma)$ resonance was therefore used as a measure of the actual target thickness. Because of the possibility of undesirable contamination by oil from the diffusion pumps, the gold backed target itself was not investigated directly.

An excitation function over the 773 keV $Al^{27}(p,\gamma)Si^{28}$ resonance was measured using a 13 cm diameter by 10 cm thick NaI(Tℓ) crystal to detect the 12.3 MeV γ rays proceeding to the ground state of Si^{28}. The apparent shift in the resonance when the MnF_2 coated side of the aluminium foil was presented to the beam (see fig 2.4) was then a measure of the energy loss of 773 keV protons in the layer. The energy loss was found to be 8.7 ± 0.6 keV, and using the compilations of proton stopping cross sections (Wh 58) (De 63), the content of fluorine was calculated as $19.5 \pm 2.5\ \mu gm/cm^2$.

The detection efficiency of the positron counting system ($2\varepsilon P_1\ \varepsilon' P_2$), was determined directly using a calibrated Na^{22} source.* The decay of Na^{22} proceeds partly (89.7 percent) by positron decay to the first excited state of Ne^{22}, and partly (10.2 percent) by electron capture to the same level (En 62). (See fig 2.5). The decay of this level gives a 1.28 MeV γ ray in coincidence with the annihilation quanta.

---

* This source was calibrated to an accuracy of $\pm$ 2.5 percent, using a 4π β-γ coincidence counter, by the Australian Atomic Energy Commission Research Establishment, Lucas Heights.

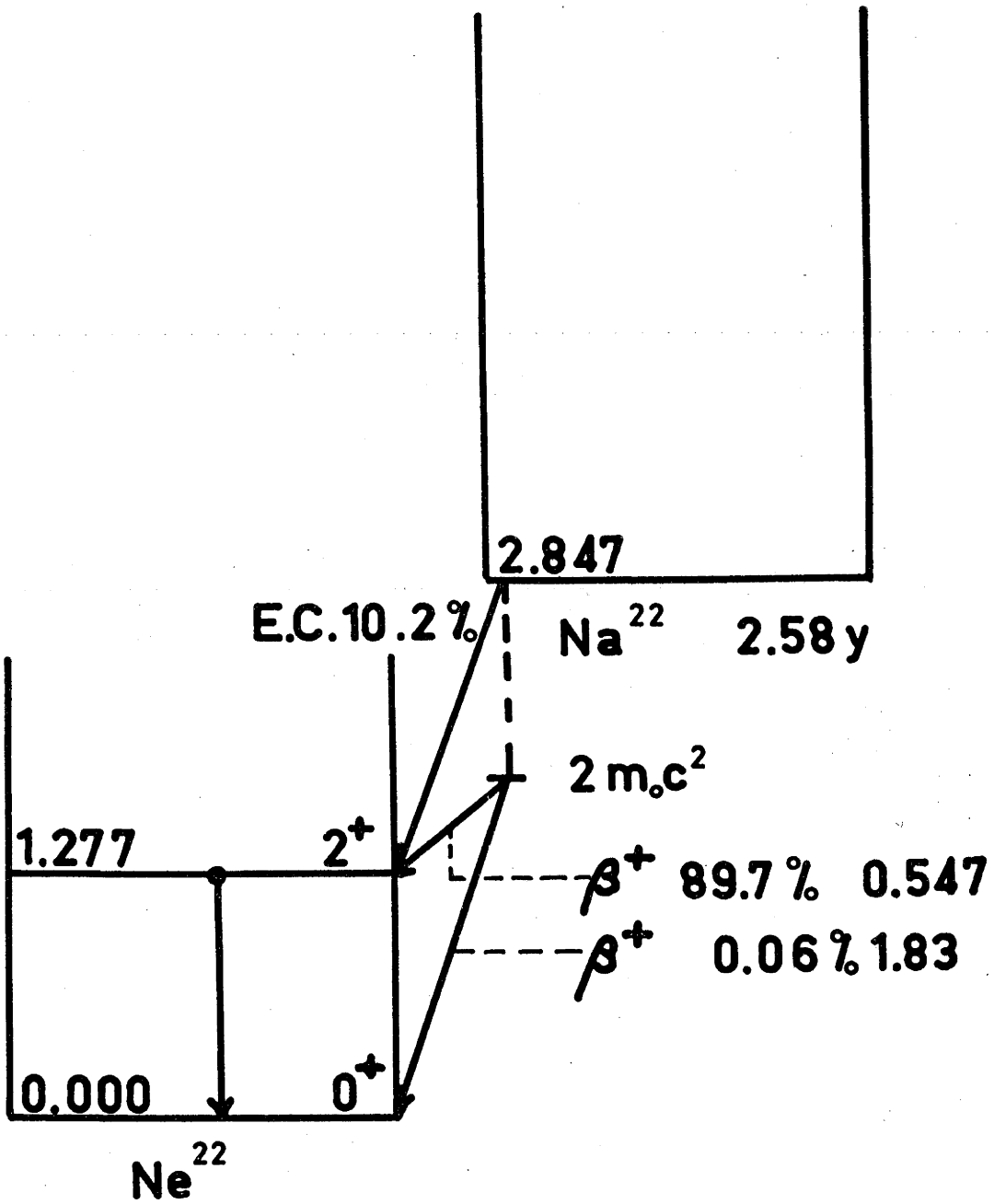

FIG. 2.5 The decay scheme of Na^{22}.

The coincidence efficiency measured with the Na^{22} source was corrected for the contribution from coincidences between an 0.511 MeV γ ray in one crystal and the Compton tail of a 1.28 MeV γ ray in the other. A spectrum of the Na^{22} γ rays obtained with the same geometry was used to estimate the fraction of the 1.28 MeV γ rays whose pulse heights fell within the window over the 0.511 MeV photopeak. Approximately 10 percent of the measured coincidences were between 0.511 and 1.28 MeV γ rays. The change in coincidence efficiency caused by the second order effect of 0.511 and 1.28 MeV pulses being recorded in the one crystal and thus removing a pulse from the 0.511 MeV photopeak, was neglected.

In deriving the cross section formula, it was assumed that the beam current was constant during the bombardment. The effect of various oscillations and changes in the beam current during bombardment were calculated (see appendix A) and it was found that a maximum error of 1 percent was introduced during normal running conditions. The integrated current was accurate to $\pm$ 1 percent and the timing of the bombardment and counting periods were accurate to $\pm$ 0.5 percent. The accuracy of the measured "equivalent constant current" was therefore $\pm$ 1.5 percent. The decay constant λ was measured and is accurate to $\pm$ 0.4 percent, and the statistical accuracies of the measured yields were better than $\pm$ 1 percent. The

distribution of errors in the cross section measurement is shown in table 2.2.

TABLE 2.2

Distribution of errors in the absolute cross section measurement

SOURCE OF ERROR	PERCENTAGE
Target thickness	$\pm$ 15%
Decay constant	$\pm$ 0.4%
Equivalent current	$\pm$ 1.5%
Counting statistics	$\pm$ 1%
Detection efficiency ($2\varepsilon P_1 \varepsilon' P_2$)	$\pm$ 2.7%
Total error	$\pm$ 16%

2.5 The $F^{19}(p,n)Ne^{19}$ Excitation Function: Experimental Procedure and Results

At time t = 0 sec., the beam was switched onto the target. Bombardment was continued for slightly more than three half-lives by which time 90 percent of the equilibrium activity was established. The effect on the number of active nuclei produced, of small errors in the bombardment time was therefore negligible. During the beam-on period, the photomultipliers were switched off by applying a

reverse bias of -90 volts between their focus grids and photocathodes. At time t = 60 secs., a switch started a timer, and also operated a fast beam stop which interrupted the beam 6 metres short of the target. At the same time, the crystals, which took 1.5 secs to move into position, began to move up to the counting position. At time t = 62 secs., the timer started the counting by removing the bias from the photomultipliers. Because of the exponential character of the decay, small errors in the time between switching off the beam and beginning the count are very important. This interval was therefore accurately controlled by the electronic timer. All other intervals were controlled manually using a stopwatch. Time coincident pulses in the two detectors were counted for 60 secs., and the photomultipliers were turned off again at time t = 122 secs. Time coincident pulses were again counted for 60 secs. between times t = 180 and t = 240 secs. Counts in the second interval were then subtracted from those in the first, a correction being made for the 0.75 percent of the Ne^{19} decay events occurring in the second interval.

By keeping the counting rate during the first 10 secs. below a predetermined figure, counting losses were always less than 1 percent. Typical values of the beam currents used were between 0.2 and 0.3 μA. During a run over a selected proton energy range, three determinations of the activity were made and averaged at

20 keV intervals. All sections of the excitation function were measured at least twice, and some energy intervals as many as four times. Relative errors on the final curve, arising from counting statistics and from the assumption of a constant current were about $\pm$ 2 percent.

The activation technique, as applied here, measures the cross section for all neutron groups from the $F^{19}(p,n)Ne^{19}$ reaction which lead to positron decay of Ne^{19}. Neutron groups to excited states in Ne^{19} above the $O^{15} + \alpha$ threshold (3.52 MeV) probably decay preferentially by particle emission and therefore are not expected to contribute significantly to the Ne^{19} activity. By comparison with the levels in F^{19}, a large number of levels are likely to be present near the $O^{15} + \alpha$ threshold. Hence for proton energies at which excitation of unbound levels in Ne^{19} is possible ($E_p \geqslant 7.94$ MeV), the measured cross section contains contributions only from those neutron groups to Ne^{19} levels below about 3.5 MeV excitation.

The absolute $F^{19}(p,n)Ne^{19}$ cross section was determined as 27 $\pm$ 4 mb at a proton energy of 5.58 MeV. Comparison with the two previously reported measurements of this cross section (Bl 51) (Gi 59) is difficult because of the small energy region in common, the thick targets used by the other workers and the lack of good error estimates. However, agreement occurs between the three groups of

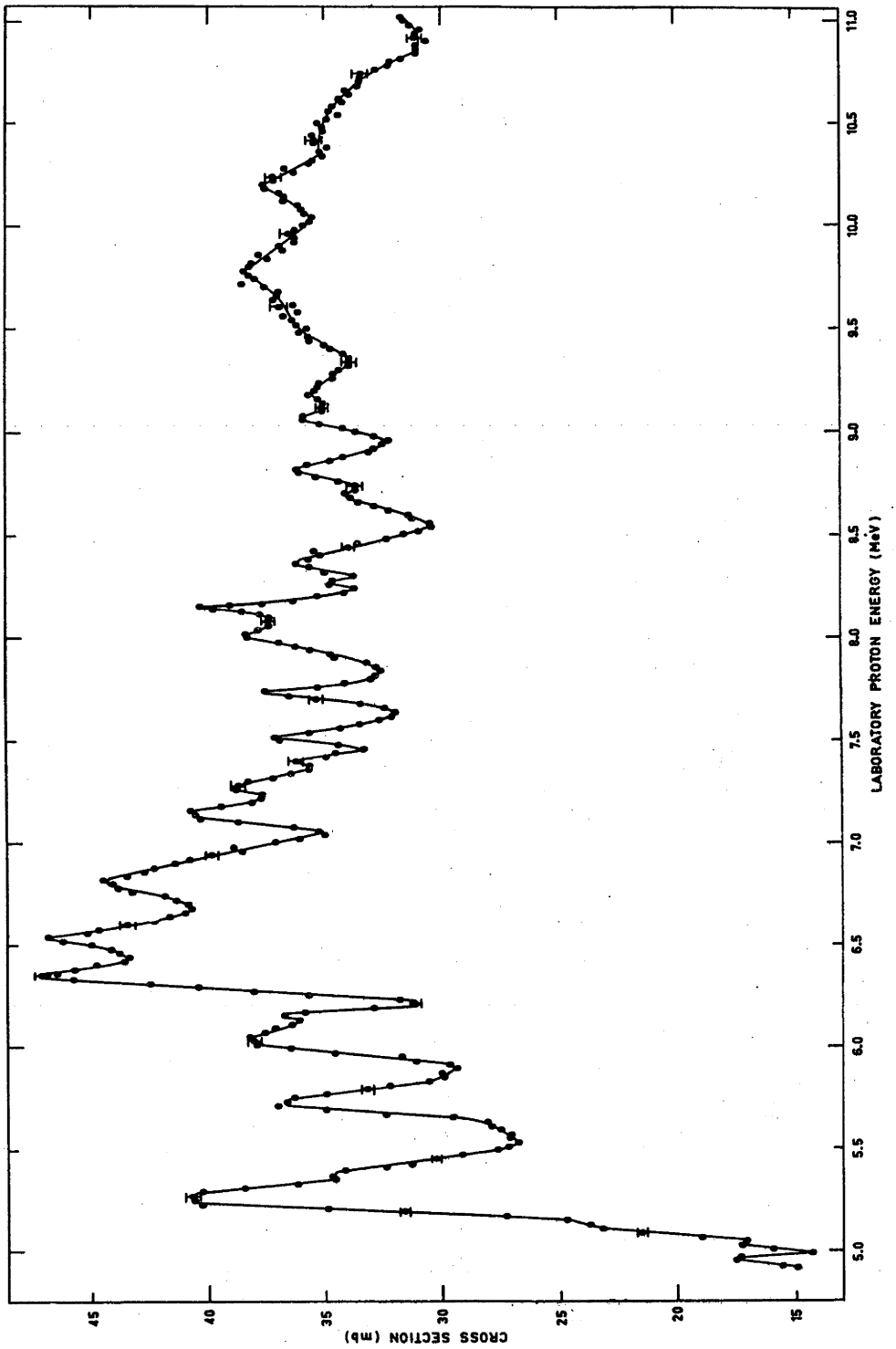

FIG. 2.6 The total $F^{19}(p,n)Ne^{19}$ cross section as a function of proton energy.

workers, to better than a factor of two, at 4.9 MeV proton energy.

The excitation function is shown in figure 2.6. Maxima occur at proton bombarding energies of 4.96, 5.03, 5.11, 5.26, 5.37, 5.73, 6.03, 6.15, 6.35, 6.53, 6.81, 7.14, 7.27, 7.41, 7.52, 7.74, 8.02, 8.15, 8.28, 8.37, 8.70, 8.82, 9.08 MeV (all $\pm$ 0.02 MeV), 9.2, 9.5, 9.8 and 10.2 MeV, corresponding to possible levels in the compound nucleus Ne^{20} at 17.55, 17.62, 17.69, 17.84, 17.94, 18.28, 18.57, 18.68, 18.87, 19.04, 19.31, 19.62, 19.75, 19.88, 19.98, 20.19, 20.46, 20.58, 20.71, 20.79, 21.11, 21.22, 21.47 (all $\pm$ 0.02 MeV), 21.6, 21.9, 22.1 and 22.5 MeV.

2.6 Discussion

A comparison of the positions of the maxima in the present (p,n) excitation function with the positions of other reported resonances above 17 MeV excitation in Ne^{20}, is shown in table 2.1. Up to an excitation energy of about 18.5 MeV, the agreement between the sets of data from the (p,n), (p,$\alpha\gamma$), (p,α_0), (p,α_π) and (α,α) reactions is very good. It is not to be expected that all reactions will show every resonance in Ne^{20}, as selection rules apply which are especially strong in reactions where an outgoing α particle is involved. The agreement evident between the levels up to 18.5 MeV excitation suggests an interpretation of the maxima over the energy range of the present (p,n) experiment, as representing individual Ne^{20} compound nucleus levels.

At excitation energies well above 18.5 MeV, the connection between the positions of the resonances seen in the different reactions becomes much less apparent. In their work on the $F^{19}(p,\alpha)$ reaction, Warsh et al. (Wa 63) studied the angular distributions of the α particles at proton energies in the range 3 to 12 MeV. They found that they could fit their data at the minima (but not at the maxima) of the total cross section by a direct interaction treatment. Teplov et al. (Te 61), who investigated the (p,α) reaction, have also suggested that in the proton energy range from 5.1 to 6.5 MeV there are sizeable contributions from both direct and compound nucleus interactions. It is probable therefore that there will be a considerable direct interaction contribution over the energy range of the present (p,n) experiment. Interference effects between this contribution and that from compound nucleus formation will have a marked influence on the structure of the excitation function. The direct interaction contribution should increase as the excitation energy increases. It is to be expected therefore, that a decreased correlation between the structure observed by different reactions will result.

Calculation has shown that if the maxima in the excitation function near 21 MeV excitation are interpreted as compound nucleus resonances, the density of levels implied is about two orders of magnitude smaller than that predicted by level density formulae.

The apparent experimental density at this energy is about one level per 100 to 150 keV, whereas the work of Lang and Le Couteur (La 54) and of Le Couteur and Lang (Le 59) predicts a density of states of about one level every 1.5 keV. Application of the formula derived by Cameron (Ca 58) gives a similar value although it is not expected to be accurate at energies so far above the neutron threshold. If the level spacing at these excitation energies is only a few keV, then it is possible that the structure observed is the result of a statistical average over many levels. The magnitude of the fluctuations which can be expected under these circumstances has been calculated, on the basis of the statistical model of the nucleus, by Ericson (Er 60). The basic assumption of the statistical model is that the intermediate state is long lived and therefore that the nucleons reach an energy equilibrium before the compound nucleus decays. Under these conditions, the formation and decay of the compound nucleus are independent and the phases of the many overlapping levels taking part in the reaction can be treated on a purely statistical basis. As well as making predictions about the magnitude of the fluctuations in the total cross section, the theory indicates, that if the angular distributions are averaged over a large energy range, they will be symmetrical about a centre of mass angle of 90^{o}.

In an effort to check the Ericson prediction, Warsh et al.

(Wa 63) averaged 12 of their angular distributions over the energy range 9.9 to 12.3 MeV. The result was not symmetric about 90^{o}. The basic assumption of the statistical model is not fulfilled by reactions of the direct interaction type. Therefore in view of the expected large contribution from direct interaction mechanisms at these energies, the magnitude and effect of both the direct interaction contribution and of interference between this and the compound nucleus contributions would have to be estimated before any theory of the statistical model nature could be effectively applied.

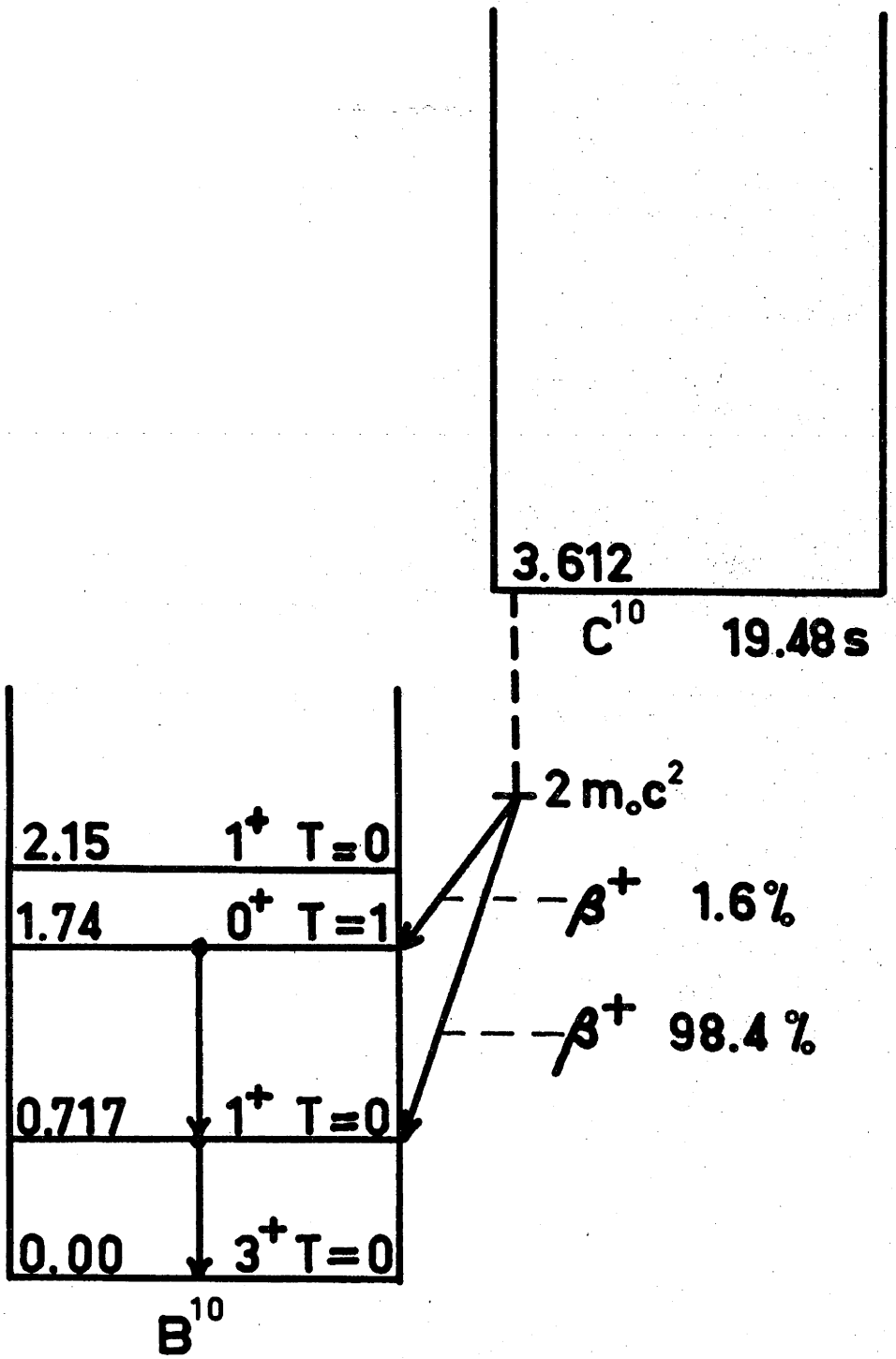

FIG. 3.1 The positron decay scheme of C^{10}.

CHAPTER 3

THE $B^{10}(p,n)C^{10}$ EXCITATION FUNCTION FROM THRESHOLD TO 10.6 MeV

3.1 Introduction

Information on high lying levels of C^{11} is scarce. The experiment described in this chapter was therefore undertaken to measure the $B^{10}(p,n)$ excitation function from the threshold (4.8 MeV) to 10.6 MeV and to search for levels in C^{11} between 13.1 and 18.3 MeV excitation. The reaction can be readily investigated using the activation apparatus described in chapter 1 since the positron decay of C^{10} (see fig 3.1) proceeds almost entirely via the 0.717 MeV level of B^{10} (Sh 53). Coincidences between the 0.717 MeV γ ray and one of the 0.511 MeV annihilation quanta then allows a unique identification of the C^{10} activity even in the presence of other likely positron activities.

Transitions to the ground state of C^{10} are inhibited by the large spin change ($\Delta J = 3$) involved. As a result, the cross section below the first excited state threshold is small, and no excitation function for the reaction has been measured.

Kalinin et al. (Ka 57) carried out a stacked foil experiment with poor energy resolution, which suggested the presence of broad resonances in the $B^{10}(p,\alpha)$ excitation function at E_p = 4.0, 5.6 and

7.8 MeV corresponding to broad levels in C^{11} at 12.3 ± 0.2, 13.8 ± 0.2 and 15.7 ± 0.2 MeV excitation energy respectively. More recent experiments in this laboratory by Ophel et al (Op 62) using the reactions $B^{10}(p,p'\gamma)$, $B^{10}(p,\alpha\gamma)$ and $B^{10}(p,\gamma_o)$ have established levels in C^{11} at excitation energies of 11.47 ± 0.01, 12.69 ± 0.01 and 13.95 ± 0.02 MeV.

3.2 Experimental Apparatus

The activation apparatus and electronic equipment used in this experiment have been described in chapter 1.

For proton energies up to 8.5 MeV, a target of electromagnetically separated boron metal (>99.9 percent B^{10}), of nominal thickness 600 μgm/cm^2 deposited on a thick tantalum backing *, was used. This target was 44 keV thick to 5 MeV protons. Preliminary measurements showed that the deposit was non-uniform, varying by about 15 percent across the 1 cm wide target. Hence, care was taken to bombard the same portion of the target throughout the experiment. For each energy measured, the beam was focussed onto the quartz viewer to a spot less than 0.2 cm in diameter located centrally to better than 0.06 cm. Reproduceable results were obtained by following this procedure.

Above a proton energy of 8.5 MeV, the large numbers of

---

* Obtained from the Harwell Electromagnetic Separator Group.

neutrons produced in the tantalum backing of the target (Ha 62) induced prohibitively high activities in the NaI detectors. For the high energy section of the experiment therefore, a self supporting boron film * containing 105 μgm/cm^2 of B^{10} was used. This target was made by vacuum evaporation of enriched boron from a tantalum crucible using electron bombardment heating. It contained 89 percent B^{10} and 8 percent B^{11} by weight, some carbon, and traces of tantalum. To prevent the C^{10} nuclei from recoiling out of the target and being lost from the counting region, a 3 mgm/cm^2 gold foil was placed directly behind the target. The beam passed through both the target and the gold foil and was collected on tantalum in a shielded section of the beam tube away from the detectors.

3.3 The Half-Life of C^{10}

At the time this experiment was carried out, only two measurements of the C^{10} half life had been reported. The first, of 8.8 sec (De 40), was in error due to an impurity in the boron powder used, and the second, by Sherr et al. (Sh 49), was 19.1 $\pm$ 0.8 sec. Because an accurate value of the decay constant is required for an absolute cross section measurement, it was necessary to measure the C^{10} decay half life.

---

* Thanks are due to Mr. F.A. Howe and associates at A.W.R.E., U.K. who made this target.

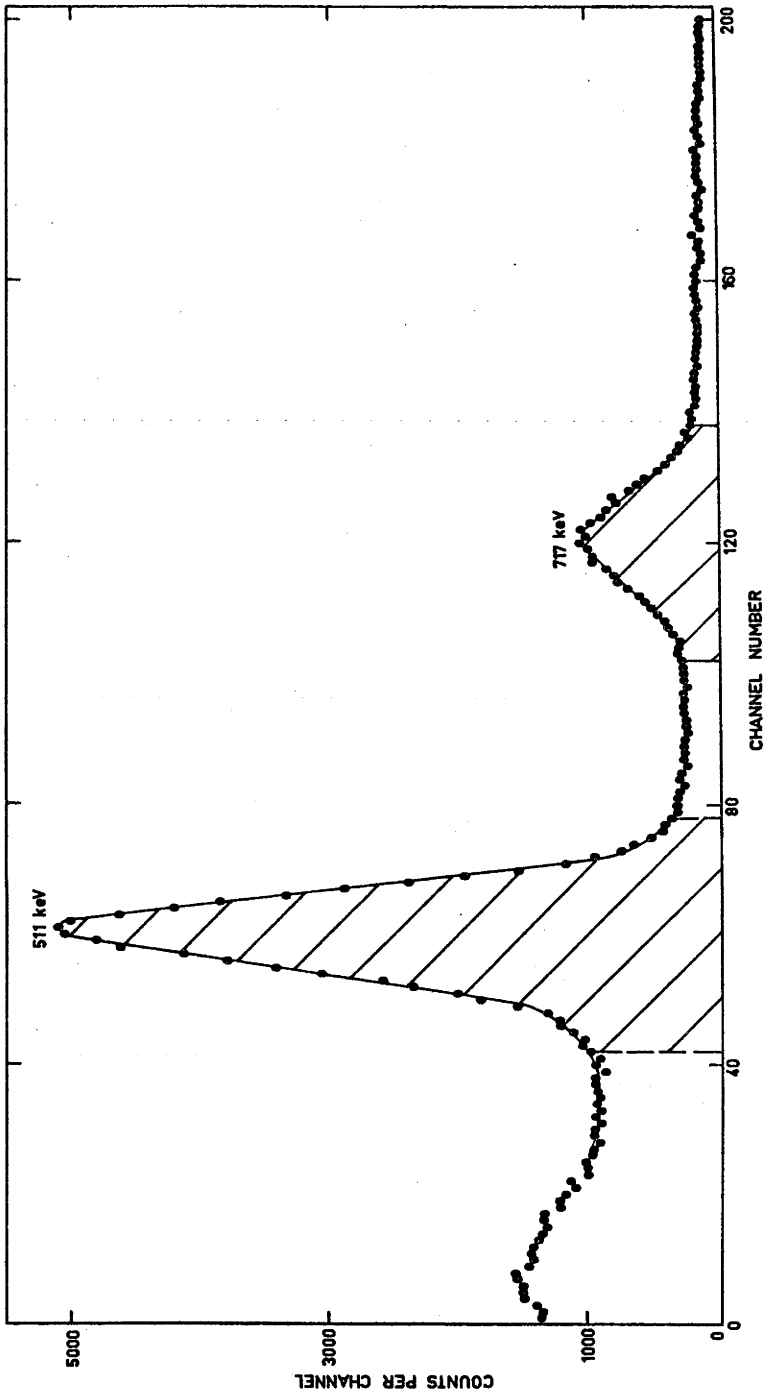

FIG. 3.2 A gamma ray spectrum taken with one of the 7.6cm x 7.6 cm spectrometers after a bombardment with 8 MeV protons. The hatched areas indicate the energy intervals selected for the coincidence measurements.

A 200 - 250 μgm/cm^2 self supporting B^{10} target (also obtained from Mr. F.A. Howe) was bombarded for 60 sec., with 0.1 μA of protons from the tandem accelerator, and the decay of the induced activity followed for 290 sec, i.e., about 15 half-lives. Since the C^{10} decay is uniquely identified by the 0.717 MeV γ rays, (see fig 3.1) the activity was measured by following the decay of counts in a single channel analyser window placed over the photo-peak of that γ ray (see fig 3.2). As in the half-life measurements described in chapter 2, statistical accuracy was increased by adding a large number of runs. A check that other positron activities were not affecting the results was also made by following the decay of the count rate of coincidences between an annihilation quantum in one crystal and an 0.717 MeV γ ray in the other. Both methods showed that the backgrounds were constant with time (see fig 3.3) and that accurate subtractions could be made.

The experimental procedure, apparatus used and the method of analysis have been fully described in chapter 2. A total of six independent measurements were made at proton bombarding energies between 7.0 and 9.2 MeV. The results for the C^{10} half-life are 19.37, 19.55, 19.62, 19.63, 19.33 and 19.40 sec (all $\pm$ 0.12 sec). From this data the half-life and its standard deviation was determined as

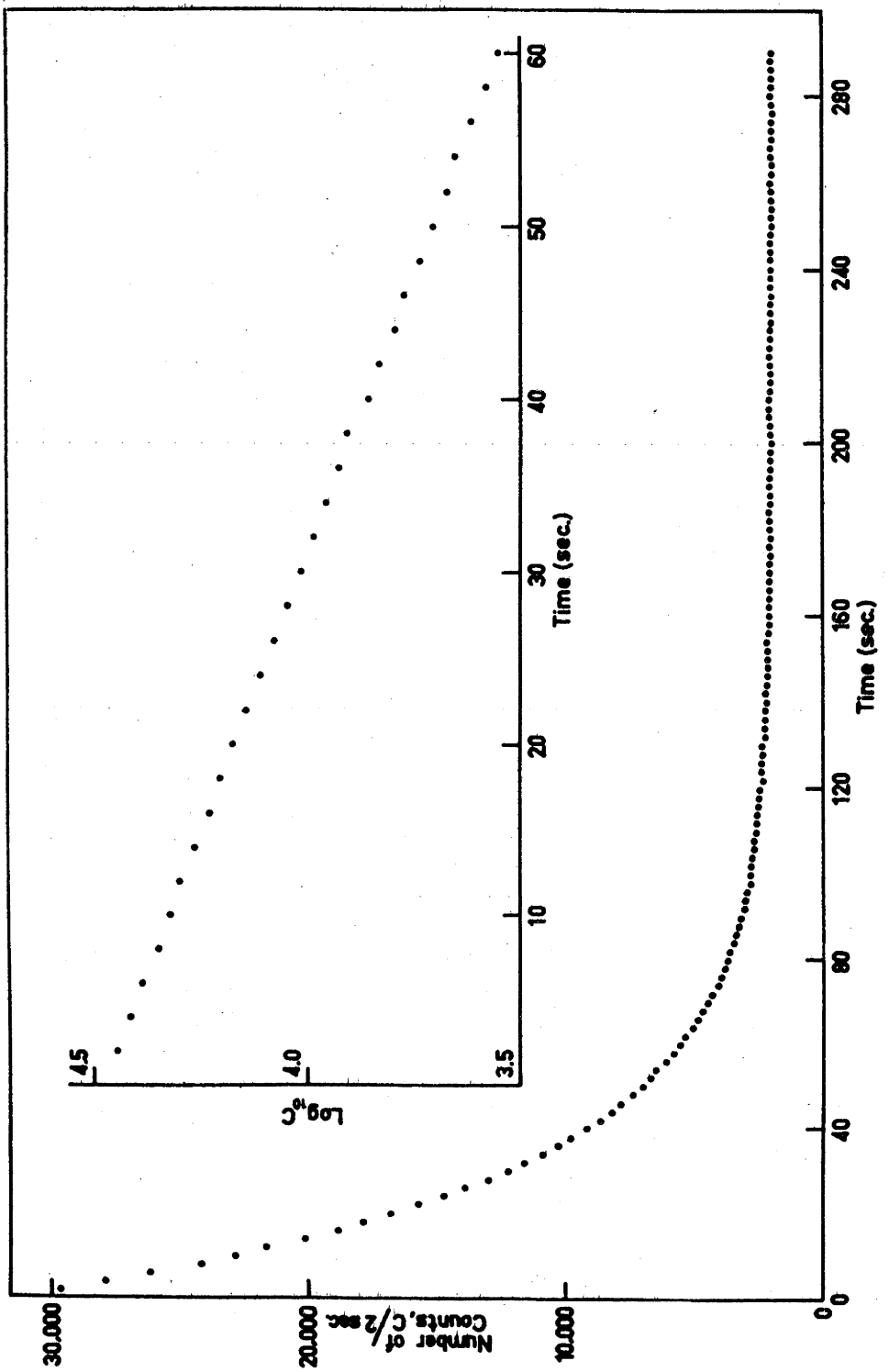

FIG. 3.3 A typical C^{10} decay curve, together with a logarithmic plot of the data after subtraction of the background. This curve consists of the sum of a number of runs, in each of which counting loss and gain-change effects were negligible.

$$\tau\ (C^{10}) = 19.48 \pm 0.05 \text{ sec.}$$

3.4 Absolute Cross Section

In chapter 2, a formula was developed for the determination of an absolute cross section using an activation apparatus. In that derivation, Ne^{19} activity was measured by the coincident counts between the two annihilation quanta. The decay of C^{10} however, has been measured by observing coincidences between an annihilation quantum in one crystal and the 0.717 MeV γ ray in the other. If the total efficiency, as defined in chapter 2, of one detector for 0.511 MeV γ rays is ε_1 then the probability that one of the annihilation quanta will be detected as a pulse in the photopeak is $2P_1\varepsilon_1$. There is no angular correlation between the 0.717 MeV γ rays and the annihilation quanta. Therefore, if the total detection efficiency of the second crystal for 0.717 MeV γ rays is ε_2, then the probability of detecting a coincident event between one annihilation quantum and the 0.717 MeV γ ray is $2P_1\varepsilon_1P_2\varepsilon_2$, where P_1 and P_2 are the ratios in the two counters of the photopeak to total counts of the respective γ rays. After making this change, the cross section formula for this experiment becomes, using the notation of chapter 2,

$$\sigma = \frac{Y\lambda M t_1 \cdot 1.60 \cdot 10^{-19}}{I \times \left[2\varepsilon_1 P_1 \varepsilon_2 P_2\right]\left[1 - e^{-\lambda t_1}\right]\left[e^{-(t_2 - t_1)\lambda} - e^{-(t_3 - t_1)\lambda}\right]} \text{cm} \qquad (3.1)$$

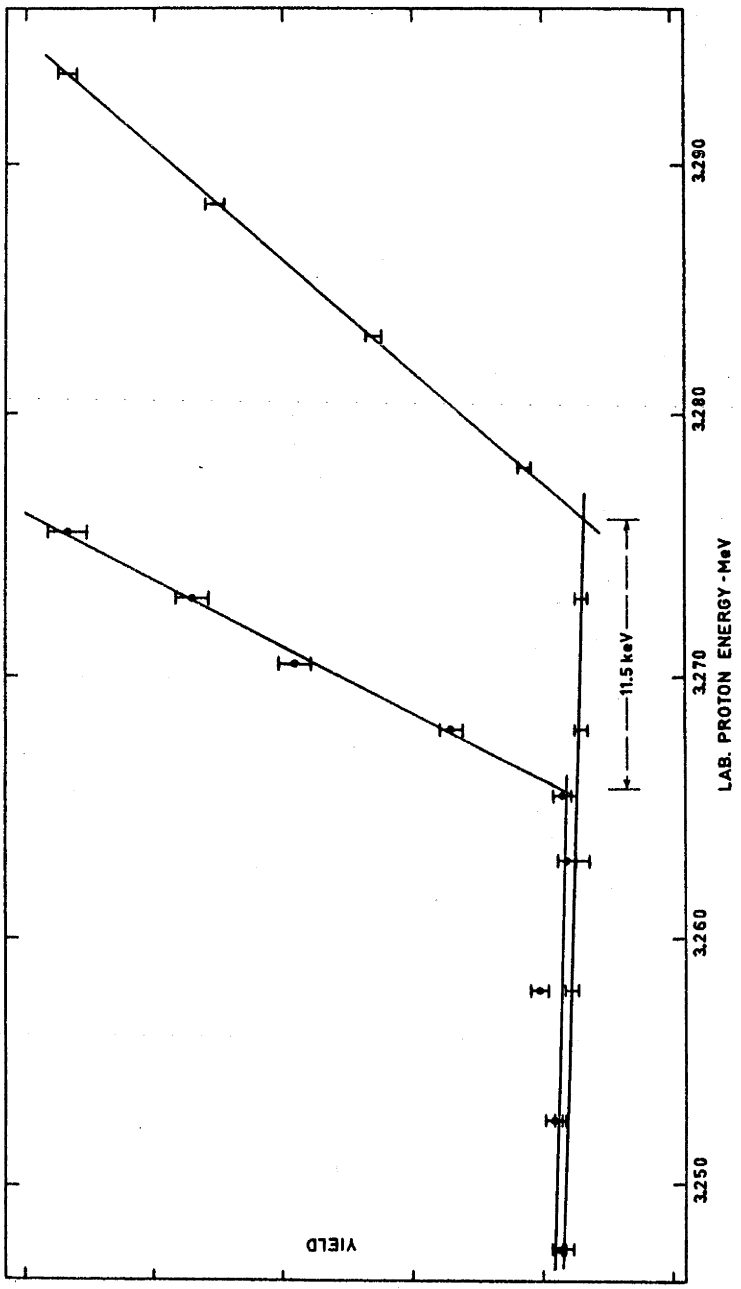

FIG. 3.4 A measurement of the thickness of the self-supporting B^{10} target. The dots represent the $C^{13}(p,n)$ threshold data taken with the slow neutron detector. The other curve shows the energy shift of the threshold when the B^{10} film was placed in front of the C^{13} target.

where here λ is the decay constant of C^{10}

x is the thickness of the target in gm/cm^2

and M is the mass of a B^{10} nucleus in gms.

The "thick" target used in this experiment between threshold and Ep = 8.5 MeV was non-uniform and unsuitable for an absolute cross section measurement. However the self supporting B^{10} target used to obtain data from Ep = 8.5 to 10.6 MeV was much more uniform. Its thickness was measured by observing the energy shift of the $C^{13}(p,n)$ threshold when the proton beam from the tandem accelerator was passed through it. The yield of slow neutrons over the region of the threshold was measured using a boron loaded plastic scintillator (type N.E. 401), placed at an angle of 0^o to the target. The apparent shift in the threshold energy when the beam had first passed through the B^{10} target was a measure of the energy lost by 3.24 MeV protons in the boron (see fig 3.4). From this energy loss, the content of B^{10} was calculated as $105 \pm 15\ \mu gm/cm^2$. The magnitude of the error in this measurement was due mainly to the very small energy loss and the effects of hysterysis in the 90^o beam-analysing magnet.

The detection efficiency of the counting system $2\varepsilon_1 P_1 \varepsilon_2 P_2$ was determined in two parts. The detection efficiency of one crystal for 0.511 MeV annihilation quanta was determined directly using the

calibrated Na^{22} source described in chapter 2. A 5 percent correction was made for the contribution in the window over the 0.511 MeV γ-ray photopeak of the Compton tail from the 1.28 MeV γ ray. Determination of the detection efficiency for the 0.717 MeV γ rays in the second crystal was more difficult however. Initially this efficiency was calculated from

$$\varepsilon = \tfrac{1}{2}\int_0^{\pi} e^{-\sum_i \tau_i y_i(\theta)} \left[1 - e^{-\tau y(\theta)}\right] \sin\theta \, d\theta \qquad (3.2)$$

where $\left[1 - e^{-\tau y(\theta)}\right] \sin\theta$ is the probability that a γ ray entering the crystal at an angle θ with respect to the line joining the source and the central axis of the crystal, will be detected in the length $y(\theta)$ of the crystal.

$e^{-\sum_i \tau_i y_i(\theta)}$ is the probability that the same γ rays will not be scattered by the thickness $y_i(\theta)$ of absorber before reaching the crystal,

the τ are the absorption coefficients for the absorbing materials and the crystal

and the subscript i represents the different absorber materials between the source and crystal.

Evaluation of this integral showed that the 0.717 MeV γ rays suffered a little over 50 percent absorption in the tantalum target holding cylinder, tantalum lining, brass target chamber walls

and the lead shielding foils on the face of the crystals. As this absorption was large, it was checked experimentally using 0.662 MeV γ rays from a Cs^{137} source. The detection efficiency without absorbers present can be accurately calculated. Therefore an ordinary uncalibrated source was used to measure the absorption by observing the count rate both with and without the absorbing material in front of the crystal. The crystal was placed within 2 cm of the source during use. Hence the count rate was extremely sensitive to small differences in this distance. The source and crystal were therefore clamped in position and an accurate replica of the appropriate section of the target chamber and lead shielding was constructed and placed between them. The absorbing material could then be placed in position and removed again without disturbing the crystal-source spacing. The value obtained for the absorption by the two methods differed by 15 percent. However the experimental value was very reproduceable and was statistically accurate to better than 1 percent. Hence the detection efficiency determined experimentally was used in the evaluation of the absolute cross section. A small correction was made for the difference in the absorption coefficients for 0.662 MeV and 0.717 MeV γ rays.

The factors contributing to the error in the absolute cross section measurement are essentially the same as those outlined in

chapter 2. Table 3.1 summarises the distribution of these errors.

TABLE 3.1

Distribution of errors in the absolute cross section measurement

SOURCE OF ERROR	PERCENTAGE
Target thickness	$\pm$ 15 %
Decay constant	$\pm$ 0.3 %
Equivalent current	$\pm$ 1.5 %
Detection efficiency $\varepsilon_1 P_1$	$\pm$ 2.5 %
Detection efficiency $\varepsilon_2 P_2$	$\pm$ 3 %
r.m.s. error on average curve (from the deviation of the measured points from the average)	$\pm$ 2 %
Total error	$\pm$ 16 %

3.5 Excitation Function, Procedure and Results

The experimental procedure was exactly the same as that used for the $F^{19}(p,n)Ne^{19}$ experiment and has been fully described in chapter 2. Counting losses were again kept to less than 1 percent. During a run over a selected energy range, at least three measurements of the yield were made at each proton energy and averaged.

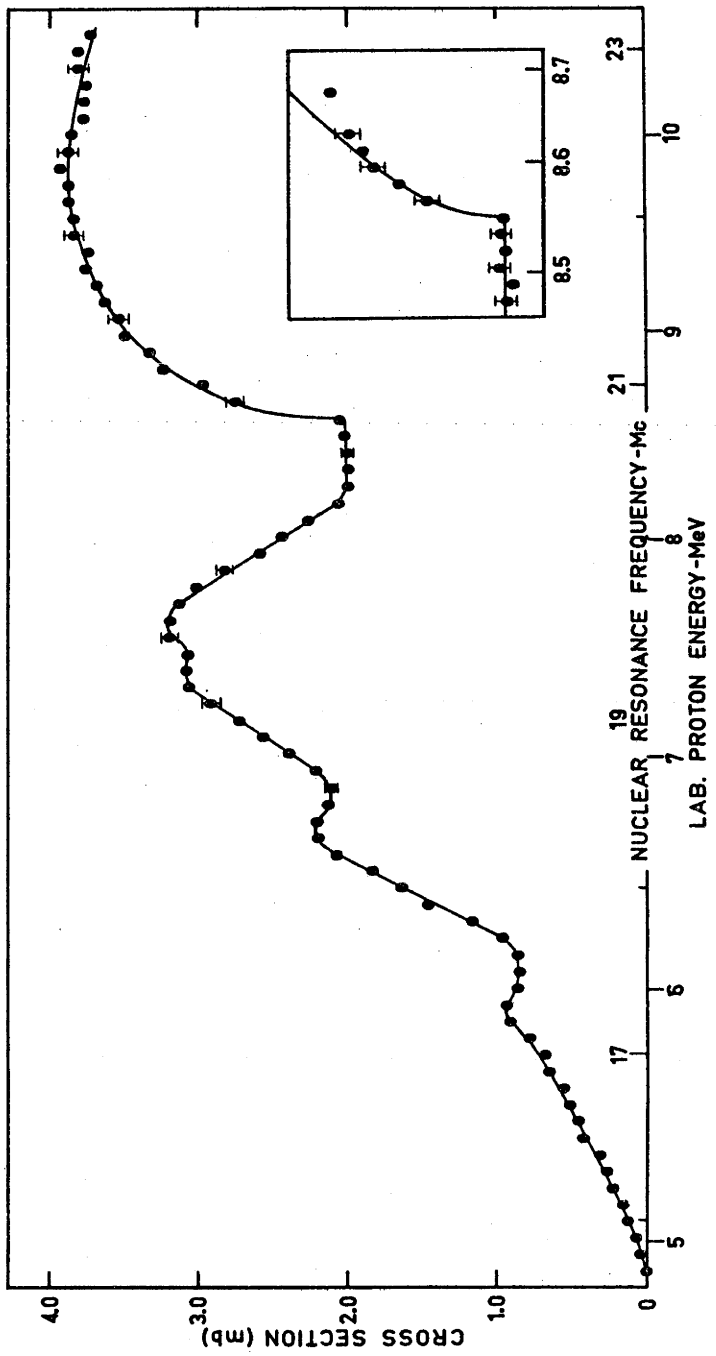

FIG. 3.5 The total $B^{10}(p,n)C^{10}$ cross section as a function of energy. The inset is a detail of the curve in the region of Ep = 8.5 MeV, the solid line being an $En^{\frac{1}{2}}$ fit to the points.

The statistical error on this average was ± 3 percent. Over the higher energy portion of the excitation function the repeatability of the curve was not good. Therefore, each energy interval was covered between six and nine times and the excitation function shown in figure 3.5 represents an average of these individual runs weighted equally after normalisation. The spread of points on the curve was much greater than the statistical error. Therefore the r.m.s. error on the average curve was obtained from the deviation of each measurement from the mean. The resulting error was ± 2 percent. This means that the structure of the curve in the region Ep = 7.5 MeV is not absolutely certain. However, the fact that the averaging has failed to smear the double peak observed in the individual runs into a single peak, suggests the existence of two resonances in this region.

The absolute $B^{10}(p,n)C^{10}$ cross section was determined as 2.0 ± 0.3 mb at a proton energy of 8.5 MeV. A cross section for the reaction has been reported by only one other group. Gibbons and Maklin (Gi 59) reported the value $\sigma \leq 2$ mb at 5.51 MeV while the present measurement gives 0.50 ± 0.08 mb at 5.51 MeV.

Although the $B^{10}(p,n)$ reaction has not been studied previously, the lower excitation energies in C^{11} reached in this experiment have been attained through the $(p,p'\gamma)$ and (p,α) reactions. Earlier results in this region show a marked lack of structure (Ka 57) (Op 62) and

indicate widely spaced broad levels, and this is supported in the present work. The maxima in the excitation function, at proton energies of 5.92 ± 0.02, 6.68 ± 0.04, 7.33 ± 0.05 and 7.60 ± 0.05 MeV correspond to broad levels in the compound nucleus C^{11} at excitation energies of 14.08 ± 0.02, 14.78 ± 0.04, 15.36 ± 0.05 and 15.61 ± 0.05 MeV.

Taking into account the broad nature of the levels, it is possible that the present level at 14.08 MeV might be identified with the level reported at 13.8 ± 0.2 MeV from the stacked foil experiment by Kalinin et al. (Ka 57). The ill-defined level of Kalinin et al. at 15.7 ± 0.2 MeV probably reflects the "double resonance" observed in this experiment near 15.5 MeV excitation.

The sharp rise in cross section at Ep = 8.55 MeV is interesting. It corresponds closely to the energy at which neutron transitions to the first excited state of C^{10} become energetically possible. Because of the large spin difference, neutron emission to the ground state of C^{10} is restricted, and the yield is low. At the threshold of the first excited state however, s-wave neutron emission becomes possible and, in the absence of resonances in this energy region, the yield above threshold may be expected to rise as for an s-wave neutron threshold. The cross section immediately above a (p,n) threshold has the form (Bl 52)

$$\sigma\,(p,n) \propto \varepsilon_n^{\ell + \frac{1}{2}}$$

where ε_n is the channel energy of the outgoing neutron,

and ℓ is its orbital angular momentum.

The channel energy is proportional to the energy of the neutron in the centre of mass. Hence for s-wave neutrons ($\ell = 0$)

$$\sigma\,(p,n) \propto E_n^{\frac{1}{2}} \qquad (3.3)$$

where E_n is the centre of mass neutron energy.

The region around Ep = 8.55 MeV was repeated in energy steps of 20 keV. If the sharp rise corresponds to the first excited state threshold, it should follow a relation approximating the form of equation 3.3. It was assumed that the background before the sharp rise was entirely due to neutrons to the ground state of C^{10} and that it remained the same under the rise. The data, after subtraction of this "ground state" contribution was then fitted by a curve of the form $\sigma \propto E_n^{\frac{1}{2}}$ (see inset in fig 3.5). The continuous line represents the fitted $E_n^{\frac{1}{2}}$ curve, and it can be seen that a reasonably good fit to the experimental data was obtained. The target thickness at this energy was only 5 keV. Hence it was assumed that the data was a good approximation to perfect energy resolution. Assuming then, that the cross section rise at Ep = 8.55 MeV is a threshold corresponding to the first excited state, then the level is located at

3.38 ± 0.03 MeV compared with the previous determination of 3.4 ± 0.2 MeV (Aj 54). In calculating this excitation energy, the $B^{10}(p,n)C^{10}$ reaction threshold value of 4.835 ± 0.025 MeV reported by Takayanagi et al. (Ta 61) was used.

It is of interest to compare this energy of the first excited state of C^{10} with the corresponding energies (Aj 59) in the other members of the isobaric triplet, Be^{10} and B^{10}. These are 3.37, 3.42 and 3.38 MeV for Be^{10}, B^{10} and C^{10} respectively. Differences in these energies could be due to different Coulomb energies in the J = 0 and J = 2 states. These have been calculated by Dr. E. Bradford (Br 62), using for simplicity, j - j coupled wave functions. The contributions to the excitation energies of the J = 2 states relative to the J = 0 states are -0.08, 0 and 0 MeV in the three nuclei. Thus the excitation energies corrected for Coulomb energies are 3.45, 3.42 and 3.38 MeV and such a linear trend could possibly be due to Thomas shifts or to increased size of the nuclei due to Coulomb repulsion.

CHAPTER 4

THE $B^{10}(p,\alpha)Be^{7}$ AND $B^{10}(p,He^{3})Be^{8}$ REACTION BETWEEN 2 AND 11 MeV

4.1 Introduction

Measurements of the excitation functions for the reactions $B^{10}(p,\alpha\gamma)$, $B^{10}(p,p'\gamma)$ and $B^{10}(p,\gamma)$ for proton bombarding energies up to 2.7 MeV, corresponding to an excitation energy of 11.2 MeV in C^{11}, have established levels in C^{11} at 9.74 ± 0.01 and 10.09 ± 0.01 MeV (Da 54) (Ch 56) (Hu 57). Bair et al. (Ba 55) have studied the $B^{10}(p,\gamma)$ reaction and have reported a broad level at 12.3 ± 0.1 MeV. Ophel et al. (Op 62), have measured the excitation functions for the above three reactions over the proton energy range 2.4 to 7.2 MeV, and have reported levels in C^{11} at 11.45 ± 0.01, 12.66 ± 0.01 and 13.91 ± 0.02 MeV. The level reported by Bair et al. at 12.3 MeV was not seen.

Levels have been reported at 9.1, 10.7 and 11.4 MeV by Andreev et al. (An 62) who studied the $B^{10}(p,p)$ reaction. From their study of the same reaction, Overley and Whaling (Ov 62) observed levels at 10.06 ± 0.02 and 10.68 ± 0.01 MeV. They also observed the latter level through the $B^{10}(p,\alpha)$ reaction.

Cronin (Cr 56) measured the $B^{10}(p,\alpha)$ excitation function between the proton energies of 0.8 and 1.65 MeV, and reported levels

at 9.76 ± 0.05 and 10.09 ± 0.05 MeV. Kalinin et al. (Ka 57), using the stacked foil method, obtained the $B^{10}(p,\alpha)$ excitation function in the range Ep = 3 to 8 MeV and found structure which indicated possible broad levels in C^{11} at 12.3 ± 0.2, 13.8 ± 0.2 and 15.7 ± 0.2 MeV.

The observation of neutron groups from the stripping reaction $B^{10}(d,n)C^{11}$ has indicated the presence of further levels in C^{11} at excitation energies of 11.26 ± 0.02 and 11.52 ± 0.02 MeV (Ce 56) (Gr 57). The experiment on the $B^{10}(p,n)C^{10}$ reaction described in the previous chapter has established levels at 14.08 ± 0.02, 14.78 ± 0.04, 15.36 ± 0.05 and 15.61 ± 0.05 MeV.

The present experiment was undertaken to extend the excitation function for the $B^{10}(p,\alpha)Be^{7}$ reaction up to a proton energy of 10.8 MeV in the hope of confirming the levels observed in other reactions and of determining some of their properties. There is only one channel spin available to the outgoing system, and this should increase the possibility of making assignments of spins, parities and reduced widths of states of the intermediate system C^{11}, by studying the angular distributions of the α particles.

Accordingly, in the experiment described in this chapter, excitation functions were taken for α particle groups from the $B^{10}(p,\alpha)Be^{7}$ reaction proceeding to the ground (α_0) and first excited (α_1) states of Be^{7}, for proton bombarding energies from 1.8 to 10.8 MeV.

Thirty angular distributions for both α_0 and α_1 were taken between proton energies of 2.8 and 7.0 MeV. Excitation functions and angular distributions for the $B^{10}(p,He^3)Be^8$ reaction were measured concurrently with the present work.

4.2 Experimental Procedure and Results

A 100 μgm/cm^2 self supporting target * (containing 89 percent B^{10} and 8 percent B^{11} by weight) was mounted on a rotatable support at the centre of a scattering chamber, and was bombarded with a 0.02 μA proton beam from the Canberra tandem accelerator. The beam entered the chamber through two 1.6 mm diameter collimating holes in carbon discs, placed 6 cm apart. Each collimating disc was followed, at a distance of 3 cm, by a carbon antiscatter disc with 3.2 mm diameter holes. The α particles were detected by a 4.5 x 4.5 mm, 300Ω-cm, gold-silicon surface barrier detector which was mounted inside the vacuum, 6.35 cm from the target, in such a manner that it could be placed at any angle in a horizontal plane, with respect to the beam axis. An aperture, 2 cm in diameter, placed 4 cm in front of the counter, provided a certain amount of collimation. The sensitive depth of the counter was adjusted, by varying the reverse bias on it, so that the α_0 group was just stopped within the sensitive depth. The scattered proton pulses were then

---

* Thanks are due to Mr. F.A. Howe and associates at A.W.R.E., U.K., who made this target.

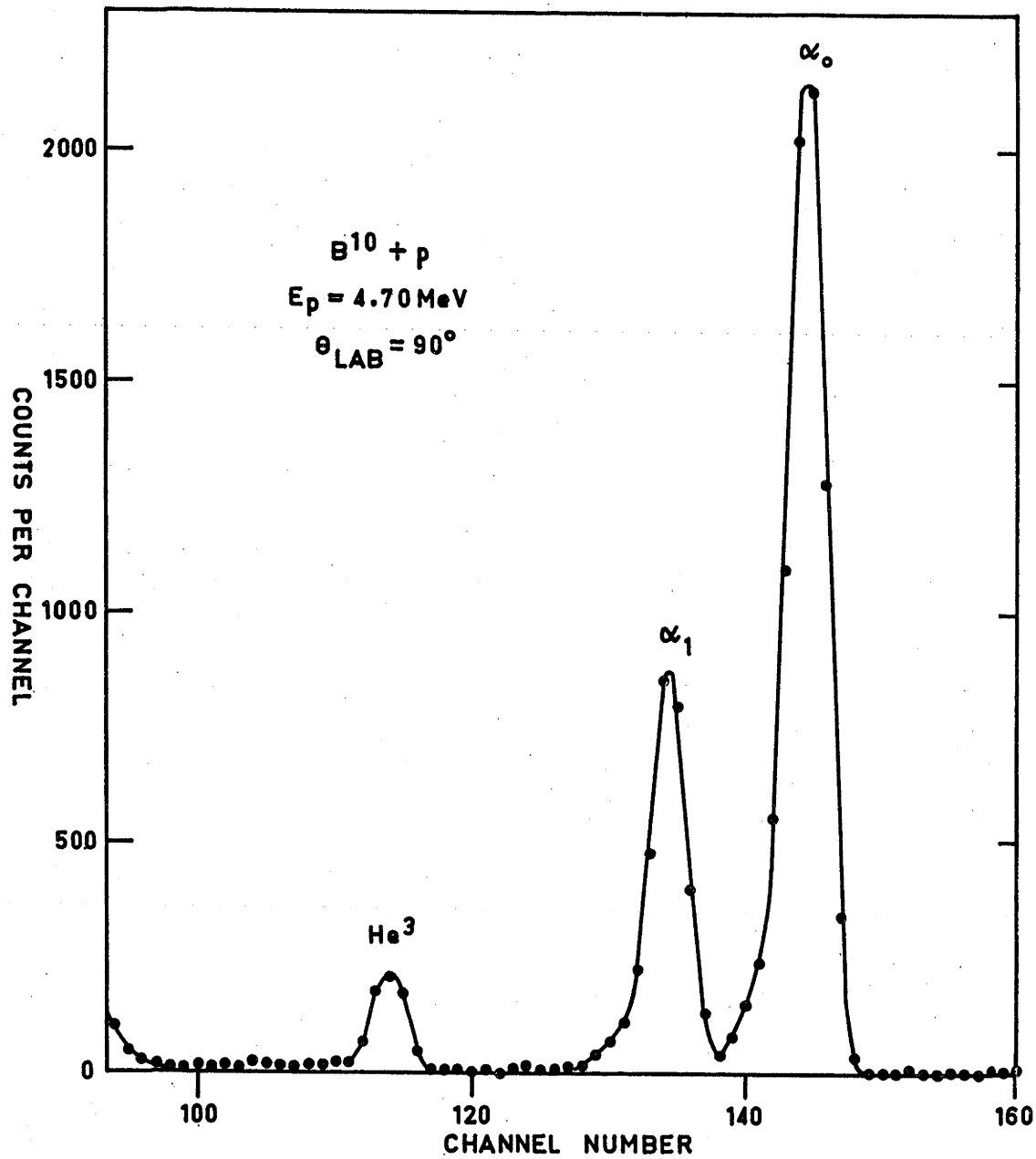

FIG. 4.1 A spectrum of helium particles from the bombardment of B^{10} by protons of energy 4.70 MeV, observed at a laboratory angle of 90^{o}.

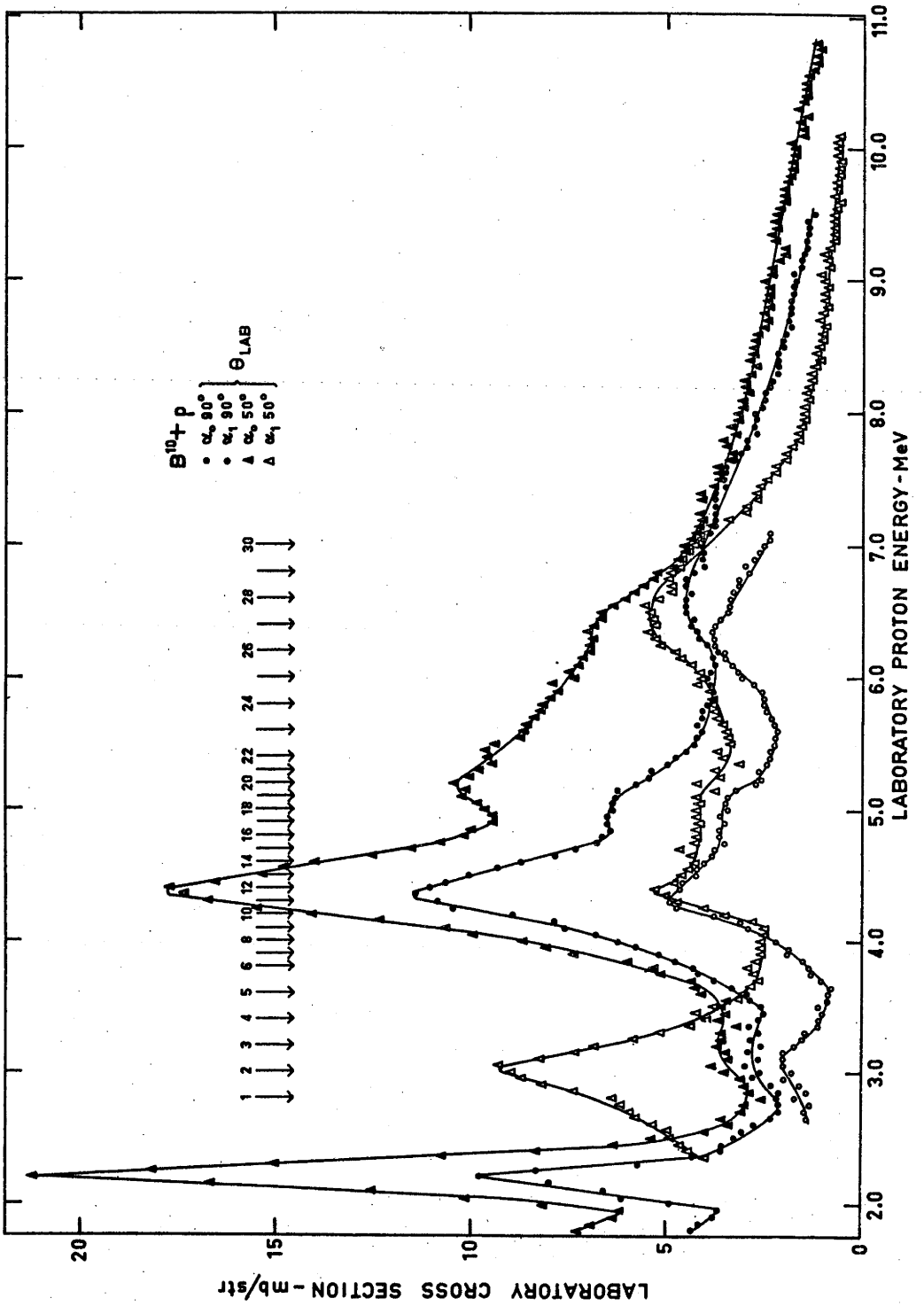

FIG. 4.2 Excitation functions for the α_0 and α_1 groups from the $B^{10}(p,\alpha)Be^7$ reaction, taken at laboratory angles of 50° and 90°. Statistical errors are of the order of the size of the triangles. The arrows indicate energies where angular distributions were measured.

small and were able to be suppressed. The pulses from the detector were amplified by an Ortec charge-sensitive preamplifier-amplifier system, and were recorded by a multichannel analyser. By keeping the dead time of the analyser below 5 percent, "pile-up" of pulses in the electronics was made negligible. A spectrum, taken at a proton energy of 4.70 MeV, is shown in fig 4.1.

To obtain absolute cross sections for the reactions, it was necessary to measure the thickness of B^{10} in the target. This was done by comparing the yields of $B^{10}(p,\alpha)$ reaction α particles from the present target and from the target of the same composition and method of manufacture, whose thickness was measured for the experiment described in chapter 3. The comparison was made at several proton energies, and the thickness of B^{10} determined as $(77 \pm 12)\,\mu gm/cm^2$. The statistical accuracy of the comparison was better than $\pm$ 2 percent.

The yields of both α_0 and α_1 were measured, as functions of proton bombarding energy, every 50 keV from 1.8 to 10.8 MeV, at laboratory angles of 50^o and 90^o. The excitation functions obtained are shown plotted as differential cross sections in fig 4.2. The α_0 excitation function at 50^o was measured up to 10.8 MeV proton energy, but that at 90^o was measured to only 9.5 MeV because of increased overlapping above this energy of the ground state α-particle group

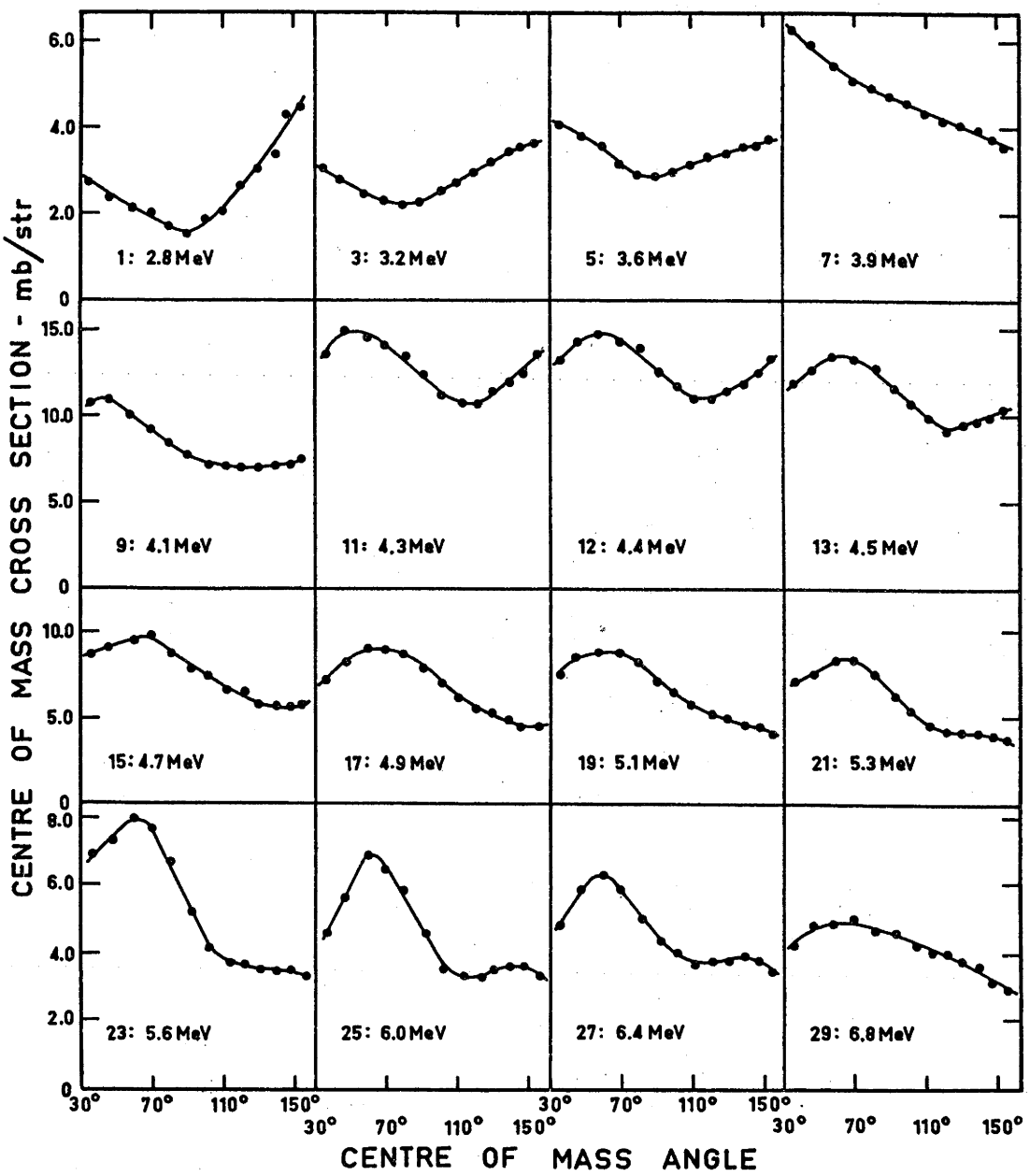

FIG. 4.3 Selected angular distributions of the α_0 group from the $B^{10}(p,\alpha)Be^7$ reaction. The curves are experimental, and the numbering corresponds to that of fig. 4.2. Statistical errors are of the order of the size of the points.

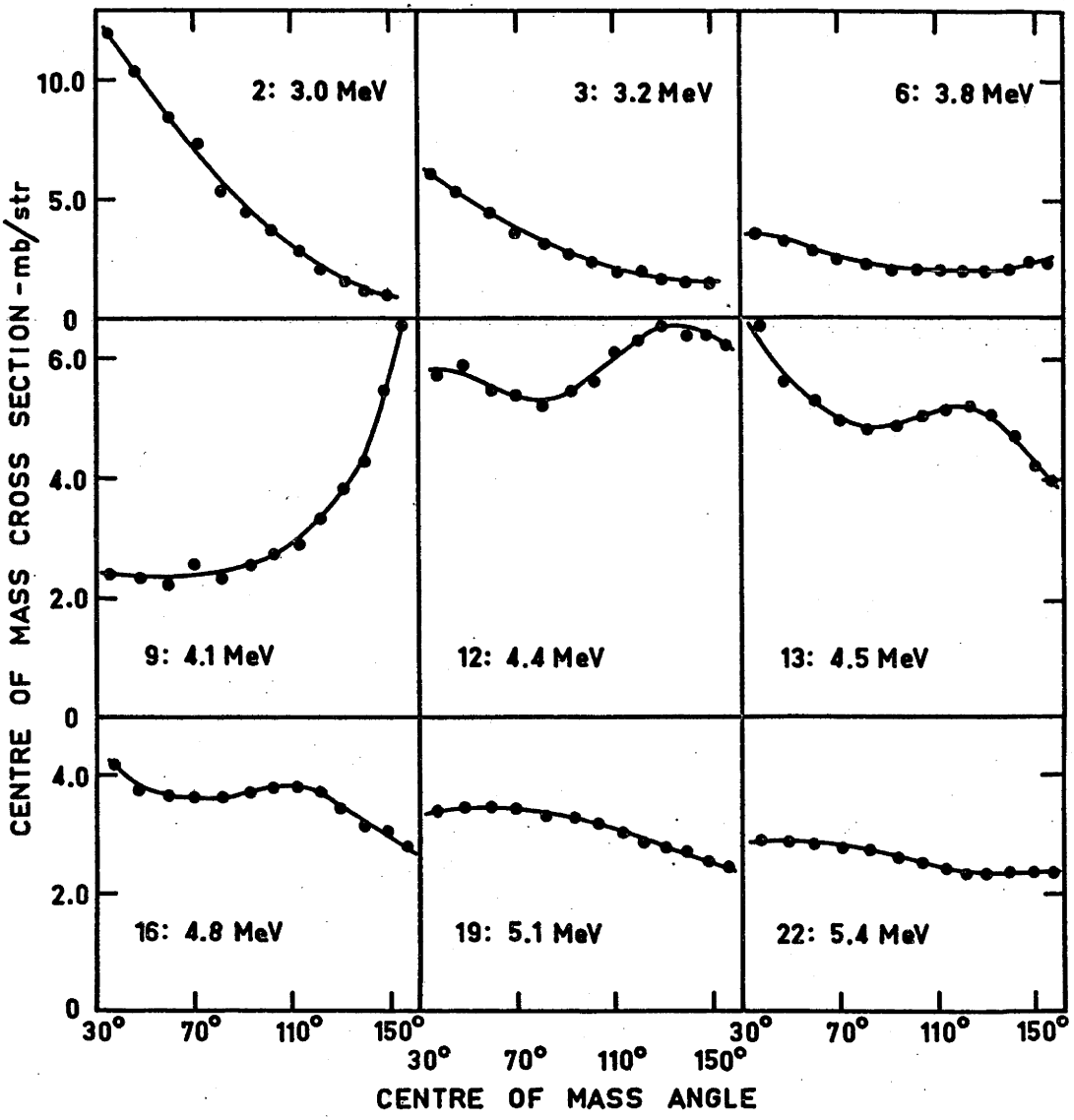

FIG. 4.4 Selected angular distributions of the α_1 groups from the $B^{10}(p,\alpha)Be^7$ reaction. The curves are experimental, and the numbering corresponds to that of fig. 4.2. Statistical errors are of the order of the size of the points.

and the He^3 group from the $B^{10}(p,He^3)$ reaction. For a similar reason the α_1 excitation function at 90^o ceases well below the corresponding one at 50^o. The lower limit of the excitation functions, namely Ep = 1.8 MeV, was imposed by the minimum energy α particles that could be detected by the solid state counter.

A value of (10 $\pm$ 2) mb/sr was obtained for the $B^{10}(p,\alpha_o)$ differential cross section at 90^o at the Ep = 2.2 MeV resonance. This is not in agreement with the (18 $\pm$ 2) mb/sr reported previously (Ov 62). (See section 4.3.3 for further details).

Angular distributions for both α_o and α_1 were measured at the thirty proton energies shown arrowed in fig 4.2, and selections of them are shown in figs 4.3 and 4.4. Most are taken with thirteen angles from $\theta_{Lab} = 30^o$ to 150^o in 10^o steps, enabling an estimate to be made of the magnitude of the contributions of terms of orders 0 to 6 to the polynomial expansion described in section 4.3.1. Measurements were not made at smaller and larger angles because of the problem of intercepting the beam with the counter assembly.

Data were taken with the target at 45^o to the beam direction. The angular range 30^o to 100^o was covered with the target foil in one position. The foil was then rotated through 90^o to enable the range of angles from 80^o to 150^o to be covered. The effective thickness of the target is a very sensitive function of the angle when it is near 45^o.

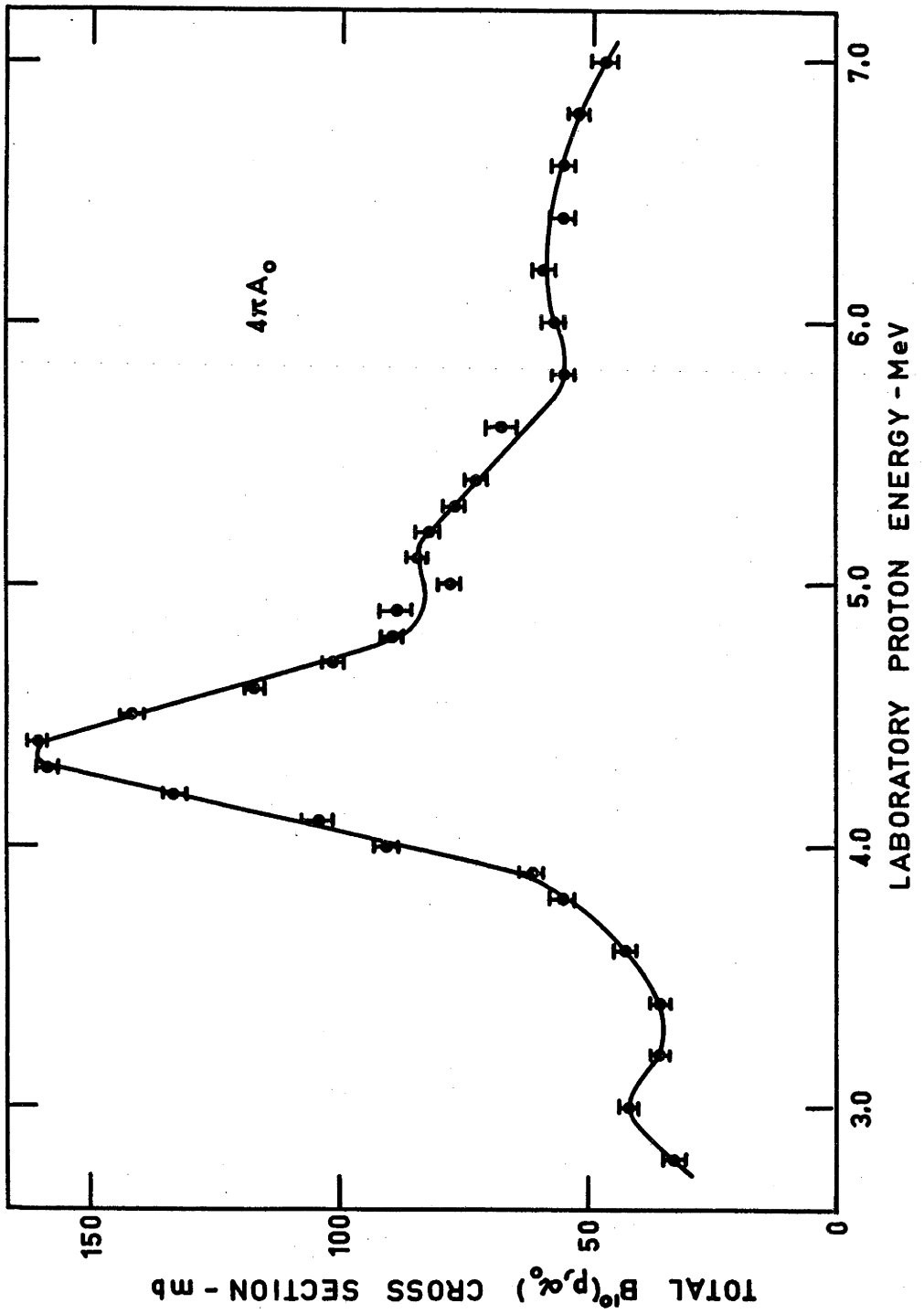

FIG. 4.5 The energy dependence of the total cross section $4\pi A_0$, for the α_0 group from the $B^{10}(p,\alpha)Be^7$ reaction, derived from a complete Legendre polynomial analysis of the α_0 angular distributions.

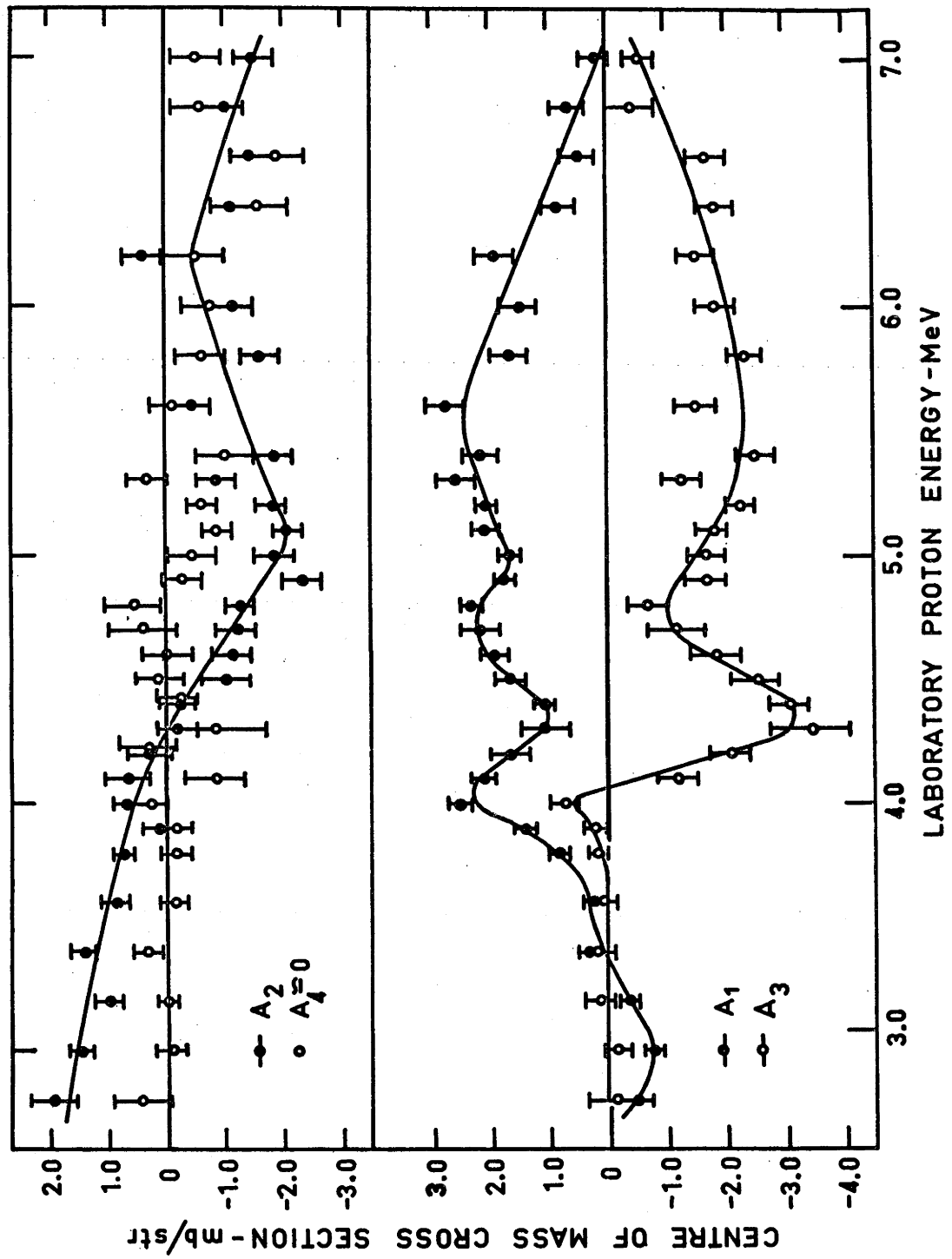

FIG. 4.6 The energy dependence of the coefficients $A_L (1 \leq L \leq 4)$ obtained from the expansion $\sum_L A_L P_L (\cos \theta)$ of the angular distributions of the α_0 group from the $B^{10}(p,\alpha)Be^7$ reaction.

Hence a monitor detector, fixed at a laboratory angle of 90^{o}, was used throughout the measurement of the angular distribution to allow normalisation of the forward and backward angle data.

4.3 Analysis and Discussion of Results

4.3.1 Least Squares Analysis of Angular Distributions

The angular distributions are most amenable to analysis in terms of resonance theory if they are expressed as a series expansion of the form

$$W(\theta) = \sum_{L=0}^{N} A_L \, P_L \, (\cos \theta) \, .$$

All of the α_o and α_1 angular distributions taken were analysed in this way on an I.B.M. 1620 computer using the least squares method of Rose (Ro 53). It was found that these thirteen-angle distributions could be expanded in a physically meaningful way with terms up to $L = 6$. The coefficients A_4, A_5 and A_6 do not differ significantly from zero over the energy range covered. The detailed results for α_o are displayed in figs 4.5 and 4.6, and those for α_1 in fig 4.7. Both residual and statistical errors were calculated (Ro 53) for all coefficients, and those quoted here are in each case the larger of the two.

4.3.2 The Ep = 2.2 MeV Level

The known resonance (Ov 62) (An 62) (Ce 56) at Ep = 2.18 MeV (10.67 MeV excitation in C^{11}) is very evident. Overley and Whaling

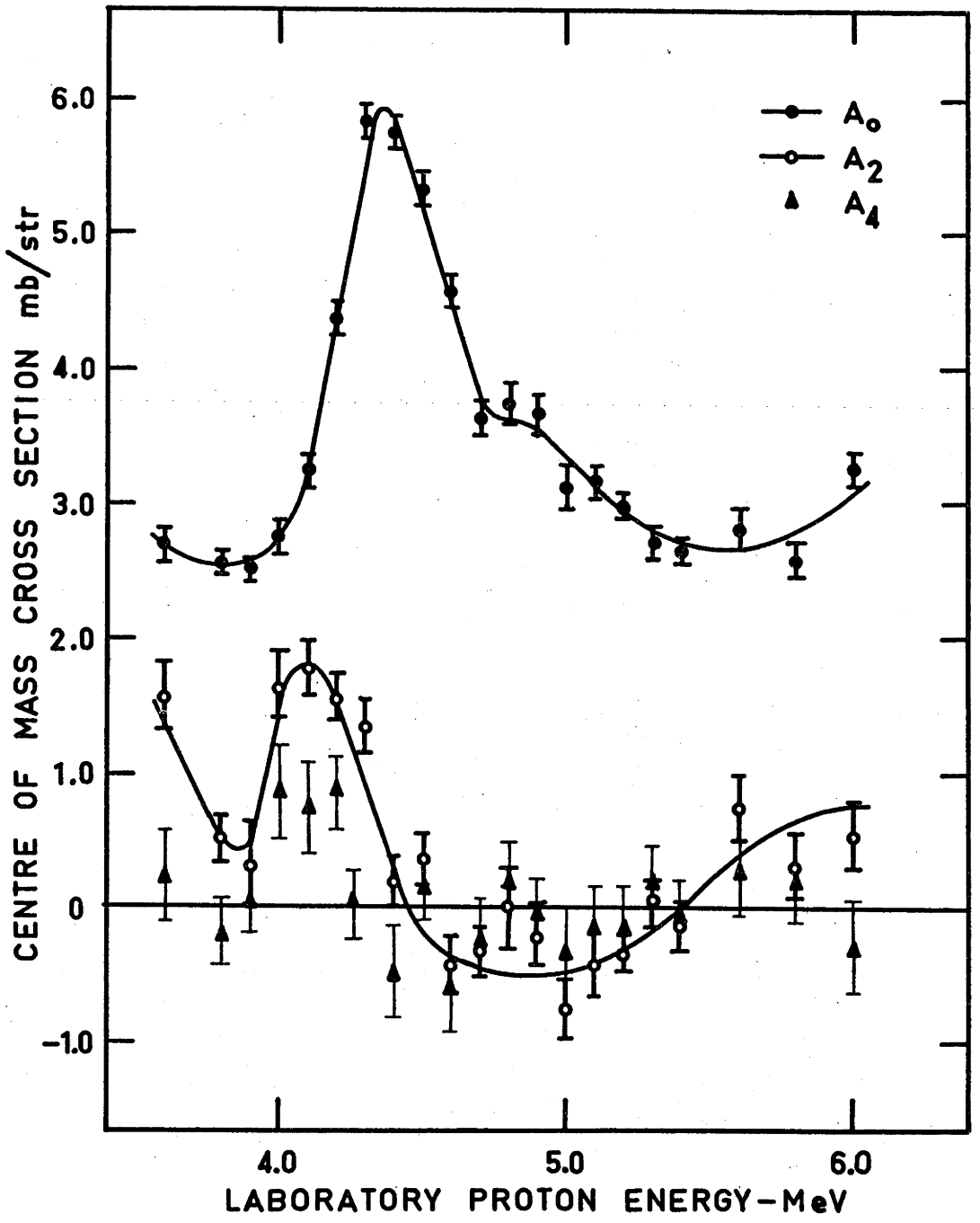

FIG. 4.7 The energy dependence of the coefficients A_L (L = 0, 2, 4) obtained from the expansion $\sum_L A_L P_L (\cos \theta)$ of the angular distributions of the α_1 group from the $B^{10}(p,\alpha)Be^7$ reaction.

(Ov 62), on the basis of their proton elastic scattering cross section and the non-resonant behaviour of the α_1 group, have suggested that the level is $J^{\pi} = 9/2^{+}$, with the proton and α_o partial widths contributing equally to the total width of 200 keV. This figure for Γ is confirmed here by a measurement of (220 $\pm$ 30) keV. Unfortunately it was not possible in the present experiment to take angular distributions over this resonance in an attempt to verify this spin and parity assignment because the low energy α-particles could not be detected at backward angles.

4.3.3 The Ep = 4.4 MeV Level

The dominant resonance in the remainder of the energy range covered is that at a bombarding energy of 4.4 MeV. This level, at 12.65 MeV excitation in C^{11}, is resonant for both α_o and α_1, and has a total width of approximately 400 keV. These values are in agreement with those of Ophel et al. (Op 62), who reported a level at 4.36 MeV, 400 keV wide, from studies of the $B^{10}(p,\alpha\gamma)$ and $B^{10}(p,p'\gamma)$ reactions. The absolute integrated cross sections ($4\pi A_o$) for the $B^{10}(p,\alpha_o)$ and $B^{10}(p,\alpha_1)$ reactions at Ep = 4.4 MeV are (160 $\pm$ 30) mb and (75 $\pm$ 15) mb respectively. The major contribution to the error is from the uncertainty in the target thickness measurement.

If it is assumed that there is only a single level in the peak

at 4.4 MeV, a lower limit on the spin value J may be imposed from a knowledge of the total cross section. The sum of the resonant reaction cross sections, measured at the peak of the resonance can be expressed in the form (Bl 52a)

$$\sigma = \frac{2J + 1}{(2s + 1)(2I + 1)} \cdot 4\pi \lambda\!\!\!^{-2} \frac{\Gamma_p \Gamma_r}{(\Gamma_p + \Gamma_r)^2}$$

where Γ_p is the partial width for the incoming channel,

Γ_r is the partial width for all open reaction channels,

I is the target nucleus spin,

s is the projectile spin,

and $\lambda\!\!\!^{-}$ is the reduced de Broglie wavelength of the incident particle. The maximum value that the expression $\Gamma_p \Gamma_r / (\Gamma_p + \Gamma_r)^2$ has is $^1/_4$ when $\Gamma_p = \Gamma_r$ so that one has the inequality

$$\sigma \leq \frac{\pi \lambda\!\!\!^{-2} (2J + 1)}{(2s + 1)(2I + 1)}$$

The lower limit on the spin of the present compound state, imposed by the integrated (p,α_0) and (p,α_1) cross sections after subtraction of an estimated background from other states, is $J \geqslant {}^{11}/_2$. However, these allowed spins all give α particle reduced widths exceeding the Wigner sum rule limit (Te 52), which suggests that the present values for the cross sections must be too large and that lower spins than $J = {}^{11}/_2$ must be considered. (It is notable that if the

present data were normalised to that of Overley and Whaling (Ov 62) at Ep = 2.2 MeV, then the integrated cross section at 4.4 MeV would be approximately 280 mb. After background subtraction, this would imply a spin $J \geq 19/2$.)

The measured total width Γ = 400 keV is more accurate than the integrated cross section, and this can be used to derive an upper limit to the possible spin values of the level. The total width of the level is the sum of the contributions from all open channels. The contribution from the (p,He^3) reaction (see fig 4.8) can be neglected, as can that from the (p,γ) reaction (Op 62). The total width is therefore given by

$$\Gamma = \Gamma_p + \Gamma_{\alpha_o} + \Gamma_{\alpha_1}$$

At the peak of the resonance $\Gamma_{\alpha_1} / \Gamma_{\alpha_o} = \sigma(p,\alpha_1) / \sigma(p,\alpha_o) = 0.37$. The maximum theoretical cross section is obtained if $\Gamma_p = 1.37\,\Gamma_{\alpha_o}$. For spins $< 11/2$ this will result in the smallest difference between the measured and the maximum theoretical cross section. Using this relation, the values $\Gamma_p = 0.20$ MeV, $\Gamma_{\alpha_0} = 0.15$ MeV and $\Gamma_{\alpha_1} = 0.05$ MeV are derived. Because of the small penetrabilities of the α particles relative to the protons, the upper limit to the possible spin values of the level are imposed by the α particles. The reduced partial widths for α_o and α_1, for different orbital angular momenta, are shown in table 4.1. Also shown is the α-particle Wigner limit

and the maximum possible spin value for each angular momentum.

TABLE 4.1

The reduced partial widths for α_o and α_1 from the $B^{10}(p,\alpha)Be^7$ reaction at the Ep = 4.4 MeV resonance

ℓ_α	$\gamma^2_{\alpha_o}$ MeV	$\gamma^2_{\alpha_1}$ MeV	Upper limit to J^π α_o	α_1	W.L. MeV
0	0.027	0.009	$^3/_2^-$	$^1/_2^-$	
1	0.030	0.011	$^5/_2^+$	$^3/_2^+$	
2	0.047	0.016	$^7/_2^-$	$^5/_2^-$	
3	0.077	0.030	$^9/_2^+$	$^7/_2^+$	$\gamma^2_\alpha \leq 1$
4	0.385	0.16	$^{11}/_2^-$	$^9/_2^-$	
5	4.78	1.90	$^{13}/_2^+$	$^{11}/_2^+$	

The above values of $\gamma^2_{\alpha_o}$ and $\gamma^2_{\alpha_1}$ are less than the Wigner limit for orbital angular momenta $\ell_{\alpha_o} \leq 4$ and $\ell_{\alpha_1} \leq 5$, giving $J \leq {}^9/_2$.

Contributions from any A_L, with L odd, must be due to interference effects from other levels. Over the region of the resonance, all A_L with L even and greater than 2, are zero. Also at the resonance (Ep = 4.4 MeV) A_2 goes through zero which suggests that the resonance contributions to both the α_o and α_1 angular distributions there are isotropic. The possible spin and parity assignments

$^9/_2^+$, $^9/_2^-$ and $^7/_2^-$ cannot give isotropic distributions. The value $^7/_2^+$ does yield an isotropic distribution for α_o and α_1 however if it is assumed that only s-wave protons contribute, the maximum possible cross sections at the peak for J = $^7/_2$ are then 64 percent of the measured values. The existence of the large resonant A_3 term in the α_o distribution could be explained as interference between the $^7/_2^+$ state and a neighbouring state of $^1/_2^-$, as such an interference would contribute an L = 3 term only.

A tentative assignment of $J^\pi = {}^7/_2^+$ was therefore adopted, and using it, partial widths Γ_p, Γ_{α_o} and Γ_{α_1} were calculated from the measured (p,α_o) and (p,α_1) total cross sections (reduced by 36 percent) and a total width of 400 keV. The dimensionless reduced widths for the state,

$$\theta = \gamma^2 \left[2\mu a^2 / (3\hbar^2)\right]$$

where μ is the reduced mass of particles A_1 and A_2

and a is the channel radius defined as

$$a = 1.40 \, (A_1^{\frac{1}{3}} + A_2^{\frac{1}{3}}) \times 10^{-13} \text{ cm.}$$

do not exceed the Wigner sum rule limits. The partial widths have not been modified by the effect of level shifts (La 58). Table 4.2 gives the properties of the 12.65 MeV state of C^{11} derived from the present experiment.

TABLE 4.2

Properties of the 12.65 MeV C^{11} level, from the $B^{10}(p,\alpha)Be^{7}$ reaction

J^{π}	LABORATORY ENERGY MeV				θ_p^2	$\theta_{\alpha_o}^2$	$\theta_{\alpha_1}^2$
	E_p	p	α_o	α_1			
$^7/_2{}^+$	4.36	0.20	0.15	0.05	0.02	0.29	0.08

4.3.4 Other Levels

The α_1 yield is peaked strongly at forward angles at Ep = 3.0 MeV (see fig 4.4), which could be due to the state which has been reported (Op 62) (An 62) (Ce 56) at 11.44 MeV excitation in C^{11}. The α_o yield is only weakly resonant at this energy. The anomaly at a proton energy of 5.10 MeV depicted by Ophel et al. (Op 62), corresponding to an excitation energy of 13.33 MeV in C^{11}, is confirmed. The broad peak at Ep = 6.3 MeV covers the region where several resonances have been observed by Kalinin et al (Ka 57) and in the $B^{10}(p,n)$ work described in chapter 3. The analysis of section 4.3.3 suggests that one of these states could be the $J^{\pi} = 1^-$ state interfering with that at 4.4 MeV.

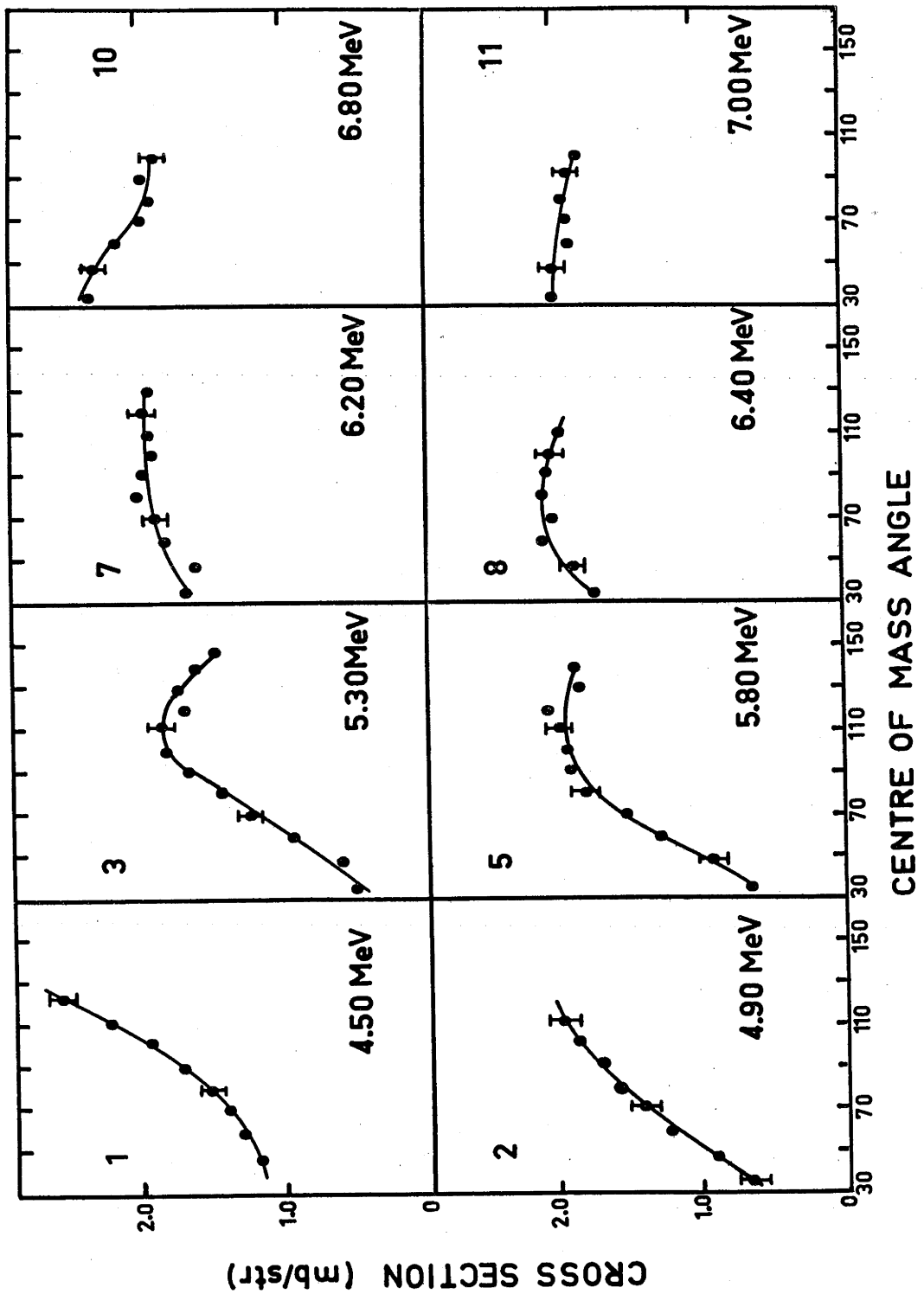

FIG. 4.9 Representative angular distributions of the ground state He^3 group from the $B^{10}(p,He^3)Be^8$ reaction over the proton energy range Ep = 4 to 7 MeV. No theoretical fitting has been attempted.

The measured excitation functions are shown in fig 4.8 together with one for the $B^{10}(p,\alpha)Be^{7}$ ground state α particles, taken at a laboratory angle of 90^{o}. The (p,He^{3}) reaction is only weakly resonant, in contrast to the (p,α) reaction. The excitation functions do pass through slight maxima at similar energies to those occurring in the (p,α) reaction. However it is significant that the $B^{10}(p,He^{3})$ angular distributions do not vary appreciably over the proton energy range 4.5 to 7.0 MeV (see fig 4.9) and this, together with the lack of structure in the excitation function, suggests a predominantly direct interaction mechanism.

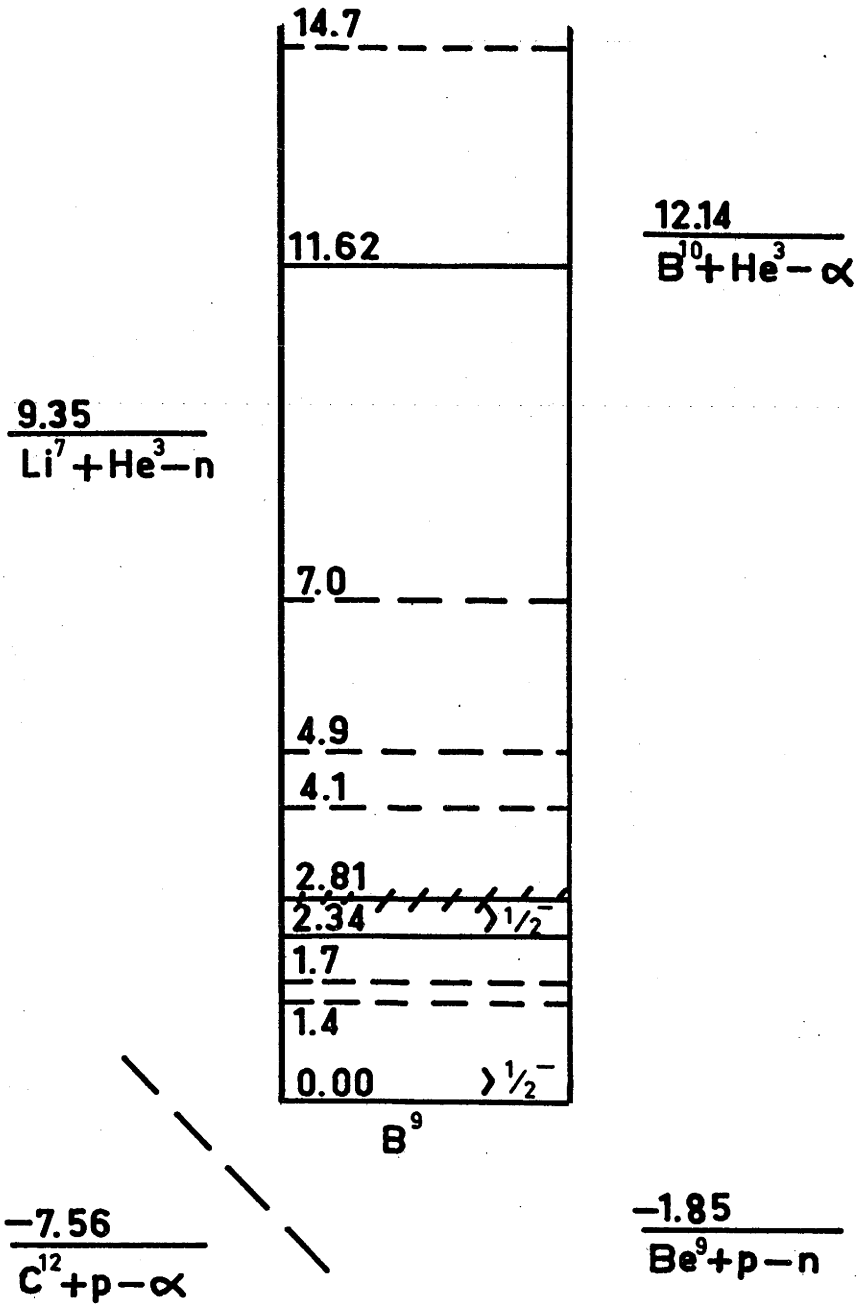

FIG. 5.1 The energy level diagram of B^9. Definitely established levels are shown as full lines and other reported levels are shown dashed.

CHAPTER 5

THE ENERGY LEVELS OF B^9

5.1 Introduction

The energy level structure of B^9 has been investigated by many workers. Most of the experiments involved measuring neutron groups, and the difficulty of these measurements has resulted in considerable uncertainty as to the number and excitation energy of the levels of B^9. Up to an excitation energy of 17 MeV, only the ground state, 2.34 and 2.81 MeV levels (La 62) and a level at 11.62 MeV (Wh 63) have been established definitely.

In figure 5.1, the definitely established levels of B^9 are shown as full lines and other reported levels are shown dashed. A possible level near 1.4 MeV has been suggested from independent studies of the $Be^9(p,n)B^9$ neutrons by Marion and Levin (Ma 59), Takayanagi et al. (Ta 61) and Saji (Sa 60). From the same experimental data Saji (Sa 60) also suggested further levels at 4.1 and 4.9 MeV excitation energy. Symons and Treacy (Sy 62) have suggested a level at 1.7 MeV from a study of the $C^{12}(p,\alpha)B^9$ reaction, while Knowles (Kn 58) suggested a possible level at 7.0 MeV from his preliminary study of the same reaction. A recent experiment on the $Li^7(He^3,n)B^9$ reaction by Dietrich et al.

(Di 63) has indicated a further level at an excitation energy of 14.70 MeV.

The present experiment was undertaken in an effort to check the reported levels, and to search for new levels in B^9 by studying α-particle spectra from the $B^{10}(He^3,\alpha)B^9$ reaction in the energy range from 3.0 to 10.5 MeV.

5.2 Experimental Procedure and Results

The apparatus used for this experiment was the same as that used for the $B^{10}(p,\alpha)Be^7$ experiment and has been described in chapter 4.

A 50 μgm/cm^2 thick self-supporting boron target * (containing 89 percent B^{10} and 8 percent B^{11} by weight) was bombarded with 0.1 μA of doubly charged He^3 ions from the Canberra tandem accelerator with helium injector. The target was mounted at 45° to the beam axis in the centre of a scattering chamber and a 300 Ω-cm surface barrier counter, also inside the chamber, was mounted 6.45 cm from the target at a laboratory angle of 90°. The reverse bias on the counter was adjusted so that the range in the counter of the ground state α-particle group from the $B^{10}(He^3,\alpha)B^9$ reaction was always less than the sensitive depth, even though the

---

* Thanks are due to Mr. F.A. Howe and associates at A.W.R.E., U.K., who made this target.

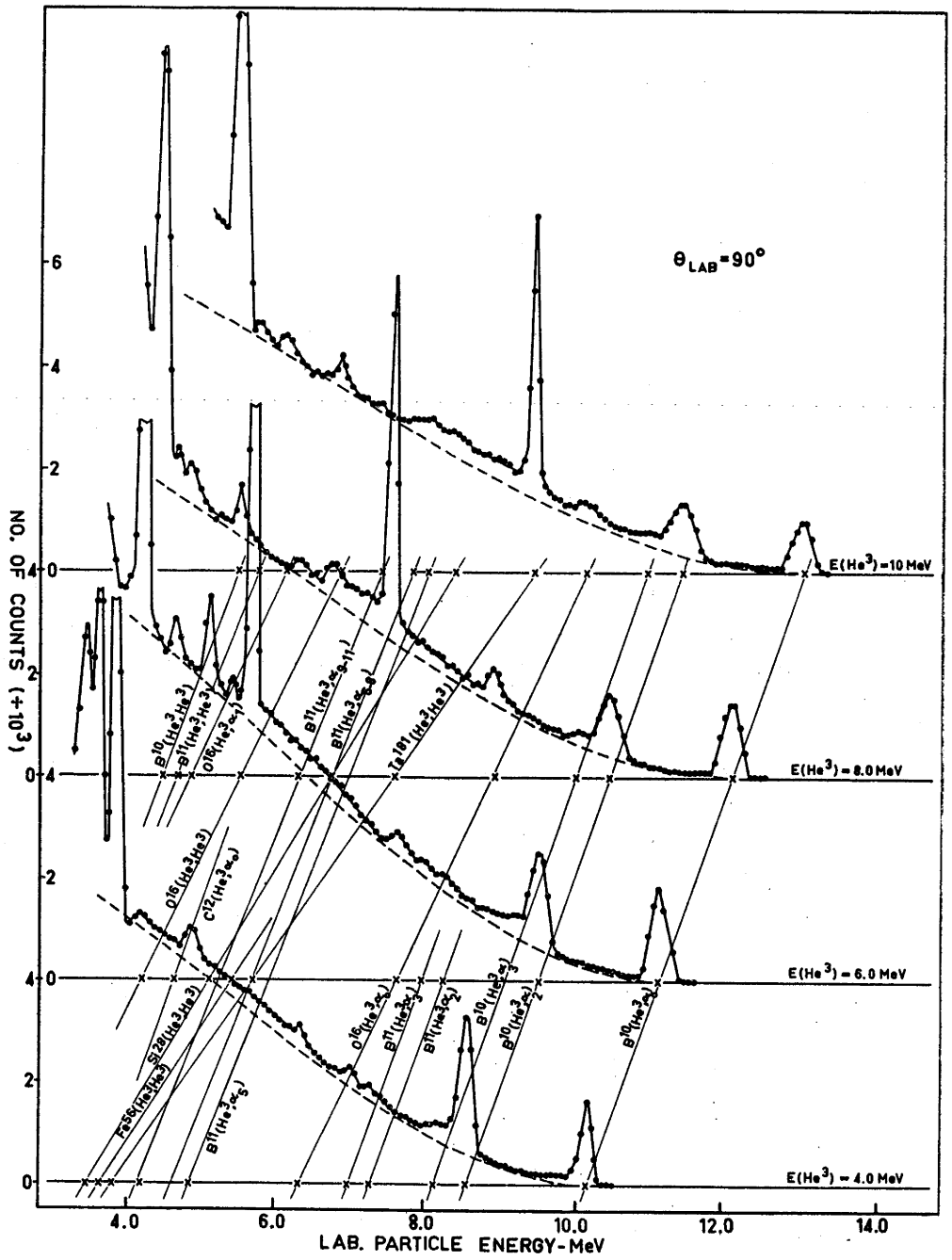

FIG. 5.2 A representation of the method used to analyse α-particle spectra from the He^3 bombardment of an enriched B^{10} target, in a search for excited states of B^9. Every second analyser channel has been plotted and statistical errors are of the order of the size of the points. The dashed curves are the fits to each α-particle continuum, of a direct four-body breakup formula of the form

$$N(E) = k E^{\frac{1}{2}} (E_{max} - E)^2$$

bias required at the maximum He^3 energy used caused a slight loss of resolution.

Spectra were recorded at a laboratory angle of 90^o every 0.5 MeV from 3.0 to 10.5 MeV incident He^3 energy. These spectra were plotted as in figure 5.2, and the positions of the various peaks were marked on the axis of each. The energy of a reaction product, when detected at a laboratory angle of 90^o, is given by

$$E_1 = \frac{(M_1 + M_2)(M_3 + M_4)}{(M_2 M_4 - M_1 M_3)} E_3 - \frac{M_4 (M_1 + M_2)}{(M_2 M_4 - M_1 M_3)} Q \qquad (5.1)$$

where E_1 and E_3 are the energy of the incident and detected particles respectively.

Q is the energy released in the reaction.

M_1 and M_2 are the masses of the incident and target nuclei respectively,

and M_3 and M_4 are the masses of the detected and recoil nuclei respectively.

The energy of the reaction products is a linear function of the incident He^3 energy. Hence the slope and intercept of the line produced by each reaction in figure 5.2 assist in the identification of the reaction. For the sake of clarity, only four of the spectra are shown in figure 5.2. As a further check on the identification, the energy of each group was compared with that calculated from

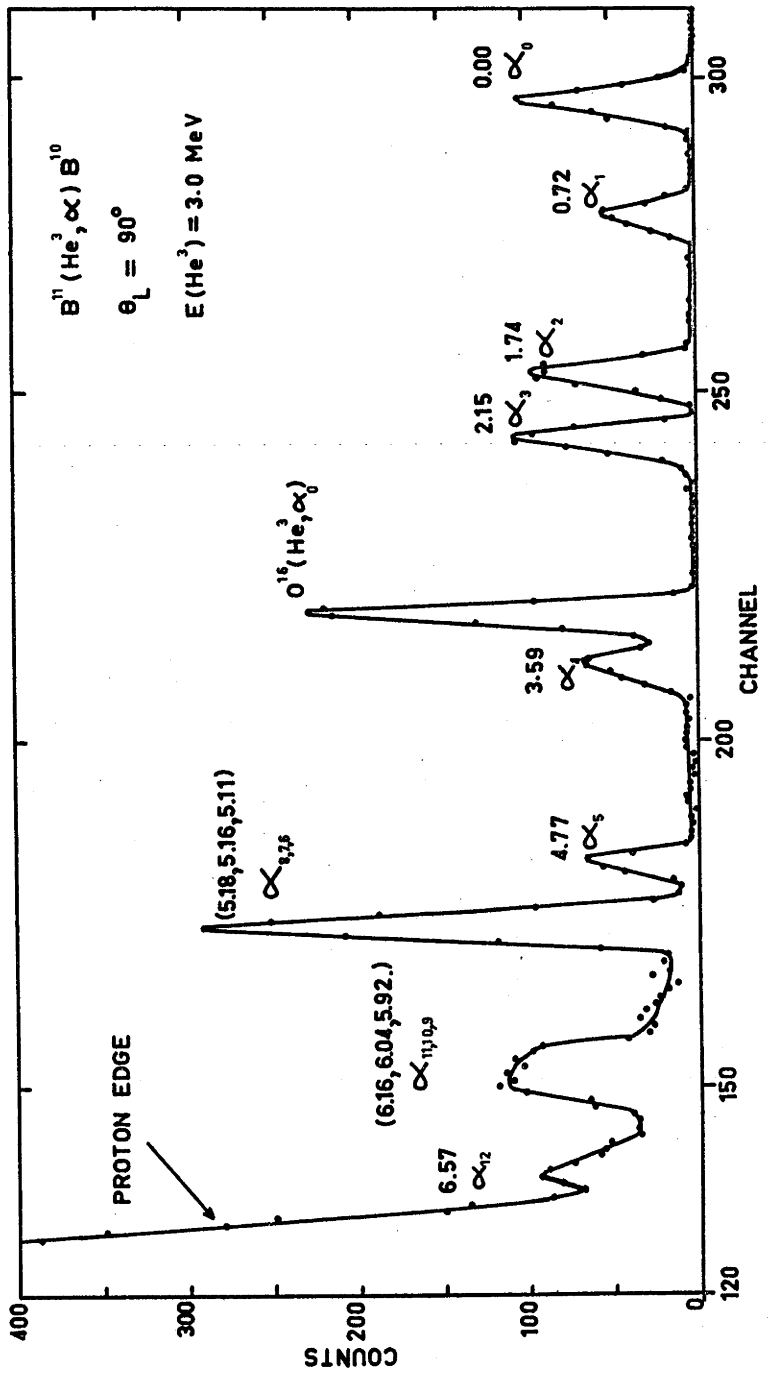

FIG. 5.3 An α-particle spectrum from the bombardment of a B^{11} enriched B_2O_3 target by 3.0 MeV He^3 particles. The groups, observed at a laboratory angle of 90^o, are labelled by the excitation energy in MeV of the B^{10} levels to which they are assigned. The group from the $O^{16}(He^3, \alpha_o)$ reaction is also observed.

the reaction kinematics. The detector energy calibration was obtained from the energy of the well-defined α-particle groups to the ground and 2.34 MeV levels of B^9 (marked α_0 and α_2 on figure 5.2).

The impurity element reactions observed were consistent with those elements reported by the supplier to be present in small amounts in the target material. Tantalum was present because the target was made by evaporation from a tantalum boat.

Alpha-particle groups from the $B^{11}(He^3,\alpha)B^{10}$ reaction behave with incident beam energy in very nearly the same manner as those from the $B^{10}(He^3,\alpha)B^9$ reaction. In order that groups from the former reaction should not be mistaken for new groups from the latter, a separate spectrum, using a B^{11} enriched B_2O_3 target, was taken for comparison. A typical spectrum is shown in figure 5.3.

Spectra from the $B^{10}(He^3,\alpha)B^9$ reaction were also recorded at laboratory angles of 50^o, 75^o, 120^o and 150^o at He^3 energies of 3.5 and 8.0 MeV, but no further α-particle groups were revealed.

No evidence was found in any of the spectra for levels of B^9 below 10 MeV excitation, other than from those previously established. In particular, the suggested levels at 4.1, 4.9 and 7.0 MeV were not observed, although the first two may have been

obscured by the very weak α_2 and α_3 peaks from the $B^{11}(He^3,\alpha)B^{10}$ reaction at low energies, and the α_0 group from the $O^{16}(He^3,\alpha)O^{15}$ reaction at higher energies. The level reported at 1.7 MeV was fitted by a reduced width (Sy 62) of 1 MeV. Such a broad level would be indistinguishable from the α-particle continuum resulting from the disintegration of N^{13} into three α particles and a proton even if its integrated yield was an appreciable fraction of that of the ground state group. This continuum, which was also seen by Povh (Po 59) and by Spencer et al. (Sp 60) makes it difficult to detect broad levels in B^9 by means of the $B^{10}(He^3,\alpha)B^9$ reaction.

A few months after this work had been completed, Whaling (Wh 63) searched for levels in B^9 using the same reaction. A double focussing magnetic spectrometer was used to analyse the reaction products. It was thus possible to discriminate much more strongly against protons and scattered He^3 particles than in the present experiment. The range of excitation from zero to 17 MeV in B^9 was investigated by Whaling using 10 MeV incident He^3 particles. Only one level, at 11.62 MeV, was seen in addition to those already definitely established (see fig 5.1), in agreement with the present results.

5.3 Discussion

The reaction mechanism in the present case is not known,

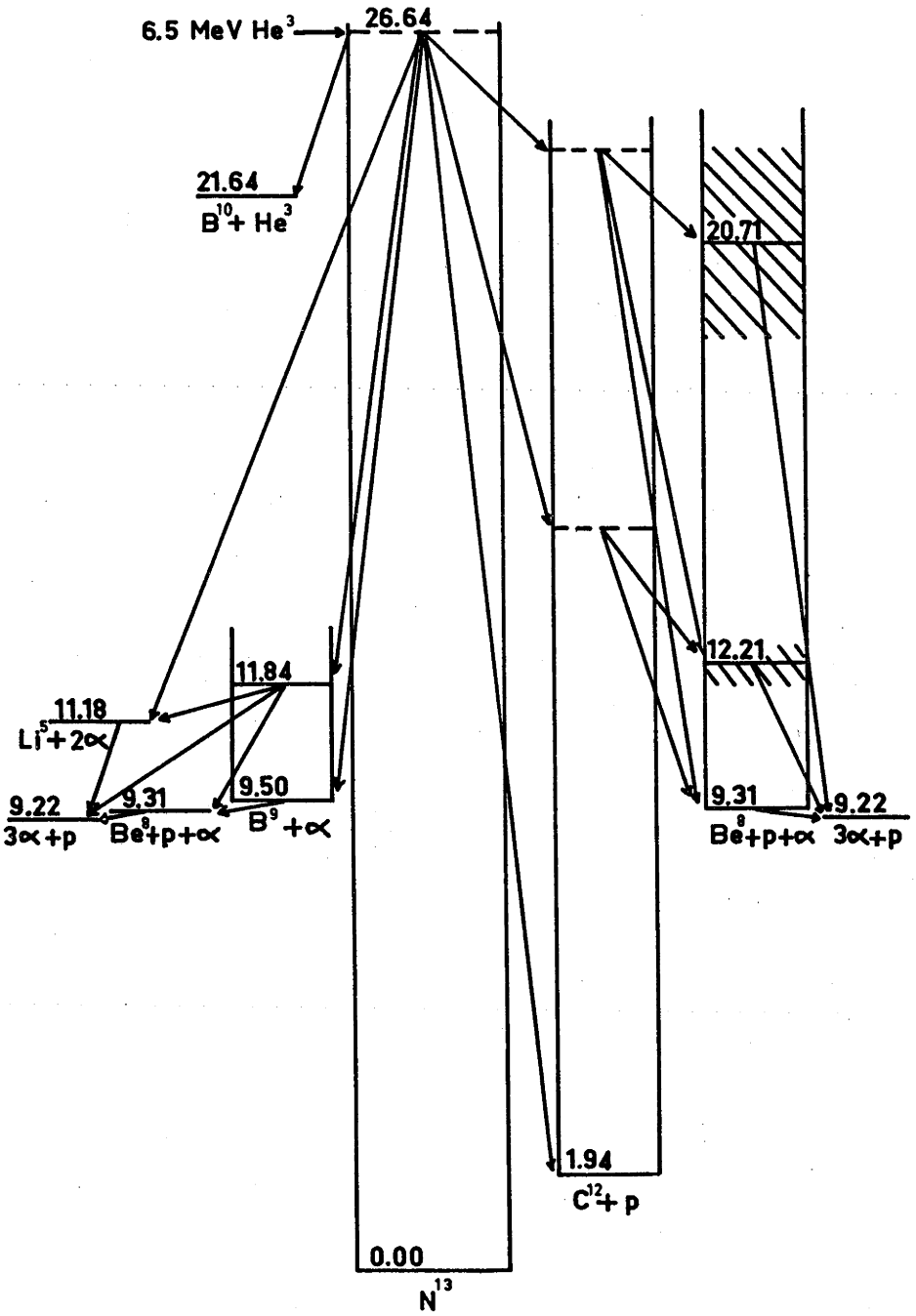

FIG. 5.4 The extremely large number of decay channels available for the excited N^{13} nucleus, produced by the bombardment of B^{10} by 6.5 MeV He^3 ions, is shown. Levels shown dashed in C^{12} represent any one of a large number of possible levels in that excited nucleus.

but if a compound nucleus is formed, this is highly unstable to break up into (3α + p). The extremely large number of decay channels available for the excited N^{13} nucleus are shown in figure 5.4. Many nuclear emulsion studies have been made of the breakup of N^{13} from highly excited states but these provide conflicting evidence on the process. Although most authors find that a proportion of the decays proceed through excited states of intermediate nuclei such as C^{12}, B^{9}, Be^{8} and Li^{5} (see for example (Ne 55)), others suggest that four-body breakup occurs (see for example (Va 63)).

If an extreme case is taken and it is assumed that the decay is purely a direct four-body process, then the energy distribution of the α-particles can be calculated. Assuming that there is no interaction between the particles, the energy distribution of one of them is (Ro 55)

$$N(E) = kE^{\frac{1}{2}} (E_{max} - E)^{2} \qquad (5.2)$$

where k is a normalization constant,

E is the particle energy in the centre of mass space,

and E_{max} is the maximum centre of mass energy available to a single particle in the breakup.

It can be shown, using the method of Lagrangian multipliers that in the centre of mass space, one particle has its maximum energy when the other three move off with equal velocities in the opposite

direction. If the spectrum is recorded at a laboratory angle of 90^{o} then an expression of the same form as equation 5.2 applies with the energies measured in the laboratory system. The dashed curves in figure 5.2 are an evaluation of equation 5.2, normalized to fit each continuum. It is worth noting that only one parameter, the vertical scale, has been adjusted when making these fits. A more critical test of the direct four-body breakup assumption would be to compare the fit in the region of the maximum of the continuum. Unfortunately, this region cannot be observed using solid state counters because of the large background of protons at lower energies.

The four-body breakup formula fits the data quite well in the energy region over which it is applied. It cannot be the whole explanation however, since the experiment itself, through the α-particle transitions to B^{9} states and proton transitions to high excited states of C^{12}, shows that these intermediate nuclei certainly take part. In fact, the α-particle background in the energy region under consideration could probably be fitted equally well by considering the breakup as a series of two-body processes. Breakup through different levels of the intermediate nuclei give rise to broad overlapping groups of α particles. Such groups are especially spread out when very broad levels such as the excited states of Be^{8} are involved. There are a large number of such decay modes available

(see fig 5.4) and it seems probable that these broad groups could be combined to fit the observed continuum.

In order to calculate the shape of the background of α particles from such a process a very large amount of experimental data on the decay mode of N^{13} would be required. Some of the data required would be:

(i) Cross sections for decay to all the excited states of C^{12} from 7.656 MeV to at least 24 MeV.

(ii) Cross sections for the decay to all levels in B^9 up to at least 16 MeV.

(iii) Branching ratios for the decay of each excited state of both C^{12} and B^9 to levels in Be^8, and also to Li^5 for some high excited states of B^9.

(iv) For each decay mode, the shape of the resulting broad α-particle group is required. This shape would be difficult to calculate when the broad excited states of Be^8 are involved.

Very few of the above measurements have been made at present, and none at all at the very high excitation energies required. Lack of this knowledge makes it impossible to carry out background subtractions which might allow evidence to be offered for or against the presence of broad states such as those suggested in the 1.4 to 1.7 MeV region.

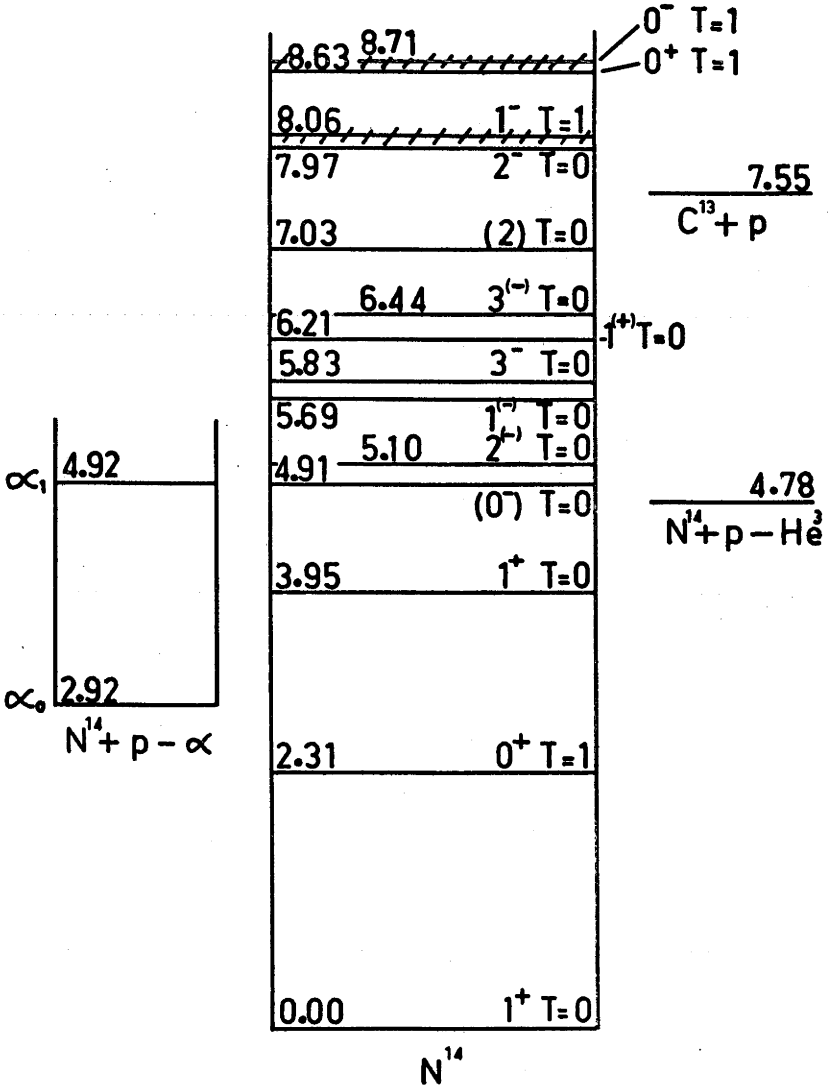

FIG. 6.1 The energy level diagram of N^{14}. Only well-confirmed levels are shown.

CHAPTER 6

ENERGY LEVELS IN N^{14} NEAR THE PROTON THRESHOLD

6.1 Introduction

The energy levels of N^{14} up to 8.71 MeV excitation energy which have been well confirmed are shown in figure 6.1. The level structure in the region immediately above the C^{13} + p threshold is of particular astrophysical interest (Ca 62) as any level existing in this region could influence the C^{12}/C^{13} abundance ratio in stars burning on the Carbon-Nitrogen-Oxygen cycle. Two reported levels fall into this category.

In his study of the neutron groups from the $C^{13}(d,n)N^{14}$ reaction, Benenson(Be 53) observed a level in N^{14} at 7.72 MeV and a possible level at 7.50 MeV in addition to the well-confirmed levels. The level reported at 7.72 MeV could influence the $C^{13}(p,\gamma)N^{14}$ reaction rate at stellar energies. In their study of the γ rays from the same reaction however, Ranken et al. (Ra 58a) saw γ rays from the well confirmed levels up to 7.03 MeV but found no evidence for levels between 7.50 and 8.6 MeV excitation. The $C^{13}(p,\gamma)N^{14}$ reaction cross section has been studied by Hebbard and Vogl (He 60) at proton energies down to 130 keV, and later by Vogl (Fo 62) down to 100 keV. Levels at 7.97 and 8.06 MeV were seen, but no evidence was found for the level reported by Benenson

at 7.72 MeV. No other levels were seen down to an excitation energy of 7.64 MeV. If a level does exist at 7.72 MeV, the work of Hebbard and Vogl shows that it would not influence the $C^{13}(p,\gamma)N^{14}$ reaction rate at stellar energies.

Burge and Prowse (Bu 56), (Ho 57) observed the inelastic scattering of protons from N^{14} using photographic emulsions. In addition to the well-confirmed levels, they reported levels at 7.40 and 7.60 MeV with possible levels at 5.95 and 6.60 MeV. The level reported at 7.60 MeV is also of considerable astrophysical interest. However the evidence provided for this level in the work of Burge and Prowse is not conclusive as the group attributed to it was suspiciously narrow, and was seen at one angle only.

Miller et al. (Mi 56) observed α-particle groups from the inelastic scattering of 21.5 MeV α particles from N^{14}. All levels reported by them up to 8 MeV excitation have been well confirmed. An additional level was reported at 8.45 MeV but no evidence was found for levels at 7.40 or 7.60 MeV. Groups from T = 1 levels would be strongly inhibited by isobaric spin selection rules however, and would not necessarily be seen with this reaction. Recently Clayton (Cl 62) has investigated the level structure of N^{14} between 4 and 8 MeV excitation energy by observing the α-particle groups from the $N^{15}(He^3,\alpha)N^{14}$ reaction. He observed all the well-confirmed

levels up to 8.06 MeV as well as a possible new level at 6.048 MeV. However, he did not find any evidence for the levels reported at 6.70, 7.40 and 7.60 MeV.

Inelastic proton scattering from N^{14} has been studied by Oda et al. (Od 60) using protons at several energies between 7.6 and 14.2 MeV. Proton groups were observed, corresponding to the well-confirmed levels up to 8 MeV excitation. However, only relatively strong groups were observed and not all levels were resolved. Further reports of inelastic proton scattering studies, by Brown (Br 63) using 10.5 MeV protons and by Donovan et al. (Do 63) using 10.2 MeV protons have recently become available. Both of these experiments revealed the well-confirmed levels in N^{14} up to 8 MeV excitation but showed no sign of levels at 6.05, 6.60, 7.40 or 7.60 MeV.

In view of the possibility of rapid changes in the inelastic proton scattering cross section with energy, it was considered desirable to observe the $N^{14}(p,p')$ reaction in a search for the 7.60 MeV level reported by Burge and Prowse using the same bombarding energy and angle of observation as were used previously.

6.2 Experimental Apparatus

The experiment was carried out using monoenergetic protons from the Canberra tandem accelerator. The beam entered a 43 cm.

FIG. 6.2 Schematic representation of the scattering chamber. Numbered items are:

1. Portion of the beam collimator and baffle system.
2. The gas target.
3. Mylar windows (1 mgm/cm^2, Al-coated on each side).
4. Thin Ni windows (0.63 micron entry, 1.26 micron exit).
5. Solid state counter.
6. Detector collimating assembly.
7. Lucite neutron moderator.
8. Electron suppressor and Faraday cup.

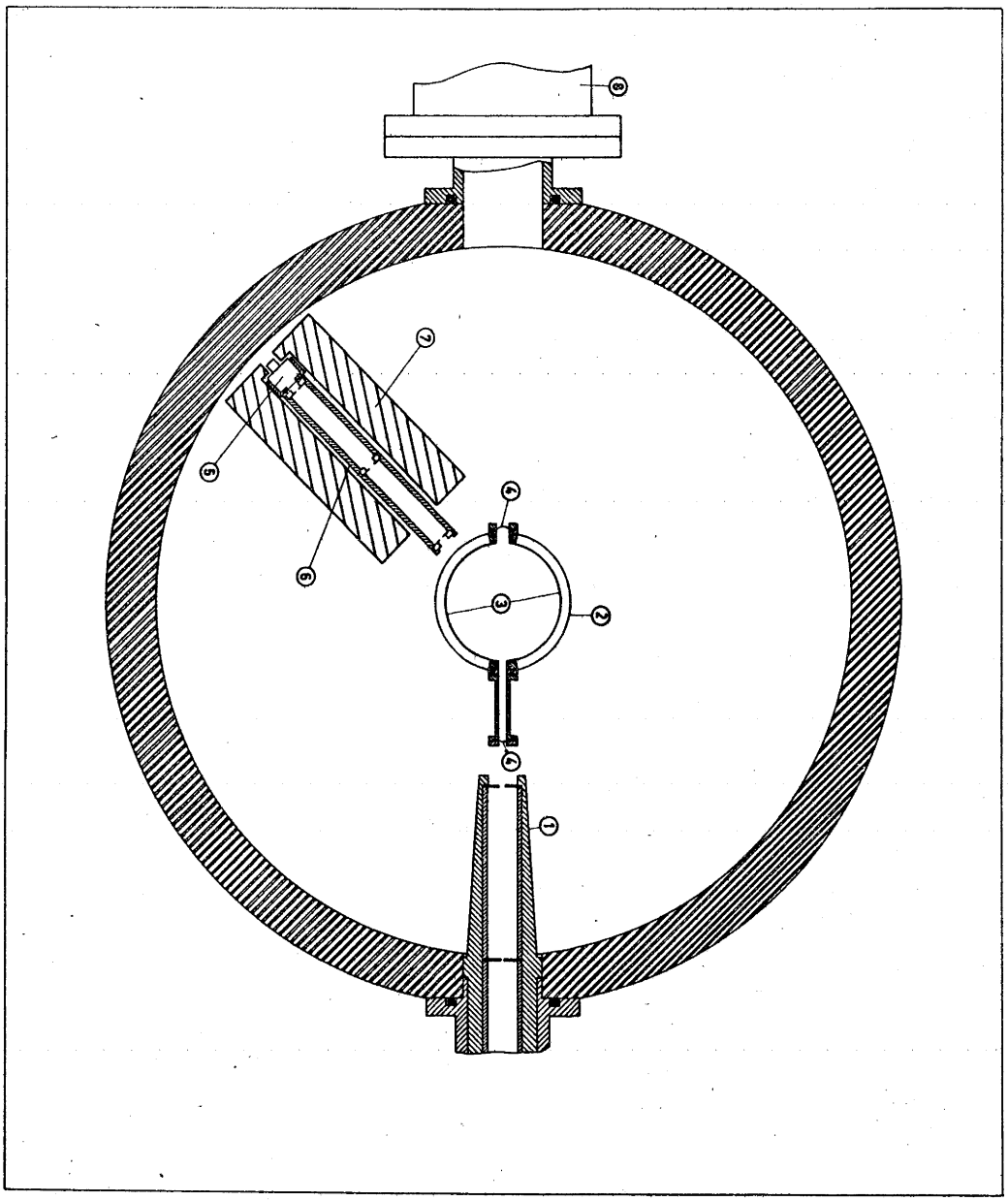
60
1
65
63
3a
3
2
3a
1

diameter scattering chamber through two collimating apertures 0.15 cm in diameter placed 20 cm. apart. An antiscatter aperture, 0.23 cm. in diameter, was placed 10 cm. behind each collimator. Beam currents of the order of 1 μA were used, and the charge was collected in a Faraday cup with both magnetic and electrostatic suppression.

A gas-cell target, already in use in this laboratory, was found to be suitable for the present experiment. Calculation showed (see appendix B) that for 10 MeV incident protons and a filling pressure of 180 mm of mercury, the energy resolution (full width at half maximum) was approximately 58 keV for a 1 MeV proton group leaving the target at a laboratory angle of 60^{o}, and was better for higher energy groups. This resolution was adequate to allow all the well-confirmed levels in N^{14} to be resolved. The experimental apparatus is shown in figure 6.2. A detailed description of the scattering chamber, gas target, beam and counter collimators is given by Ohlsen and Young (Oh 63). The beam entered and left the 7.6 cm. diameter gas target through Ni foils of thickness 0.63 micron and 1.20 micron respectively. The entrance foil was mounted on a 5.7 cm. "snout" and was 10.3 cm. from the centre of the target. The purpose of the snout was to prevent protons scattered by the Ni foil from illuminating the front slit of the counter collimator.

The reaction products left the target through an aluminium coated mylar foil 1 mgm/cm^2 thick. The filling gas was dry oxygen-free nitrogen, and various filling pressures between 40 and 180 mm of mercury were used. A small tray containing KOH pellets was mounted inside the target lid in order to help eliminate the build up of water vapour.

Two 6000Ω-cm gold-silicon surface barrier detectors of 50 mm^2 area, and capable of stopping 8 MeV protons were mounted inside the scattering chamber, 19 cm from the centre of the target. Two rectangular collimating slits were placed between each counter and the target. The dimensions of the collimator systems are given, following the notation of Silverstein (Si 59), in table 6.1.

TABLE 6.1

NOTATION	DESCRIPTION	DIMENSION
$2b_1$	front slit width	0.30 cm
$2b_2$	rear slit width	0.30 cm
ℓ	rear slit height	0.50 cm
R_o	distance from centre of target to rear slit	18.5 cm
h	distance between slits	13.2 cm
	slit thickness	0.038 cm
	angular resolution	2^o

An antiscatter slit 0.40 cm. wide and 0.60 cm high was placed midway between the front and rear slits. Pulses from the counters were amplified by charge-sensitive preamplifiers and Ortec model 203 amplifiers operated in their double delay line mode, and spectra were recorded on 400 channel pulse-height analysers.

6.3 Experimental Procedure

Data were recorded at laboratory angles of 60^{o}, 90^{o} and 120^{o} every 20 keV between the proton energies of 9.30 and 10.00 MeV, and every 100 keV between 10.00 and 10.50 MeV. Initially, spectra were taken with maximum permissible bias on the counters to enable all inelastic proton groups to be stopped within the depletion layer. Peaks from the well confirmed levels in N^{14} were used to provide an energy calibration for the counters. Other proton groups were then identified, both by their calculated energy, and by their energy variation with angle. In addition to their energy variation with incident beam energy and angle of observation, α-particle and He^{3} groups were identified by their increased energy loss in an 0.88 mgm/cm^{2} mylar foil which could be placed in front of the counters. Helium peaks were also typically about twice as broad as proton peaks.

The energy loss of the incident beam in reaching the centre of the target, and of the reaction products in leaving the target, was

calculated, using the stopping cross sections compiled by Whaling (Wh 58). The stopping cross section for low energy reaction products (below about 2 MeV) varied markedly along their path length in the target gas and in the mylar. The procedure adopted at these energies therefore, was to use the stopping cross section appropriate to the energy of the particle entering the absorber to calculate a first order energy loss. This was used to find an approximate average energy of the particle in the absorber, and the stopping cross section appropriate to this energy was then used to obtain a corrected energy loss. Values obtained in this way agreed with those obtained by numerical integration to within the accuracy of reading the stopping cross section curves. In calculating the energy loss in the mylar window, a slight correction was made to the nominal thickness in order to achieve consistency between the proton and heavy particle calibration curves. This correction made negligible difference to the proton calibration.

In all spectra recorded, a very large background of low energy pulses was evident. Part of this was probably due to pile-up of pulses from β particles from the target. If V is the reverse bias applied to the counter, then the sensitive volume is proportional to $V^{\frac{1}{2}}$. For the highly penetrating β particles therefore, the energy deposited in the depletion layer will be roughly proportional to $V^{\frac{1}{2}}$.

It follows that the energy of pile-up pulses will also be proportional to $V^{\frac{1}{2}}$. Substantial reduction in the energy of pile-up pulses from β particles can therefore be gained by lowering the counter bias. Part of the background was also caused by Si(n,p) and Si(n,α) reactions induced in the counter depletion layer by the large flux of neutrons originating in the beam collimator, target and Faraday cup. For single neutron-induced pulses, if n is the number of reactions per second per unit volume of the counter, the number recorded per second is proportional to $nV^{\frac{1}{2}}$. If the resolving time of pulses from the counter is τ, the number of double neutron-induced pulses recorded is proportional to $n^2\tau V$. Lowering the counter bias will therefore greatly reduce the number of those background pulses, especially those at higher energy caused by multiple pulse detection. In the present experiment, the background in the proton energy region corresponding to the excitation energy near the C^{13} + p threshold, was reduced by a factor of three. This background was reduced by a further factor of two under low bias conditions, by surrounding the counter by a 2.5 cm. thick lucite neutron moderator (see fig 6.2) which lowered the average energy of the neutrons incident on the counter. In all the spectra recorded in the investigation of the excitation region near the C^{13} + p threshold, the counter bias was reduced until the broad group due to the partially

FIG. 6.3 A pulse-height spectrum of charged particles from the N^{14} + p reaction, taken at a laboratory angle of 60^{o} and a proton reaction energy of 9.45 MeV. Proton groups are labelled by the energy of the appropriate level in N^{14} and heavy particle groups are labelled by the reaction producing them. The expected position of the peaks from levels reported at 7.40 and 7.60 MeV are marked by arrows. A target-gas filling pressure of 180 mm of mercury was used and the charge incident on the target was 100 μC of protons. In the region between the peaks, the statistical errors are approximately the magnitude of the plotted points.

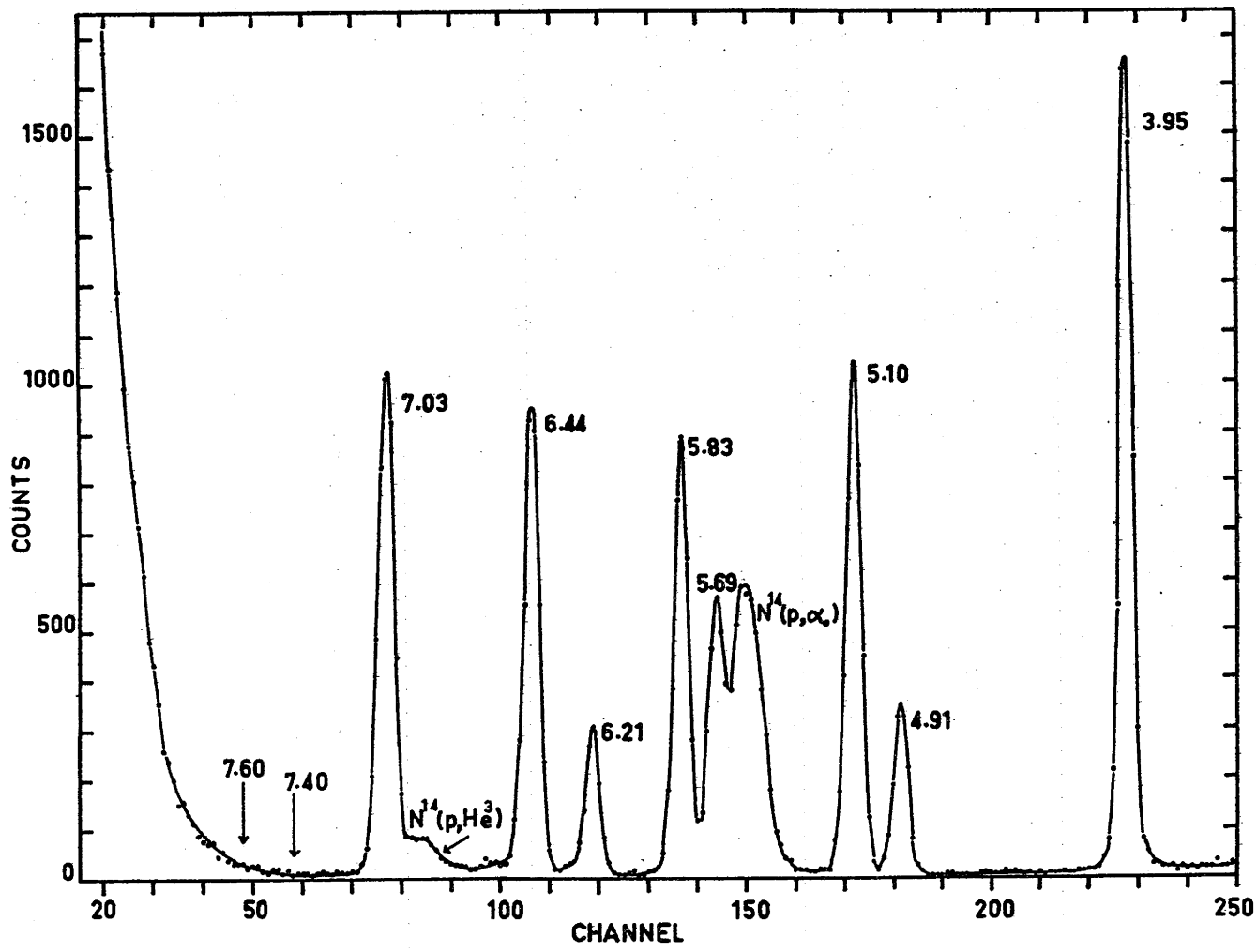
1500
1000
500
0
COUNTS
20
50
100
150
200
250
CHANNEL
7.60
7.40
7.03
$N^{14}(p,He^3)$
6.44
6.21
5.83
5.69
$N^{14}(p,\alpha_1)$
5.10
4.91
3.95

stopped elastic protons was just above the region of interest.

6.4 Results and Discussion

6.4.1 The Energy Levels of N^{14}

Spectra were taken at sufficiently close intervals in energy, so that the whole of the reaction energy range between 9.15 and 9.85 MeV was investigated. All spectra showed similar characteristics. Figure 6.3 shows a spectrum taken at the same proton reaction energy (laboratory energy at the target centre) and angle of observation as was used by Burge and Prowse (Bu 56). The expected position of the peaks from the levels reported by these workers at 7.40 and 7.60 MeV are shown by arrows on the figure. Figure 6.3 shows clearly that no proton groups to these states occur in the present spectrum. At higher proton energies, states of higher excitation appear out of the low energy background, demonstrating that the equipment works satisfactorily for low energy protons.

Of particular interest is the ground state α-particle group from the $N^{14}(p,\alpha)$ reaction shown in fig 6.3. Tracks from this α-particle group should be visible on the emulsions exposed by Burge and Prowse. Accordingly, the properties of this group of tracks have been calculated. The range of protons and α particles in the emulsions was obtained from the Nuclear Emulsion section of this Laboratory (Br 63a), and the geometry and gas pressure of the

experiment was obtained from the publication by Burge and Prowse (Bu 56). It was found that the group would have a track-length distribution whose mean length, width at half height and intensity correspond closely to the properties of the group attributed to inelastic protons from a level at 7.60 MeV in N^{14}. The intensity is measured relative to the proton group to the 7.03 MeV state of N^{14}, shown in the same histogram (Bu 56). At the other angles used by Burge and Prowse, the α-particle group would not be visible. Burge and Prowse found that the analysis of their emulsions was made difficult by a concentration of background grains near the surface. In some of their work this surface deposit was removed by rubbing the emulsions with cotton wool dipped in alcohol. It seems probable therefore, that the ends of the α-particle tracks could easily have been mistaken for proton tracks. In order to check this hypothesis, Dr. Burge has re-examined his emulsions at 60^{o} and checked the present calculations. He has indicated (Bu 63) that the conclusions reached here appear to be well founded, and that the group concerned could easily be the $N^{14}(p,\alpha)$ group. Positive identification of the tracks, as resulting from α particles, was made difficult by their shortness and by the removal of the surface layer of the emulsion.

Following the initial survey, several fixed energies were

FIG. 6.4 A portion of a spectrum of charged particles from the N^{14} + p reaction, taken at a laboratory angle of 60^{o} and an incident proton reaction energy of 10.14 MeV. An incident charge of 10^{4} μC of protons and a gas-filling pressure of 60 mm of mercury were used. A broad proton group, caused by elastic scattering from hydrogen accumulating as water vapour in the gas target, and a first excited state α-particle group from the $N^{14}(p,\alpha)$ reaction are visible. The portion of the spectrum expanded by 10 shows two weak proton groups from known levels in C^{12} and N^{15} at 7.66 and 7.57 MeV excitation respectively. The bulge labelled 'A' is caused by a low-energy proton group from the $N^{14}(p,p')$ reaction to a level in N^{14} at an excitation energy of approximately 8.57 MeV.

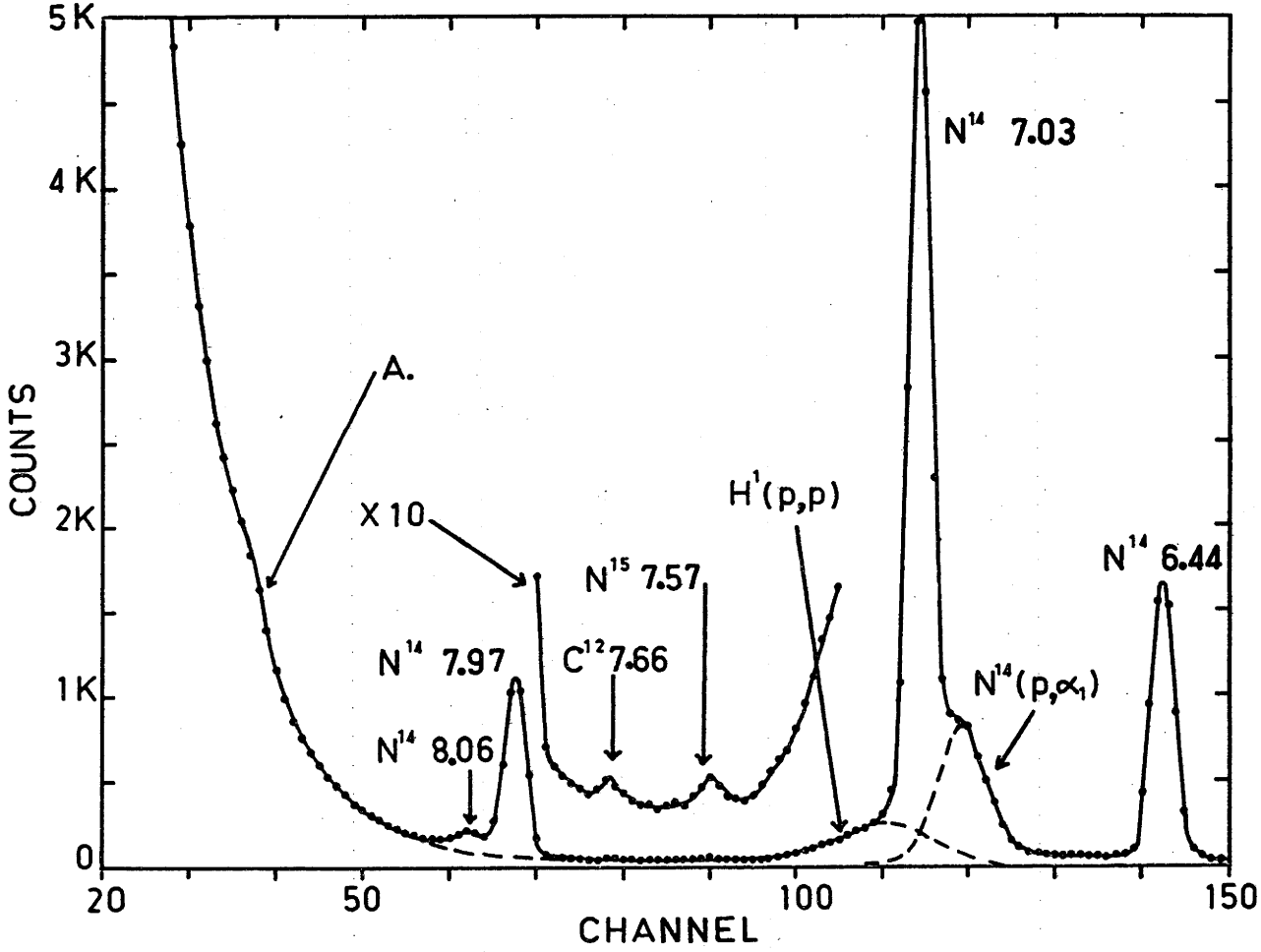
5K
4K
3K
2K
1K
0
COUNTS
20
50
100
150
CHANNEL
A.
X 10
N14 7.97
N14 8.06
C12 7.66
N15 7.57
H1(p,p)
N14 7.03
N14(p,α1)
N14 6.44

selected and bombardments made to obtain good statistics for the known proton groups and to investigate more closely the regions between these groups. The spectrum of fig 6.4 is typical of all the spectra obtained with good statistics every 100 keV between 9.95 and 10.45 MeV (reaction energy) at angles of 60^{o} and 90^{o}, and at 10.25 MeV at an angle of 120^{o}. Statistical accuracy is high, typical errors being of the order of the size of the plotted points on the expanded portion of the curve. Two further proton groups, to the 7.97 and 8.06 MeV levels of N^{14} are clearly visible above the low energy background. The cross section of the group to the 8.06 MeV level is very small for all energies and angles observed, even though it is not inhibited by any known selection rules. A proton group, marked A on the figure, is also evident on the side of the rising background. At higher incident proton energies, this group was fully resolved. Because of its low energy, it could not be positively identified by kinematics at other angles. However because of the intensity of the group, it was attributed to a level in N^{14} at an excitation energy of (8.57 ± 0.05) MeV. The energy calibration technique, which was previously tested on the group to the 7.97 MeV level when this group was of comparable energy, is believed to be satisfactory. The position of this level is not in agreement with the well-confirmed level in this region at 8.63 MeV (Aj 59). However,

there is a relatively large background under the group which probably contains a contribution from the broad proton group resulting from the breakup of the excited N^{14} nucleus into C^{13} + p. It is possible therefore, that a small group from the 8.63 MeV level could have been obscured. The present level could possibly be identified with the level reported by Miller et al. at (8.45 ± 0.07) MeV (Mi 56).

Also present in this spectrum (fig 6.4) is the first-excited-state α-particle group from the $N^{14}(p,\alpha)$ reaction, and a broad group from the $H^1(p,p)$ reaction resulting from water vapour present in the target. The expanded section of the spectrum shows proton groups from the 7.57 MeV level of N^{15} and the 7.66 MeV level of C^{12}. Other C^{12}, N^{15}, and O^{16} peaks were also observed in other regions of the spectrum.

None of the spectra taken provided evidence for groups to the levels of N^{14} reported at 7.40 and 7.60 MeV. A group to the N^{14} level, of the same magnitude as that to the 7.57 MeV level of N^{15} (see fig 6.4), would have a laboratory cross section of 11.5 μb/sr. An upper limit of 2 μb/sr is therefore set to the cross section of a group (which would appear as a statistically significant peak) to any level in N^{14} near the C^{13} + p threshold.

An upper limit of 5 μb/sr has been found for the cross section to a 6.05 MeV state of N^{14} suggested by Clayton (Cl 62). In some of

the spectra, a weak group appeared at an energy close to that expected for this level. It was demonstrated however, both by the energy variation of this peak with the angle of observation, and by recording a spectrum with air in the target, that the group was from the 6.13 MeV level of O^{16}. It was estimated from the intensity of the group, that up to 0.5 percent O^{16} was present in the target when badly contaminated with water vapour.

In summary, it may be said that although proton groups to all the well-confirmed levels in N^{14} up to 8.06 MeV excitation were observed, no evidence was found for the levels reported at 6.0, 6.6, 7.4 and 7.6 MeV (Bu 56), or at 6.05 MeV (Cl 62). A proton group, possibly corresponding to a new level in N^{14} at 8.56 MeV was seen. An upper limit of 2 μb/sr has been placed on the inelastic proton scattering cross section from any level of astrophysical importance at an excitation in N^{14} near the C^{13} + p threshold.

6.4.2 Excitation Functions and Levels in O^{15}

Angular distributions of the first nine inelastic proton groups from the $N^{14}(p,p')$ reaction have been measured by Brown (Br 63). For these measurements an incident reaction proton energy of 10.36 MeV was used. An attempt is being made by Brown to fit these distributions by a direct interaction distorted wave calculation leading to N^{14} states of configurations proposed by Warburton and Pinkston. It is therefore of interest to look at these cross sections

FIG 6.5 The excitation function, at three angles of the proton group to the 2.31 MeV state of N^{14}. At the higher energies there is a pronounced minimum in the angular distribution at 90^{o}.

FIG. 6.6 The excitation function, at three angles, of the proton group to the 3.95 MeV state of N^{14}. The O^{15} levels corresponding to the resonances shown in figs. 5.10 and 5.12 appear to have some influence on the cross section. This is particularly noticeable at 90^{o}. The angular distribution is varying with energy near 10.4 MeV proton reaction energy.

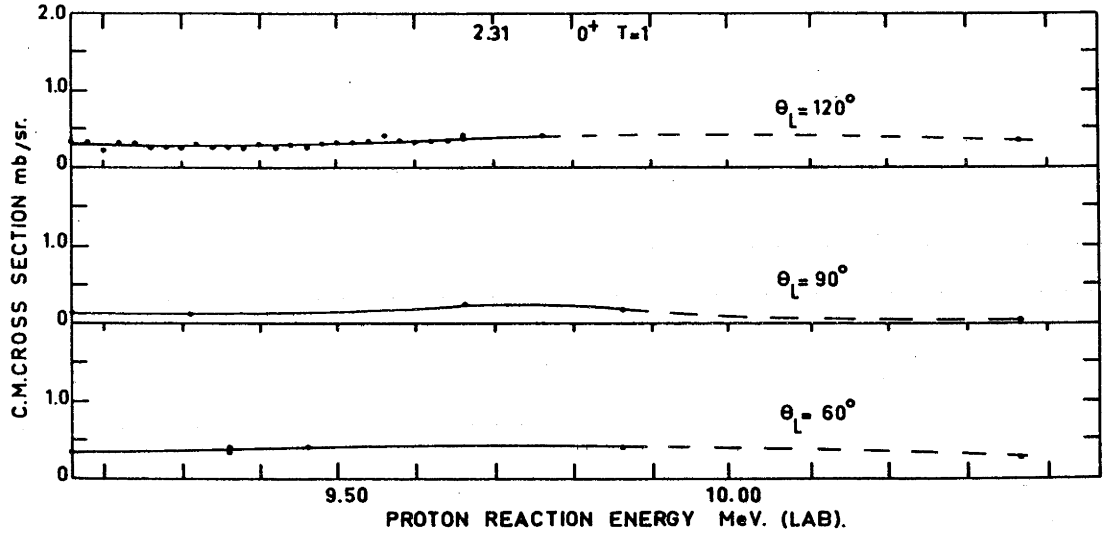
2.31 0+ T=1
θL = 120°
θL = 90°
θL = 60°
C.M.CROSS SECTION mb/sr.
2.0
1.0
0
9.50
10.00
PROTON REACTION ENERGY MeV. (LAB).

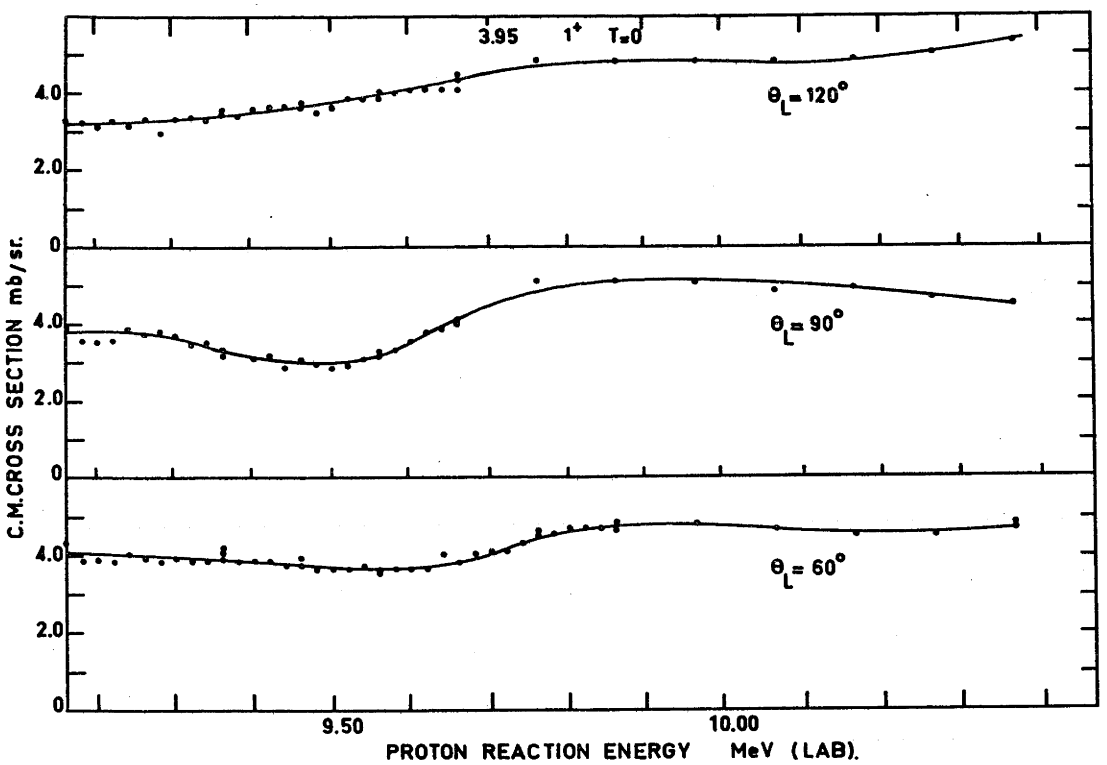
3.95 1+ T=0
θL = 120°
θL = 90°
θL = 60°
C.M.CROSS SECTION mb/sr.
4.0
2.0
0
9.50
10.00
PROTON REACTION ENERGY MeV (LAB).

X63-545

FIG. 6.7 The excitation function, at three angles, of the proton group to the 4.91 MeV state of N^{14}. The O^{15} levels corresponding to the resonances shown in figs. 5.10 and 5.12 may have some influence on the cross section. The angular distribution is varying with energy near 10.4 MeV proton reaction energy.

FIG. 6.8 The excitation function, at three angles, of the proton group to the 5.10 MeV state of N^{14}. The cross section is influenced by the O^{15} levels corresponding to the resonances shown in figs. 5.10 and 5.12. This is evident from the significant changes in the angular distributions over much of the energy range shown.

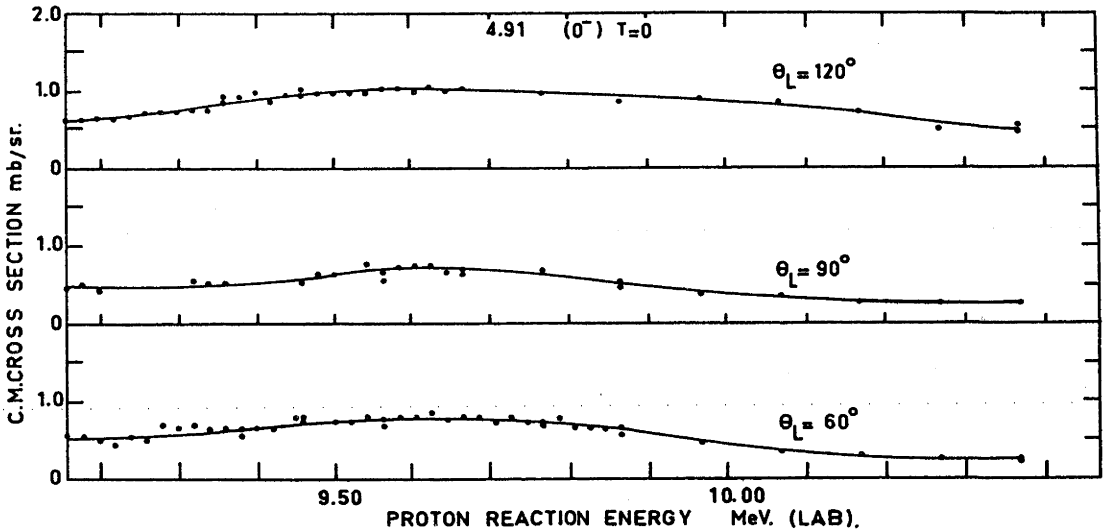
4.91 (0⁻) T=0
θL= 120°
θL= 90°
θL= 60°
2.0
1.0
0
C.M.CROSS SECTION mb/sr.
9.50
10.00
PROTON REACTION ENERGY MeV. (LAB).

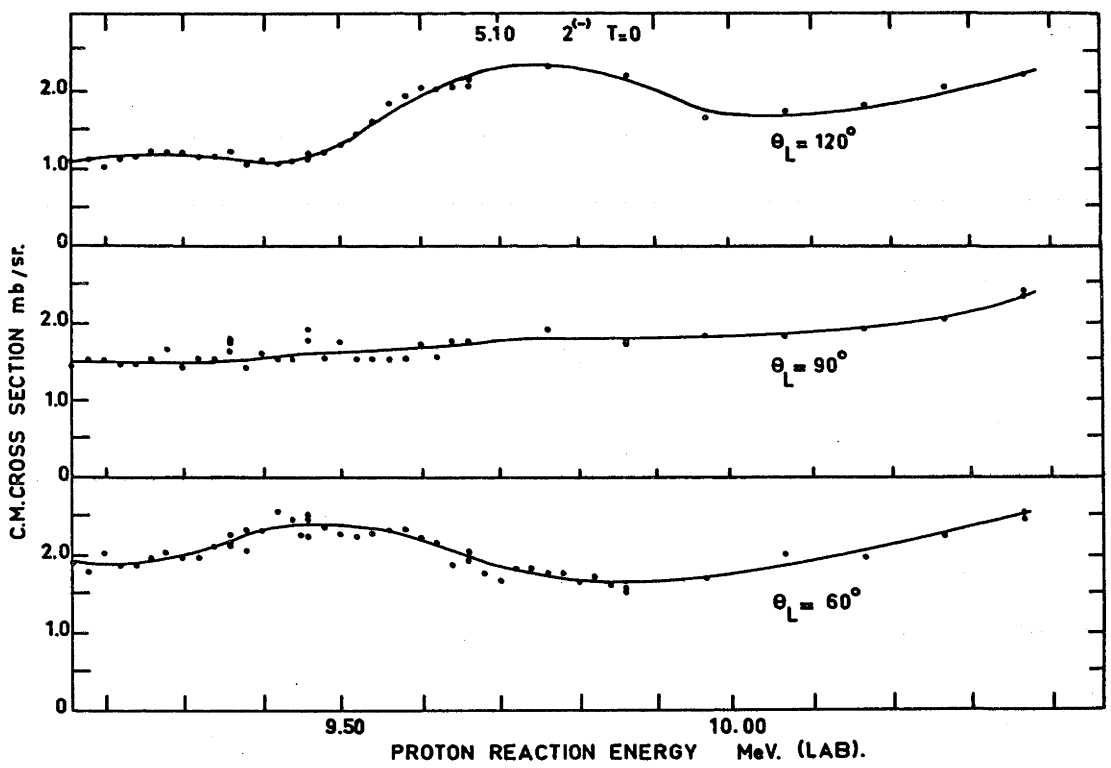
5.10 2(-) T=0
θL= 120°
θL= 90°
θL= 60°
2.0
1.0
0
C.M.CROSS SECTION mb/sr.
9.50
10.00
PROTON REACTION ENERGY MeV. (LAB).

FIG. 6.9 The excitation function, at three angles, of the proton group to the 5.69 MeV state of N^{14}. Both the cross section and angular distributions are influenced by the levels in O^{15} corresponding to the resonances shown in figs. 5.10 and 5.12.

FIG. 6.10 The excitation function, at three angles, of the proton group to the 5.83 MeV state of N^{14}. The prominent resonance at a proton energy of 9.58 MeV corresponds to an O^{15} level at 16.25 MeV excitation. The peaks at different angles are slightly displaced, possibly because of the influence of the nearby resonance shown in fig. 5.12.

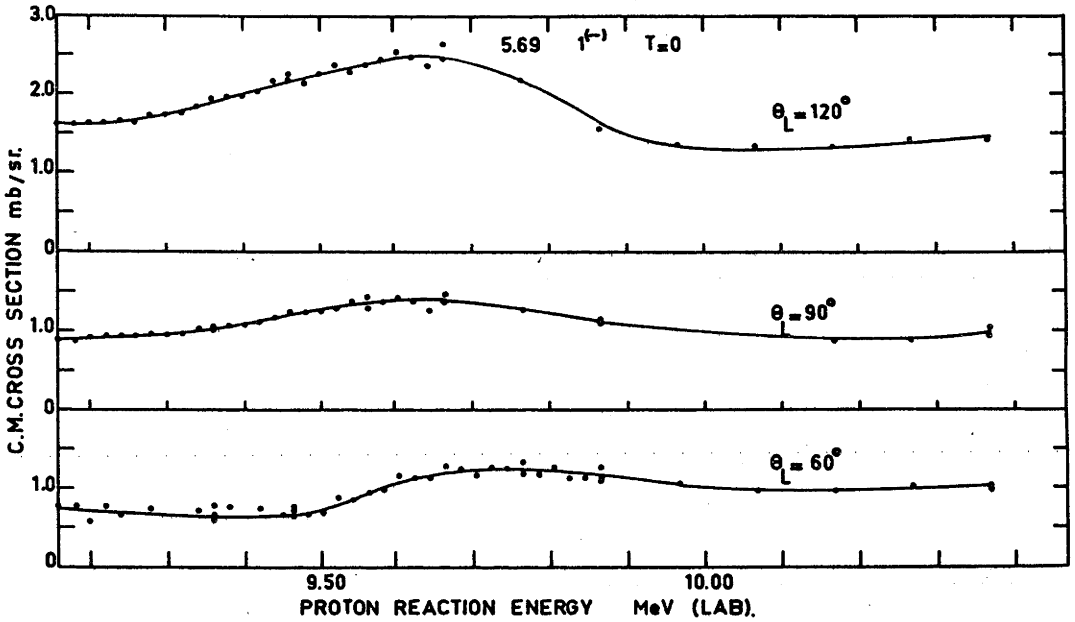
5.69 1(−) T=0
θL=120°
θ=90°
θL=60°
C.M.CROSS SECTION mb/sr.
3.0
2.0
1.0
0
9.50
10.00
PROTON REACTION ENERGY MeV (LAB).

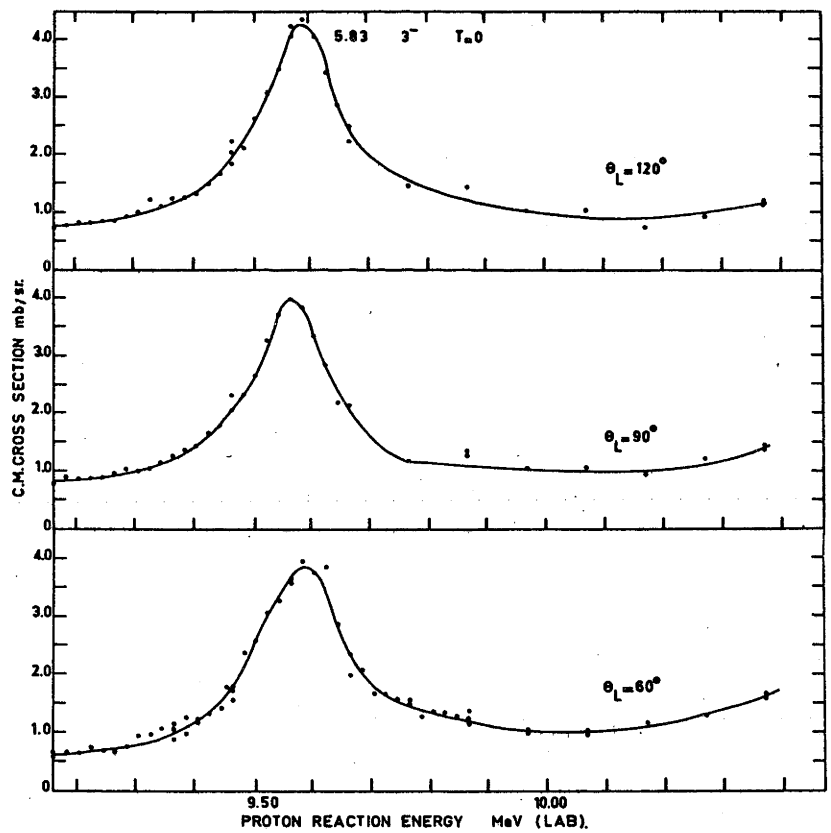
5.83 3− T=0
θL=120°
θL=90°
θL=60°
C.M.CROSS SECTION mb/sr.
4.0
3.0
2.0
1.0
0
9.50
10.00
PROTON REACTION ENERGY MeV (LAB).

FIG. 6.11 The excitation function, at three angles, of the proton group to the 6.21 MeV state of N^{14}. The cross section is influenced by the O^{15} levels corresponding to the resonances shown in figs. 5.10 and 5.12. The angular distribution is varying with energy near 10.4 MeV proton reaction energy.

FIG. 6.12 The excitation function, at three angles, of the proton group to the 6.44 MeV state of N^{14}. The prominent resonance at a proton energy of 9.38 MeV corresponds to an O^{15} level at 16.04 MeV excitation. The peaks at the different angles are slightly displaced, possibly because of the influence of the nearby resonance shown in fig. 5.10. The angular distribution is varying with energy near 10.4 MeV proton reaction energy.

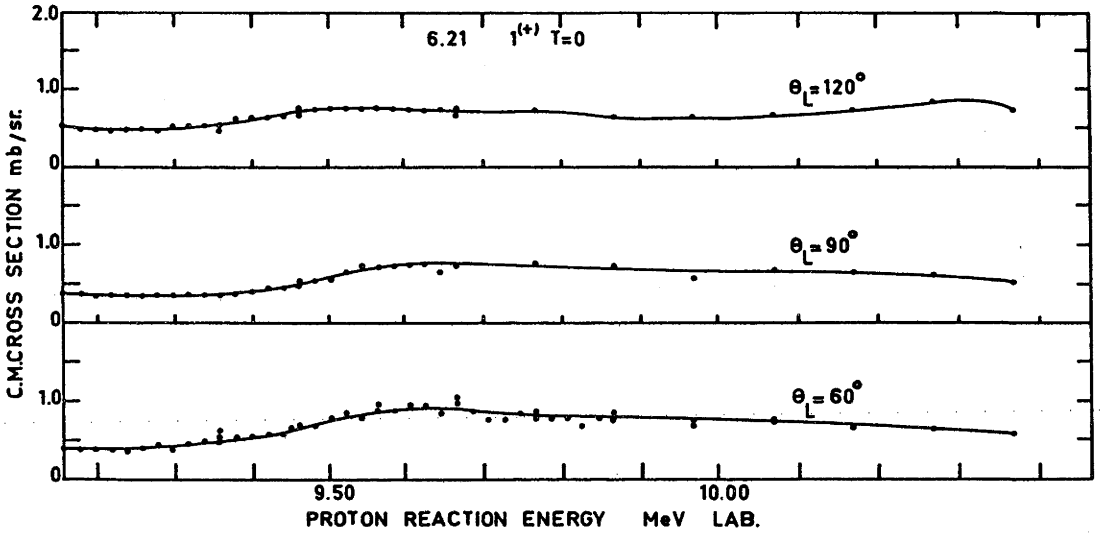
6.21 1(+) T=0
θL=120°
θL=90°
θL=60°
C.M.CROSS SECTION mb/sr.
2.0
1.0
0
9.50
10.00
PROTON REACTION ENERGY MeV LAB.

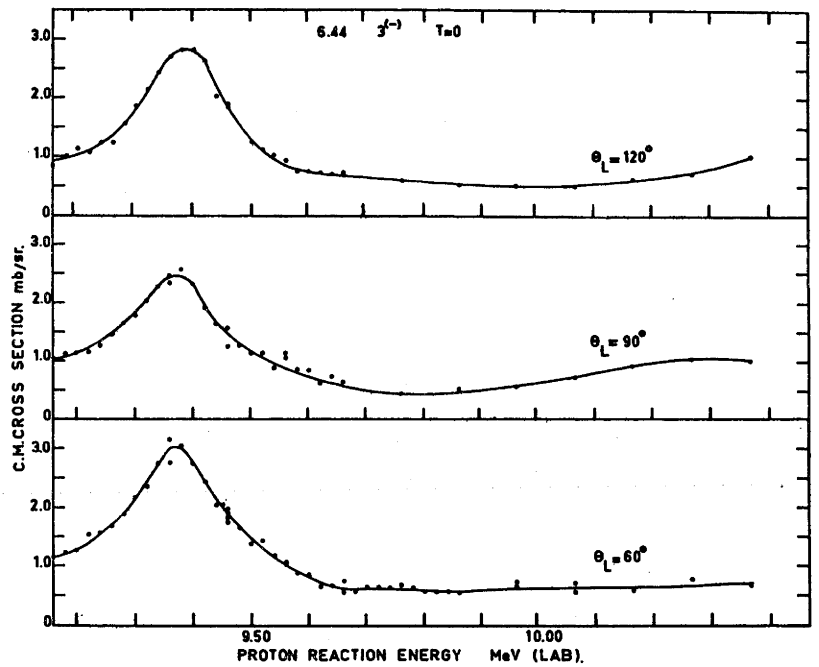
6.44 3(-) T=0
θL=120°
θL=90°
θL=60°
C.M.CROSS SECTION mb/sr.
3.0
2.0
1.0
0
9.50
10.00
PROTON REACTION ENERGY MeV (LAB).

FIG. 6.13 The excitation function, at three angles, of the proton group to the 7.03 MeV state of N^{14}. The cross section is influenced by the O^{15} levels corresponding to the resonances shown in figs. 5.10 and 5.12. The angular distribution is varying with energy near 10.4 MeV proton reaction energy.

FIG. 6.14 The excitation function, at two angles, of the proton group to the 7.97 MeV state of N^{14}. This group was insufficiently resolved at 120^{o} for all energies used.

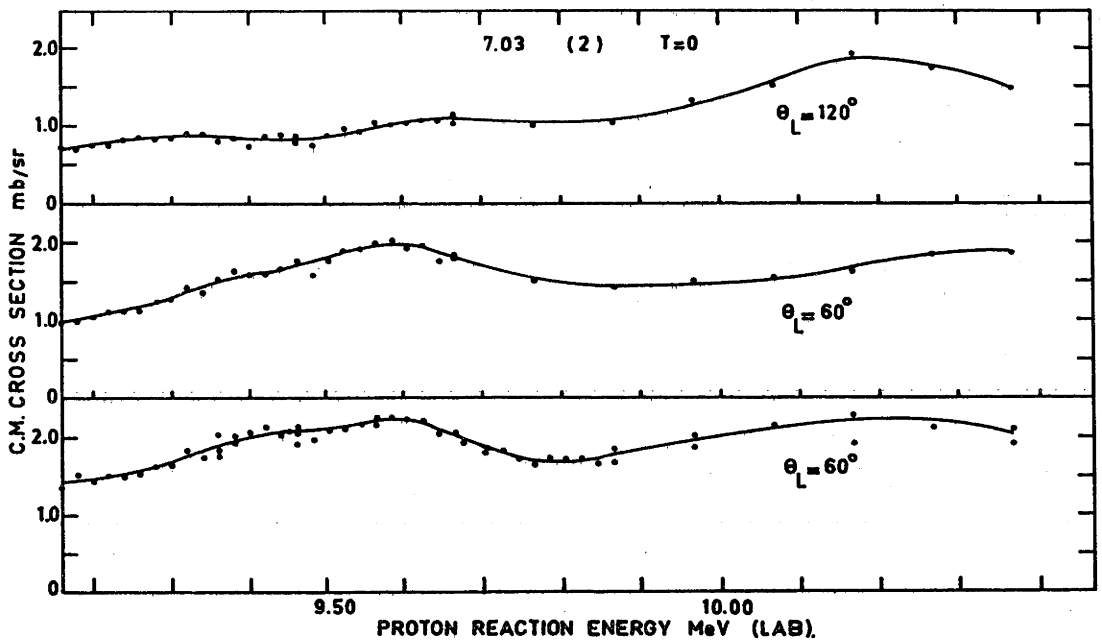
7.03 (2) T=0
θ_L=120°
θ_L=60°
θ_L=60°
C.M. CROSS SECTION mb/sr
2.0
1.0
0
9.50
10.00
PROTON REACTION ENERGY MeV (LAB).

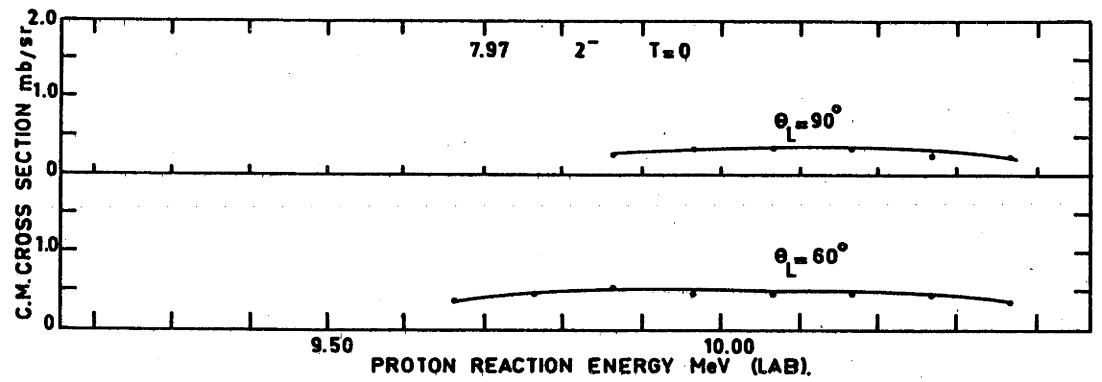
7.97 2⁻ T=0
θ_L=90°
θ_L=60°
C.M. CROSS SECTION mb/sr
2.0
1.0
0
9.50
10.00
PROTON REACTION ENERGY MeV (LAB).

as a function of energy in order to indicate the contribution of compound nucleus effects.

Excitation functions for inelastic proton groups from all the well-confirmed levels in N^{14} up to 7.97 MeV have been extracted from the data at laboratory angles of 60^{o}, 90^{o} and 120^{o} between the proton energies of 9.30 and 10.50 MeV (see figs. 6.5 to 6.14). The cross sections, which were calculated using the formula derived by Silverstein (Si 59), are accurate to $\pm$ 10 percent.

Quite large and rapid variations in cross section are shown by two groups. The groups to the 5.83 MeV level (fig 6.10) and to the 6.44 MeV level (fig 6.12) show marked peaks at proton reaction energies of 9.58 and 9.38 MeV respectively. These peaks correspond to separate levels in the compound nucleus, O^{15}, at 16.24 and 16.04 MeV. Most of the other groups are influenced by these compound nucleus levels, and some show anomalies near 10.4 MeV. The cross sections are least affected by compound nucleus formation in the proton reaction energy region near 10.0 MeV. Angular distributions taken in this energy region would therefore be most likely to be amenable to a direct interaction treatment.

Information on the level structure of O^{15} at the excitation energy reached here, is scarce. The only previous report was of levels at 16.1 and 16.5 MeV by Towle and Macefield (To 61). In

that experiment, neutrons from the $C^{12}(He^3,n)O^{14}$ reaction were studied by a time of flight technique and with a long counter.

It is of interest to note that the two groups showing the strongest evidence for compound nucleus formation, populate levels in N^{14} with the highest spin (J = 3). Two separate levels in O^{15} are involved, each with a width of approximately 170 keV. These two levels have a moderate, but not strong, influence on the cross sections for proton groups to the N^{14} states with J = 2 or 1, and a weak or negligible influence on the cross sections for proton groups to N^{14} states with J = 0. The ways in which the O^{15} levels break up appear to be strongly correlated with the magnitudes of the spins of the residual N^{14} states. In order that residual levels with J = 3 should be preferred to those with J = 2 or 1, a spin for the O^{15} levels of at least $^5/_2$ is indicated. A spin $\geqslant {}^9/_2$ is probable, because the barrier penetrabilities for the inelastic protons are not significantly different for orbital angular momenta $\ell_{p'} \leqslant 2$. An upper limit ($\leqslant {}^{13}/_2$) of the spins of the O^{15} states may be obtained from the total widths of the states by application of the Wigner limit. The limit to the spin is obtained, independent of any assumption concerning the relative magnitudes of the elastic and inelastic proton partial widths.

It should be noted that many of the angular distributions of

the inelastic proton groups are changing significantly with energy near a proton reaction energy of 10.3 MeV. It is therefore likely that an additional level in O^{15}, just above an excitation energy of 16.9 MeV, is influencing the cross sections and angular distributions of these groups.

APPENDIX A

THE EFFECT OF VARYING BEAM CURRENTS ON CROSS SECTIONS MEASURED BY AN ACTIVATION TECHNIQUE

In deriving the formula for cross section determinations when using an activation apparatus (see chapter 2), a constant current was assumed. In actual fact, the beam current from the tandem accelerator is not absolutely constant with time. In this appendix therefore, the effect on the accuracy of the cross section measurement of different types of beam current variation is calculated. In all cases treated, the value of the current integrated over the bombardment period was the same. Hence any differences in the number of active nuclei produced are a measure of the error introduced by assuming a constant current. Three different examples have been calculated.

(a) Constant current

With a constant current, the rate of reactions k, is proportional to the beam current. However the radioactive nuclei decay at a rate proportional to the number N, present at any time. The number decaying is $N\lambda$ where λ is the decay constant. Hence the rate of build up of active nuclei is given by

$$\frac{dN}{dt} = k - \lambda N \qquad \text{A.1}$$

Integration from the beginning of the bombardment to time $t = t_1$ seconds, gives as the number of active nuclei present at time t_1

$$N(t_1) = \frac{k}{\lambda}(1 - e^{-\lambda t_1}) \qquad \text{A. 2}$$

(b) A small sinusoidal ripple on a constant current

If the amplitude of the oscillation is ka (where $a \ll 1$) then the rate of build up of active nuclei is given by

$$\frac{dN}{dt} = k(1 + a \sin \omega t) - N\lambda \qquad \text{A. 3}$$

where ω is the angular frequency of the oscillation in radians / second.

Integration over the time $t = 0$ to $t = t_1$ gives as the number of active nuclei produced

$$N(t_1) = \frac{k}{\lambda}(1 - e^{-\lambda t_1}) + \frac{ka}{(\lambda^2 + \omega^2)}(\lambda \sin \omega t_1 - \omega \cos \omega t_1 + \omega e^{-\lambda t_1}) \qquad \text{A. 4}$$

For oscillations in which $\omega \gg \lambda$, equation A. 4 can be approximated by

$$N(t_1) = \frac{k}{\lambda}(1 - e^{-\lambda t_1}) + \frac{ka}{\omega}(e^{-\lambda t_1} - \cos \omega t_1) \qquad \text{A. 5}$$

The number of active nuclei given by equations A. 2 and A. 5 differ by the term

$$\frac{ka}{\omega}(e^{-\lambda t_1} - \cos \omega t_1) \qquad \text{A. 6}$$

(c) A slow linear change in current

Suppose the beam current at the beginning of the bombardment is $I(1 - b)$, and at the end of the bombardment is $I(1 + b)$ where $b \ll 1$. Then the rate of build up of active nuclei would be

$$\frac{dN}{dt} = k\left[1 + b\left(\frac{2t}{t_1} - 1\right) - N\lambda\right] \qquad A.7$$

Integrating from the beginning of the bombardment to time $t = t_1$ secs., gives as the number of active nuclei produced,

$$N(t_1) = \frac{k}{\lambda}(1 - e^{-\lambda t_1}) - \frac{kb}{\lambda}(1 - e^{-\lambda t_1}) + \frac{2kb}{t_1}\left(\frac{t_1}{\lambda} - \frac{1}{\lambda^2} + \frac{e^{-\lambda t_1}}{\lambda^2}\right) \qquad A.8$$

In this case, the number of active nuclei produced differs from that of the steady current by the term

$$\frac{2kb}{t_1}\left(\frac{t_1}{\lambda} - \frac{1}{\lambda^2} - \frac{e^{-\lambda t_1}}{\lambda^2}\right) - \frac{kb}{\lambda}(1 - e^{-\lambda t_1}) \qquad A.9$$

On several occasions the beam current from the Tandem Van de Graaff accelerator was recorded on a Brown Recorder. The recorder trace showed three types of beam current variation. Two are of the oscillatory type, and the other is a slow linear change. Of the two oscillatory types, one had a frequency of about 2 cycles per sec., and was associated with the frequency of revolution of the belt in the accelerator. The magnitude of the oscillation was typically about $a = 0.01$. The second type of

oscillatory variation which had a frequency of approximately 0.2 cycles per second, was often seen, but was of unknown origin. Its magnitude was typically about a = 0.02. Typical variations of the linear change type, observed during the bombardment time, were up to about b = 0.03, i.e., a 6 percent change from beginning to end of the bombardment.

The decay constant for Ne^{19} (chapter 2) is $\lambda = 0.0398$ per sec. The target was bombarded for 60 seconds. Hence the number of active nuclei produced by the steady current is (from equation A.2)

$$N(60) = 22.6\,k \qquad A.10$$

By substituting the above values in equations A.6 and A.9, and by letting $\cos\omega t_1 = -1$ in equation A.6, the maximum differences in the activity produced are

(i) for the fast oscillation $\pm$ 0.001k

(ii) for the slower oscillation $\pm$ 0.02k

(iii) for the linear change $\pm$ 0.2k.

By comparison with the steady current yield (equation A.10) these represent differences of $\pm$ 0.005, $\pm$ 0.1 and $\pm$ 1 percent respectively.

The decay constant for C^{10} (chapter 3) is $\lambda = 0.0355$ per sec., which is not very different from the value for Ne^{19}. It is concluded therefore, that for both the $F^{19}(p,n)Ne^{19}$ and the

$B^{10}(p,n)C^{10}$ experiment, quite large amplitude oscillations can be tolerated provided they have a fairly high frequency. Linear drifts however, can lead to much greater errors. Under normal operating conditions, the variations in beam current from the tandem accelerator can introduce an error of up to $\pm$ 1 percent into the cross section measurement.

APPENDIX B

THE ENERGY RESOLUTION OBTAINABLE USING A GAS TARGET

This appendix describes calculations which were carried out to determine the energy resolution of the proton groups from the $N^{14}(p,p')$ reaction,, obtainable with the gas target described in chapter 6. Broadening of the groups is introduced both by the geometry of the system and by energy straggling in the filling gas and containing foils.

Energy straggling in an absorber is produced by statistical fluctuations in the average number of collisions a particle makes per unit length. The derivation of energy straggling formulae is well documented (Li 37), and only the results will be quoted here. Using a quantum mechanical approach, the variance in the energy loss by monoenergetic particles in unit length of an absorber is found to be

$$P = 4\pi e^4 z^2 N \left[Z' + \sum_n k_n \frac{I_n Z_n}{m v^2} \log \frac{2mv^2}{I_n} \right] \text{ergs}^2/\text{cm} \qquad \text{B.1}$$

where ze is the charge of the incident particle in $(\text{erg-cm})^{\frac{1}{2}}$,

e is the proton charge in $(\text{erg-cm})^{\frac{1}{2}}$,

N is the number of absorber atoms per cm^3,

m is the mass of an electron in gms,

v is the velocity of the incident particle,

the k_n are numerical constants of order unity,

Z_n is the number of electrons in the nth shell of the absorber atom,

I_n is their average excitation energy,

Z' is the total number of "effective" electrons defined as the number of electrons in the atom excluding those in the inner shells for which $I_n > 2mv^2$, and the summation is over all shells which are not excluded.

The variance of the energy loss of particles passing through a thickness Δx of absorber, is therefore $P.\Delta x$, and the full width at half maximum of the energy distribution is $\Delta E = 2.4 \left[P.\Delta x\right]^{\frac{1}{2}}$.

When using equation B.1, several simplifying assumptions may be made. The constants k_n take the value $k = 4/3$ for hydrogen-like electrons, and this value can be used to obtain approximate results for any atom. Approximate results may be obtained by using tabulated values (Se 53) of the average ionization potential over all electron shells involved in the absorption. By using the average values of I and k, the summation term in equation B.1 reduces to

$$\frac{4\,I\,Z'}{3mv^2} \log \frac{2mv^2}{I} \qquad \text{B.2}$$

In general, Z' is somewhat smaller than the total number of electrons, Z, in the absorber atom. However an upper limit on the straggling is obtained if Z' is replaced by Z in equation B.1. Making this substitution, and using equation B.2, the variance equation becomes

$$P = 4\pi z^2 e^4 Z N \left[1 + \frac{4I}{3mv^2} \log \frac{2mv^2}{I}\right] \text{ergs}^2/\text{cm} \qquad \text{B.3}$$

Typical values of the second term in the square brackets, for straggling in 1 mgm/cm^2 thick mylar, range from 0.02 for 10 MeV protons to 0.2 for 1 MeV protons.

The various contributions to the energy spread of an inelastic proton group from the $N^{14}(p,p')$ reaction are listed below. The example has been taken of a proton group leaving the reaction volume of the target at a laboratory angle of 60^o, with 1 MeV energy. A target-gas pressure of 180 mm of mercury, and a 10 MeV incident proton beam are assumed.

The widths at half maximum, ΔE, for the approximately gaussian energy distributions resulting from energy straggling, have been calculated for the following absorbers.

(i) For the 10 MeV incident protons passing through the 0.63 micron Ni entrance foil ΔE = 16 keV.

(ii) For the incident beam passing through 10.3 cm of gas (at 180 mm of mercury pressure) to the centre of the

target ΔE = 38 keV.

(iii) For the 1 MeV reaction proton group passing through 3.8 cm of gas to the target chamber window ΔE = 24 keV.

(iv) For the reaction proton group passing through the nominal 1 mgm/cm^2 mylar target chamber window ΔE = 23 keV.

These energy distributions are independent of one another and can therefore be combined to give a distribution of width

$$\Delta E = \left[16^2 + 38^2 + 24^2 + 23^2\right]^{\frac{1}{2}}$$

$$= 53 \text{ keV}$$

The finite size of the counter and length of beam visible to the counter, introduce further spreads into the energy of an observed proton group. Four factors which contribute to the energy spread introduced by the geometry are:

(i) The incident beam loses energy in the gas as it progresses along the section visible to the counter. The maximum difference in the beam energies viewed by the counter is 5 keV.

(ii) Reaction protons, originating at opposite ends of the length of beam visible to the counter, must travel through different amounts of gas to reach the counter. The maximum spread in reaction proton energies due to this effect is 17 keV.

(iii) The finite angular resolution, and the reaction kinematics result in an energy distribution with a maximum width of 16 keV.

(iv) With the counter at a laboratory angle of 60^{o}, a section of beam 0.35 cm long is visible to the complete area of the counter defined by the rear collimator slit. A further section of the beam approximately 0.2 cm long is visible only to part of the defined area of the counter. The detection efficiency is different for different parts of the beam visible to the counter. Hence the efficiency distribution, which is trapezoidal along the visible length of beam, must be folded with each of the above three energy distributions.

The four geometrical contributions are not independent. However, they can be combined with each other, and with the straggling distributions. The result is a full width at half maximum of approximately 58 keV for the energy spread of a 1 MeV proton group, emerging from the gas target at a laboratory angle of 60^{o}.

REFERENCES

(Aj 54) F. Ajzenberg and W. Franzen, Phys. Rev. 95 (1954) 1531.

(Aj 59) F. Ajzenberg-Selove and T. Lauritsen, Nuclear Physics 11 (1959) 1.

(An 62) G.B. Andreev, A.S. Deinenko and I.Ya. Malakov, Izv. Akad. Nauk. SSSR 26 (1962) 1134.

(Ba 55) J.B. Bair, J.D. Kington and H.B. Willard, Phys. Rev. 100 (1955) 21.

(Ba 62) S. Bashkin and T.R. Ophel, Nucl. Instr. 15 (1962) 112.

(Be 53) R.E. Benenson, Phys. Rev. 90 (1953) 420.

(Bl 51) J.P. Blaser, F. Boehm, P. Marmier and P. Scherrer, Helv. Phys. Acta. 24 (1951) 465.

(Bl 52) J.M. Blatt and V.F. Weisskopf, "Theoretical Nuclear Physics", p. 394, John Wiley and Sons (1952).

(Bl 52a) J.M. Blatt and L.C. Biedenharn, Revs. Mod. Phys. 24 (1952) 258.

(Br 60) C. Broude and H.E. Gove, Proc. of the International Conference on Nuclear Structure, Kingston, Canada (U. of Toronto Press, 1960), p. 754; Private communication.

(Br 62) E. Bradford, private communication.

(Br 63) R.E. Brown, Astrophys. Journal, 137 (1963) 338.

(Br 63a) T.A. Brinkley, private communication.

(Bu 56) E.J. Burge and D.J. Prowse, Phil. Mag. 1 (1956) 912.

(Bu 63) E.J. Burge, private communication.

(Ca 58) A.G.W. Cameron, Can. J. Phys. 36 (1958) 1040.

(Ca 62) G.R. Caughlan and W.A. Fowler, Astrophys. Journal 136 (1962) 453.

(Ce 56) M. Cerino, Nuclear Physics 2 (1956) 113.

(Ch 56) G.B. Chadwick, T.K. Alexander and J.B. Warren, Can. J. Phys. 34 (1956) 381.

(Cl 62) D.D. Clayton, Phys. Rev. 128 (1962) 2254.

(Cr 52) D.S. Craig, D.J. Donahue and K.W. Jones, Phys. Rev. 88 (1952) 808.

(Da 54) R.B. Day and T. Huus, Phys. Rev. 95 (1954) 1003.

(De 40) L.A. Delsasso, M.G. White, W. Barkas and E.C. Creutz, Phys. Rev. 58 (1940) 586.

(De 63) D. Demirlioglu and W. Whaling, to be published.

(Di 63) F.S. Dietrich, J.L. Honsaker and J.W. Davies, Bull. Amer. Phys. Soc. 8 (1963) 120.

(Do 63) P.F. Donovan, J.F. Mollenauer and E.K. Warburton, Phys. Rev. (1963) In press.

(En 62) P.M. Endt and C. Van der Leun, Nuclear Physics 34 (1962) 1.

(Er 60) T. Ericson, Advances in Physics, 9 (1960) 425.

(Fa 58) U. Farinelli and R. Malvano, Rev. Sci. Inst. 29 (1958) 699.

(Fo 62) W.A. Fowler (1962) private communication.

(Ge 59) D.S. Gemmell, A.H. Morton and W.I.B. Smith, Nuclear Physics 10 (1959) 45.

(Gi 59) J.H. Gibbons and R.L. Macklin, Phys. Rev. 114 (1959) 571.

(Gr 57) A. Graüe and B. Trumpy, Phil. Mag. 2 (1957) 138.

(Ha 62) L.F. Hansen, R.C. Jopson, H. Mark and C.D. Swift, Nuclear Physics 30 (1962) 389.

(He 60) D.F. Hebbard and J.L. Vogl, Nuclear Physics 21 (1960) 652.

(Ho 57) A. Hossain and A.N. Kamal, Indian J. Phys. 31 (1957) 553.

(Hu 57) S.E. Hunt, R.A. Pope and W.W. Evans, Phys. Rev. 106 (1957) 1012.

(Hu 62) W.E. Hunt, M.K. Mehta and R.H. Davis - from the Ph.D. Thesis of K.L. Warsh, Florida State University.

(Ka 57) S.P. Kalinin, A.A. Ogloblin and Y.M. Petrov, Soviet J. of Atomic Energy 2 (1957) 193.

(Ka 58) H.B. Knowles, Bull. Amer. Phys. Soc. 3 (1958) 330.

(La 54) J.M.B. Lang and K.J. Le Couteur, Proc. Phys. Soc. A 67 (1954) 586.

(La 58) A.M. Lane and R.G. Thomas, Revs. Mod. Phys. 30 (1958) 257.

(La 62) T. Lauritsen and F. Ajzenberg-Selove, Nuclear Data Sheets, Sets 5 and 6 (1962).

(Le 59) K.J. Le Couteur and D.W. Lang, Nuclear Physics 13 (1959) 32.

(Li 37) M.S. Livingston and H.A. Bethe, Revs. Mod. Phys. 9 (1937) 245.

(Ma 55) J.B. Marion, T.W. Bonner and C.F. Cook, Phys. Rev. 100 (1955) 91.

(Ma 59) J.B. Marion and J.S. Levin, Phys. Rev. 115 (1959) 144.

(Mi 56) D.W. Miller, B.M. Carmichael, U.C. Gupta, V.K. Rasmussen and M.B. Sampson, Phys. Rev. 101 (1956) 740.

(Ne 55) J.L. Need, Phys. Rev. 99 (1955) 1356.

(Od 60) Y. Oda, M. Takeda, N. Takano, T. Yamazaki, C. Hu, K. Kikuchi, S. Kobayashi, K. Matsuda and Y. Nagahara, J. Phys. Soc. Japan 15 (1960) 760.

(Oh 63) G.G. Ohlsen and P.G. Young, Nuclear Physics, in press.

(Op 62) T.R. Ophel, R.N. Glover and E.W. Titterton, Nuclear Physics 33 (1962) 198.

(Ov 62) J.C. Overley and W. Whaling, Phys. Rev. 128 (1962) 315.

(Po 59) B. Povh, Phys. Rev. 114 (1959) 1114.

(Ra 58) W.A. Ranken, T.W. Bonner and J.H. McCrary, Phys. Rev. 109 (1958) 1646.

(Ra 58a) W.A. Ranken, T.W. Bonner, J.H. McCrary and T.A. Rabsen, Phys. Rev. 109 (1958) 917.

(Re 55) J.B. Reynolds, Phys. Rev. 98 (1955) 1289.

(Ro 53) M.E. Rose, Phys. Rev. 91 (1953) 610.

(Ro 55) I.L. Rosental, J.E.T.P. (U.S.S.R.) 28 (1955) 118; J.E.T.P. (Soviet Physics) 1 (1955) 116.

(Sa 60) Y. Saji, J. Phys. Soc. Japan 15 (1960) 367.

(Se 53) Experimental Nuclear Physics, E. Segre Ed. John Wiley and Sons Inc. (1953).

(Sh 49) R. Sherr, H.R. Meuther and M.G. White, Phys. Rev. 75 (1949) 282.

(Sh 53) R. Sherr and J.B. Gerhart, Phys. Rev. 91 (1953) 909.

(Si 59) E.A. Silverstein, Nucl. Instr. 4 (1959) 53.

(Sp 60) R.R. Spencer, G.C. Phillips and T.B. Young, Nuclear Physics 21 (1960) 310.

(Sy 62) G.D. Symons and P.B. Treacy, Phys. Lett. 2 (1962) 175.

(Ta 61) S. Takayanagi, N.H. Gale, J.B. Garg and J.M. Calvert, Nuclear Physics 28 (1961) 494.

(Te 52) T. Teichmann and E.P. Wigner, Phys. Rev. 87 (1952) 123.

(Te 61) I.B. Teplov, O.P. Shevchenko and E.K. Ruuge, Zhur. Eksp. i Theoret. Fiz. 39 (1960) 923; Soviet Physics J.E.T.P. 12 (1961) 640.

(To 61) J.H. Towle and B.E.F. Macefield, Proc. Phys. Soc. 77 (1961) 399.

(Va 63) S.S. Vasilyev, V.V. Komarov and A.M. Popova, Nuclear Physics 40 (1963) 443.

(Wa 63) K.L. Warsh, G.M. Temmer and H.R. Blieden, Phys. Rev. 131 (1963) 1690.

(Wh 58) W. Whaling, Handbuch der Physik, (Springer-Verlag, Berlin 1958) Vol. 34.

(Wh 63) W. Whaling, private communication.

(Wi 52) H.B. Willard, J.K. Bair, J.D. Kington, T.M. Hahn, C.W. Snyder and F.P. Green, Phys. Rev. 85 (1952) 849.